



HAL
open science

Assessment of heat pump operating faults coupled with building energy simulation using Petri net model

Minh Toàn Vo

► **To cite this version:**

Minh Toàn Vo. Assessment of heat pump operating faults coupled with building energy simulation using Petri net model. Civil Engineering. Université de La Rochelle, 2021. English. NNT : 2021LAROS023 . tel-03685404

HAL Id: tel-03685404

<https://theses.hal.science/tel-03685404>

Submitted on 2 Jun 2022

HAL is a multi-disciplinary open access archive for the deposit and dissemination of scientific research documents, whether they are published or not. The documents may come from teaching and research institutions in France or abroad, or from public or private research centers.

L'archive ouverte pluridisciplinaire **HAL**, est destinée au dépôt et à la diffusion de documents scientifiques de niveau recherche, publiés ou non, émanant des établissements d'enseignement et de recherche français ou étrangers, des laboratoires publics ou privés.



École doctorale n° 618 : Sciences pour l'ingénieur (EUCLIDE)

THÈSE de DOCTORAT
La Rochelle Université
Spécialité Génie Civil

Minh Toàn VÕ

Soutenu le 29 Septembre 2021
à La Rochelle Université

**Assessment of heat pump operating faults coupled
with building energy simulation using Petri net
model**

Devant le jury composé de :

Christian INARD,	Professeur, LaSIE	Président
Monica SIROUX,	Professeure, INSA Strasbourg	Rapporteuse
Gilles FRAISSE,	Professeur, LOCIE	Rapporteur
Cong-Toan TRAN,	Docteur-Ingénieur de recherche, Mines ParisTech	Examineur
Emmanuel BOZONNET,	HDR, LaSIE	Directeur de thèse
Charles PELE,	Docteur-Chef de division, CSTB	Co-encadrant

Laboratoire des Sciences de l'Ingénieur pour l'Environnement (LaSIE)

UMR CNRS 7356, 17042 La Rochelle Cedex 1 - France

Acknowledgments

Completion of this doctoral dissertation was possible with the support of several people during my thesis. I would like firstly to acknowledge the Scientific and Technical Centre for Building (CSTB), the Energy and Environment Department (DEE), and the Laboratory of Engineering Science for Environment (LaSIE) for their financial support.

I would like to thank Emmanuel Bozonnet (LaSIE) and Charles Pele (CSTB) for their supervision and their availability. They welcomed me to their team and helped me go through this adventure. This helps me to realize how the research should be done. Without their support, it would not be possible to conduct and finish this research.

Besides, I would like to acknowledge DEE members (CSTB) for their supports at various phases of this thesis. In particular, I thank Christophe Barras, who enlightened me the first glance of research in fault analysis field, which was entirely new for me. He gradually developed my interest in this topic, especially Petri net models. Additionally, discussions with Jean-Marie Alessandrini, Jean-Baptiste Videau, Tianyun Gao have been illuminating. They are very good at referring me to publications, ideas, and relevant people to support my substantive work. Their contributions of time and ideas made my Ph.D. experience productive and stimulating. Advices, suggestions and comments given by Antoine Breitwiller, Laurent Reynier, Anthony Rey on Python, COMETH, pyCOMETH, Maestro have been great helps in my simulation phase. I received generous support from Mr. Payne Vance and his group (National Institute of Standards and Technology, USA) in heat pump modelling works. I also thank Simon Thebaut, who proposed LaTeX format for my dissertation, which saves me a lot of time in writing.

I would like to thank the committee members: Monica Siroux, Gilles Fraise, Christian Inard and Tran-Cong Toan, who accepted and took the time to review and examine my work. I would also like to express my gratitude to Mateusz Bodgan and Phillipe Rivière, who supported me and criticized constructively. Their insightful comments, encouragement, and also their questions incited me to widen my research from various perspectives.

I had a wonderful time thanks to all my colleagues, past and present Ph.D. students, and friends in both cities Paris and La Rochelle. Thank you everyone, including Chloé, Emilie, Melanie, Gaby, Rafael, Dima, Raphael, NicolasC, Christophe, Thomas, Islem, Lorena, NicolasB, Elodie, Madeleine, Simon, Emilien, Jean-Baptiste, and others if I forgot to mention (sorry). I would like to thank my fellow doctoral students from LaSIE, as Hien, Louis, Anais, Fanny and Simon for their feedbacks, cooperation and of course friendship. In addi-

tion, I would like to express my thanks to all the administration staff: Jennifer De La Corte Gomez, Isabelle Hirsch (DSSM), Caterina Dagui, and Despierre Laurie Annie (DEE) and Karine Planchet (LaSIE) for their administration supports in both academic process and business trips.

Last but not least, I send a special thanks to my families for supporting me spiritually throughout this journey and my life in general. Words cannot express how grateful I am to my parents, my siblings, my welcome family Béatrice Martineau, Bibi, Bénédicte & Vincent Brocard, Sylviane Rivière and Marie Calvez. I would also like to thank my partner, Mathieu Montagut, who is tremendously helpful in this process. I cannot thank you enough for encouraging me throughout this experience.

Nomenclature

Abbreviations

AEI	Annual energy impact
AFI	Annual financial impact
ASHP	Airsource heat pump
BES	Building energy simulation
COMETH	BES tool developed by CSTB
CSTB	Scientific and Technical Centre for Building
DEE	Energy and Environment Department
DSSM	Doctoral Studies & Services Manager
EHPA	European Heat pump association
EPBD	Energy Performance of Buildings Directive
EPC	Energy Performance Certificate
EU	European Union
FDD	Fault detection and diagnostic
GHG	Green house gas
HVAC	Heating, ventilation, and air conditioning
NEEAP	The National Energy Efficiency Action Plan
NF	French standard
NF EN	European standard
NF EN ISO	International standard
NZEB	Nearly Zero-energy Buildings
PV	Photovoltaic
RT	French building thermal code
TXV	Thermostatic expansion valve

Symbols	Description	Unit
A	Area	m^2
C_{nn}	Correction coefficient in RT2012 calculation	
C_{ep}	Primary energy consumption per year and per square meter of building	$kWh_{EP}/(m^2 \cdot yr)$
COP	Coefficient of performance	
D	Hydraulic diameter	m
EER	Energy efficiency ratio	
F	Fault ratio	$\%$
K	Global exchange coefficient of the heat exchanger	$W/(m^2 \cdot K)$
$LMTD$	Logarithmic mean temperature	$^{\circ}C$
PLF	Partial load factor	
PLR	Part load ratio	
Q	Heat transfer rate	W
\mathcal{R}	Global thermal resistance	$m^2 \cdot K/W$
S	Heat exchanger surface	m^2
T	Temperature	K
W	Compressor power	W

Symbols	Description	Unit
c_p	Specific heat at constant pressure	J/K
e	Thickness	m
h_c	Convection heat transfer coefficient	$W/(m^2 \cdot K)$
h	Specific enthalpy	kJ/kg
q_{mr}	Mass flow rate	kg/s
q_v	Volumetric flow rate	m^3/h
t	Fouling time	month
ρ	Density	kg/m^3
η_{CPs}	Compressor isentropic efficiency	
λ	Thermal conductivity	$W/(m \cdot K)$

Subscripts	Description
a	air
aux	auxiliary components
CD	condenser
CP	compressor
EX	expansion valve
EV	evaporator
ext	exterior
i	inlet
ini	initial
int	interior
n	nominal
o	outlet
r	refrigerant

Abstract

France building thermal code RT and energy performance labels, have been developed to improve the intrinsic performance of buildings and energy systems. However, the regulations define a conventional performance, which is not intended to predict actual consumption, which could be changed if we take into account the system faults.

In this research, we focus on the building operation, and the fault appearance in energy systems. Indeed, systems sometimes operate with a lower efficiency than that measured under nominal laboratory conditions. The causes are numerous and can be due to (1) the design, (2) the installation or the maintenance process, and (3) fault occurrence during the building operation. These can reduce the performance of the overall system to a large extent.

Among the three fault types mentioned above, operating faults (3) are more difficult to control because they occur randomly during normal use. They are not taken into account in the design process. Besides, the current tools for building energy simulation do not consider these operating faults. We propose to develop a method to model these operating faults and to associate them with a building simulation model. This coupling potentially supports to describe how the system works, to get the system performance in practice, and to assess the building energy consumption during the operation.

In the building sector, heating takes a share of approximately 70% of the energy needs. Among heating systems, the heat pump gives an efficient and sustainable solution for both heating and cooling. Moreover, aerothermal heat pumps have spread rapidly in recent years and now dominate residential sales in France, accounting for nearly 97.5% of the market in 2018. We therefore decided to choose the air-to-air heat pumps to study this subject. We focus on, three operating faults: refrigerant leakage, condenser fouling, and evaporator fouling. They are the most frequent faults, and evolve undetectably over time until they start to create energy problems.

In order to solve the question about the fault integration into building energy simulation, the study proposes a method composed of two parts. In the first place, we developed physical models of a heat pump in order to predict the coefficient of performance of the heat pump, as a function of the use intensity, and operating fault. We built an operating fault database, based on an experimental model of heat pump, and physical equations, in order to perform simulations. Then, a Petri net model – the mathematical and graphical modeling, was proposed to determine a priori structure of fault evolution. It describes any evolution of operating fault from a fault-free state to a state with a specific fault level. When operating

fault occurs and evolves to a higher level, the Petri net applies this new fault level in the heat pump model and results in the heat pump performance, particularly COP and EER in this research. This model can regulate a singly imposed fault or with some faults together.

In the second step, we apply a notion of uncertainty of fault database to take into account different working cases and generalize the fault occurrence model. We coupled it with the dynamic energy simulation tool COMETH - a building simulation model developed by CSTB, to simulate the annual energy consumption. This allows us to determine the global uncertainty on energy consumption and to show a propagation on the system performances. As many operating faults occurs during the heat pump life cycle, we use Petri net model to regulate the occurrence of various operating faults. It shows the occurrence order of each fault, which helps us combine all operating faults together and analyze their impacts. This method allows to analyze fault impacts on the performance of a machine and on the whole energy consumption of the building.

For research purposes, the method was applied to a residential building in Paris, respecting the intrinsic performances of the RT2012 requirements. We analyzed the impact of these three heat pump operating faults in a case study over 15 years. In a first approach, the operating fault is imposed separately. A refrigerant leakage of about 30% can result in an average 32% increase in heating consumption and a 5% rise in cooling capacity. For interior and exterior fouling, a 30% reduction in airflow increased the average heating consumption by 15% and 10%, respectively. Then, as operating faults occur cumulatively, we model all three operating faults together. The building consumption remarkably increased from the third year, in which the primary energy consumption of the building exceeds $60\text{kWh}/\text{m}^2/\text{year}$. If there is no maintenance intervention, the operating faults impact more and more on the primary energy consumption. At the 15th year, the building energy consumption C_{ep} can increase approximately $120\text{kWh}/\text{m}^2/\text{year}$, double the standard value. The results underline the possibility of the proposed methodology. By using the Petri net model, three models as the heat pump model, the fault model and the building model are coupled to analyze the impact of operating faults on the annual building energy consumption.

Résumé

La réglementation thermique des bâtiments en France (RT) et les labels de performance énergétique, ont été développés pour améliorer la performance intrinsèque des bâtiments et des systèmes énergétiques. Toutefois, la réglementation définit une performance conventionnelle, qui n'a pas vocation à prédire la consommation réelle, laquelle pourrait être modifiée si l'on tient compte des défauts de fonctionnement du système.

Dans cette recherche, nous nous concentrons sur le fonctionnement du système, auquel nous associons une notion d'apparition de défauts. En effet, les systèmes fonctionnent parfois avec une efficacité inférieure à celle mesurée dans des conditions nominales de laboratoire. Les causes sont nombreuses et peuvent survenir (1) lors de la conception, (2) lors du processus d'installation ou de maintenance, et (3) lors de l'utilisation des systèmes. Ceux-ci peuvent réduire dans une large mesure les performances de l'ensemble du système.

Parmi les trois types de défauts mentionnés ci-dessus, les défauts de fonctionnement (3) sont plus difficiles à contrôler car ils se produisent de manière aléatoire lors d'une utilisation normale. Ils ne sont pas pris en compte dans le processus de conception. Par ailleurs, les outils actuels de simulation énergétique des bâtiments ne prennent pas en compte les défauts de fonctionnement. Nous proposons de développer une méthode pour modéliser les défauts de fonctionnement et les associer à un modèle de simulation de bâtiment. Ce couplage permet de décrire le fonctionnement du système, d'obtenir les performances du système dans la pratique et d'évaluer la consommation d'énergie du bâtiment pendant son fonctionnement.

Dans le secteur du bâtiment, le chauffage représente environ 70% des besoins en énergie. Parmi les systèmes de chauffage, la pompe à chaleur constitue une solution efficace et durable pour le chauffage et la climatisation. Par ailleurs, les pompes à chaleur aérothermiques se sont rapidement répandues ces dernières années et dominent désormais les ventes résidentielles en France, représentant près de 97.5% du marché en 2018. Nous avons donc décidé de choisir les pompes à chaleur air-air pour étudier ce sujet. Trois défauts de fonctionnement sont considérés dans cette étude : les fuites de réfrigérant, l'encrassement du condenseur et l'encrassement de l'évaporateur. Ces défauts sont les plus fréquents et évoluent de manière indétectable dans le temps jusqu'à ce qu'ils commencent à créer de graves problèmes de confort et engendrent l'augmentation de la consommation énergétique.

Afin de résoudre la question de l'intégration des défauts dans la simulation énergétique des bâtiments, l'étude propose une méthode composée de deux parties. En premier

lieu, nous avons développé des modèles physiques d'une pompe à chaleur afin de prédire le coefficient de performance COP/EER de la pompe à chaleur, en fonction de l'intensité d'utilisation et des défauts de fonctionnement à un niveau donné. Pour le faire, nous avons construit une base de données de défauts pendant la phase d'utilisation, utilisé un modèle expérimental de pompe à chaleur et des équations physiques.

Ensuite, un modèle de réseau de Petri - la modélisation mathématique et graphique, a été proposé pour déterminer a priori la structure de l'évolution des défauts. Il décrit toute évolution d'un défaut de fonctionnement d'un état sans défaut à un état avec un niveau de défaut spécifique. Lorsque le défaut de fonctionnement se produit et évolue vers un niveau plus élevé, le réseau de Petri applique ce nouveau niveau de défaut dans le modèle de pompe à chaleur. La performance de la pompe à chaleur, en particulier le COP et l'EER, évolue en conséquence. Ce modèle fonctionne avec un défaut seul ou avec plusieurs défauts combinés.

Dans un deuxième temps, nous appliquons une notion d'incertitude dans la base de données des défauts pour prendre en compte différents cas de fonctionnement et généraliser le modèle d'occurrence des défauts. Nous l'avons couplé à l'outil de simulation énergétique dynamique COMETH - un modèle de simulation de bâtiment développé par le CSTB, pour simuler la consommation énergétique annuelle. Cela nous permet de déterminer l'incertitude globale sur la consommation d'énergie et de montrer une propagation sur les performances du système. Comme de nombreux défauts de fonctionnement se produisent pendant le cycle de vie de la pompe à chaleur, nous utilisons notre modèle de réseau de Petri pour réguler l'apparition de divers défauts de fonctionnement. Il montre l'ordre d'apparition de chaque défaut, ce qui nous aide à combiner tous les défauts de fonctionnement et à analyser leurs impacts. Cette méthode permet d'analyser l'impact des défauts sur les performances d'une machine et sur la consommation énergétique globale du bâtiment.

La méthode a été appliquée à un bâtiment résidentiel à Paris, en respectant les performances intrinsèques des exigences de la RT2012. Nous avons analysé l'impact de ces trois défauts définis pour l'étude sur une période de 15 ans. Dans une première approche, le défaut de fonctionnement est imposé séparément. Une fuite de réfrigérant de 30% peut entraîner une augmentation moyenne de 32% de la consommation de chauffage et de 5% de la capacité de refroidissement. Pour l'encrassement intérieur et extérieur, une réduction de 30% du débit d'air peut augmenter la consommation moyenne de chauffage de 15% et 10%, respectivement. Ensuite, comme les défauts de fonctionnement se produisent de manière cumulative, nous modélisons les trois défauts de fonctionnement ensemble. La consommation du bâtiment peut augmenter remarquablement à partir de la troisième année, au cours de laquelle la consommation d'énergie primaire du bâtiment dépasse 60kWh/m²/an. En l'absence d'intervention de maintenance, les défauts de fonctionnement ont un impact de plus en plus important sur la consommation d'énergie primaire. A la 15ème année, le Cep peut augmenter d'environ 120 kWh/m²/an, soit le double de la valeur standard.

Les résultats soulignent la possibilité de la méthodologie proposée. En utilisant le mod-

èle de réseau de Petri, trois modèles tels que le modèle de pompe à chaleur, le modèle de défaut et le modèle de bâtiment sont couplés pour analyser l'impact des défauts de fonctionnement sur la consommation énergétique annuelle du bâtiment.

Contents

Acknowledgments	iii
Nomenclature	v
Abstract	vii
Résumé	ix
Contents	xiii
1 Introduction	1
1.1 Building faults	1
1.2 Heating and cooling systems, heat pumps	2
1.3 Importance of heat pump faults	5
1.4 Objectives	8
2 State of the art	11
2.1 Description of heat pump technology	11
2.1.1 Heat pump components	11
2.1.2 Refrigerant and regulation evolution	15
2.1.3 Heat transfer mechanism	17
2.2 Heat pump models without faults	18
2.2.1 Refrigerant cycle model	18
2.2.2 Empirical models	23
2.3 Heat pump operating faults	28
2.3.1 Fault definition	29
2.3.2 Petri nets, fault occurrence model	42
3 Operating fault impact on heat pump performance	49
3.1 Heat pump calculation without faults	49
3.1.1 Refrigerant cycle model	50
3.1.2 Benchmark of the refrigerant cycle model with a standard model . . .	52
3.2 Heat pump calculation with faults	53
3.2.1 Refrigerant cycle model	53

3.2.2	Benchmark of the refrigerant cycle model with the empirical model . . .	56
3.3	Combination of operating faults	58
4	Dynamic evolution of coupled building and heat pump simulation taking into account operating faults	65
4.1	Coupled building and heat pump models – static fault ratio	66
4.1.1	The simulation process without fault illustrated for the reference case study	66
4.1.2	The simulation process with a static fault ratio	73
4.2	Integration of fault evolution with Petri net model	76
4.2.1	Impact of an elementary operating fault	80
4.2.2	Impact of fault combination	85
	References	99
	Appendices	103
A	Heat pump types	105

Chapter 1

Introduction

1.1 Building faults

It is reasonable to expect that the buildings are constructed and used in a manner that is stable, safe, and fit for purpose during longer lifetimes ranging from 50 to 100 years. Unfortunately, buildings appear to have the defects. According to the British Standard BS 3811:1964 [BSI, 1993] about the glossary of maintenance management terms, building faults are defined as the deterioration of building features and services to unsatisfactory quality levels of user requirements. They can result from design error by the architect, lack of adherence to the design by the technician, system malfunction, or any combination of them. Common types of building faults are related to the building envelopes and HVAC systems (heating, ventilation, and air conditioning), such as structural faults, inadequate insulation or soundproofing, faulty electrical wiring and/or lighting, insufficient or defective drainage systems, insufficient or incorrect ventilation, cooling or heating systems, etc. Based on the United States Commercial Buildings Energy Consumption Survey (CBECS), Kim et al. [2018] identified a total of 47 building faults, and identified the most important ones reported in Table 1.1.

Table 1.1 shows the significant impacts of the studied faults on the annual energy impact (AEI) and the annual financial impact (AFI) during its operation. The excessive infiltration through the building envelope has the most significant impact with the highest prevalence, AEI and AFI. Air-duct leakage has the second-largest energy impact, which causes higher energy use for both heating and cooling. As incorrect HVAC on/off modes, inappropriate setpoints/thermostat schedules, and zone temperature sensor bias, three other building operating faults are also among the 20 top faults in terms of energy and financial impact. In addition, seven out of the 20 top-priority faults occur in vapor compression systems, such as air-conditioning, heat pumps, and refrigeration equipment, which account for an essential part in substantial energy and financial impacts. In this thesis, faults in vapor compression systems have been studied.

Table 1.1: List of 20 top-priority faults in buildings Kim et al. [2018]

Fault	AEI, trillion Btu/yr	AFI, million \$/yr
Excessive infiltration through the building envelope	47.00	1,127
Air-duct leakage	40.92	1,047
Incorrect HVAC on/off modes	22.50	920
Nonstandard refrigerant charging	14.56	587
Inappropriate lighting schedules	13.16	393
Inappropriate set points/schedule for thermostats	12.04	492
Condenser fouling	5.35	274
Insufficient evaporator airflow	5.19	914
Inappropriate electric line voltage	3.82	355
Oversized equipment at design	3.27	90
Improper time-delay setting in occupancy sensors	2.91	87
Biased zone temperature sensor	1.90	60
Compressor flow fault	1.87	244
Economizer damper stuck at certain position	1.75	53
Fan motor degradation	1.25	128
Refrigerant liquid line restriction	1.12	133
Presence of non-condensable in refrigerant	0.98	29
Condenser fan degradation	0.43	91
Biased economizer sensor	0.18	56
Occupancy-sensor malfunction	0.05	1

Other authors also shared the same results and have highlighted energy waste caused by HVAC faults. Norford et al. [1994] showed that up to 12% of excess energy consumption could come from HVAC equipment, which does not operate as specified. Roth et al. [2004] and Katipamula and Brambley [2005] found that degraded equipment wastes an estimated 15% to 30% of heating and cooling energy in commercial buildings. Based on those studies, we can assume that the energy consumption in the building will constantly increase if we do not face this challenge. This raised a high demand for studying about HVAC faults to meet the requirement of energy consumption in buildings; for example, the primary energy consumption of the new residential building in the French H2b zone cannot exceed 50 kWh/m²/year [CSTB, 2012].

1.2 Heating and cooling systems, heat pumps

According to the annual report of IEA [2019] about the energy demand in residential buildings, among the energy demand of building, heating and cooling demands account for important part. Fig.1.1 shows the share of residential energy consumption by end use in IEA countries in 2017.

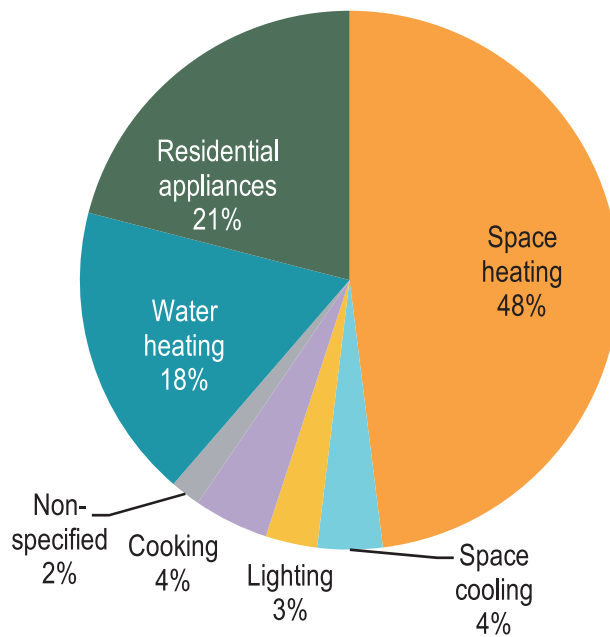


Figure 1.1: Share of residential energy consumption by end use in IEA countries in 2017 [IEA, 2019]

Over half (52%) of residential building energy consumption is accounted essentially from heating and cooling, followed by the appliances by 21% and domestic hot water by 18%. We focus, therefore, on the fault of heating systems in this research. Among heating systems, heat pumps provide an efficient and sustainable solution for heating and cooling compared to other heating systems. Replacing the oil, gas boiler, and pure electrical heater, the heat pump system has cut the global CO₂ emissions considerably. According to European Heat Pump Association (EHPA), based on 11.8 million heat pumps installed in Europe from 2005 to 2018, a reduction of 32.8 Mton of CO₂ emissions is estimated [Nowak, 2019]. About 75% of the energy used in heat pumps is renewable, whereas 25% of the energy is generated by electricity. If the electricity is generated by renewables (PV, wind, hydro), the heat pump is 100% renewable and CO₂-neutral. Electrically driven heat pumps are considered key in the energy transition.

Additionally, Bettgenhauser et al. [2013] predicted that the CO₂ equivalent emissions would be reduced by 40% if 50% of all new buildings and 30% of retrofitted buildings are equipped with heat pumps in 2030. Furthermore, regarding energy efficiency, a heat pump transfers the heat from the environment (air, water, or ground) to provide heat for space heating/cooling and water heating. For each kW of electricity consumed by a heat pump, about 3kW (or higher) of thermal energy is generated, for example. This corresponds to a 300% efficiency, which is higher than direct electric heating, condensing gas/oil boiler, and conventional gas/oil boiler of 100% efficiency, 90-96% efficiency and 70-80% efficiency, respectively. With its efficiency, heat pumps are encouraged to use in buildings and other sectors. Indeed, recent years have shown strong growth in the international heat pump market. The EU market is expanding quickly, with around 1.3 million households purchasing a

heat pump in 2018 (12% annual average growth since 2015). Indeed, France has a leading position in heat pump sales for years in Europe, followed by Italy and Spain [IEA, 2019]. They are responsible for nearly half of all sales in the European Union. Concerning the residential sector, almost 20 million households purchased heat pumps in 2019, accounting for 5% of global building heating demand. It is predictably increased to 22.1% in 2030 [Abergel, 2020].

Besides, among three types of heat pumps, based on the energy sources as air source, water source, and ground source, the air source heat pumps (ASHP) are found commonly in Europe. Fig.1.2 shows the share of heat pump sales in Europe in 2013. The heat pump types are explained in Annexes B.

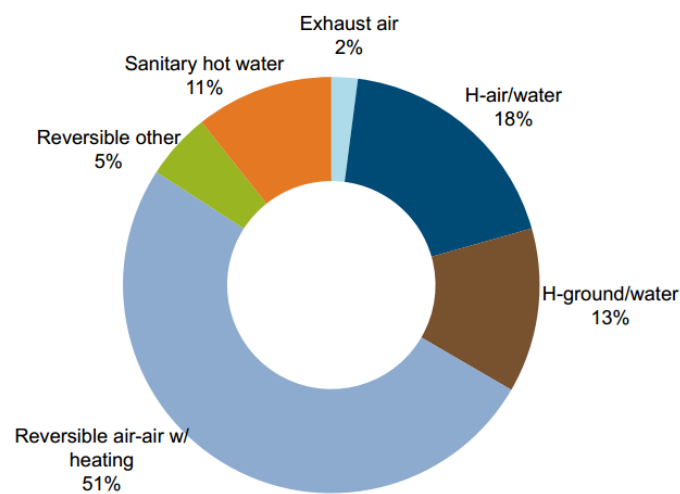


Figure 1.2: Split of sales by product category in EU-21, 2013 [EHPA, 2014]

As we can see from Fig.1.2, the ASHP accounted for approximately 70% of total heat pump sales in Europe in 2013, of which 51% is the air-to-air heat pumps. They have become more widespread in recent years, for example the heat pump sales in France which is presented in Fig.1.3.

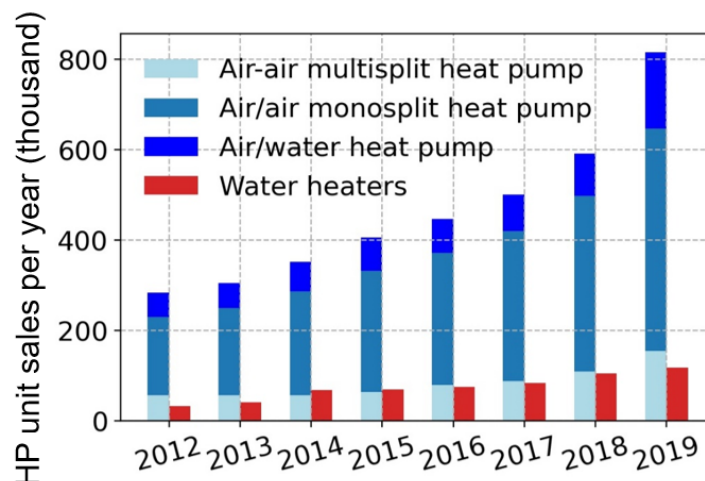


Figure 1.3: Sales of aerothermal heat pumps and water heaters in France [Deboyser, 2020]

As can be seen from Fig.1.3, air-to-air heat pumps have dominated French heat pump sales. 650,000 air-to-air heat pump units sold in 2019 represent around 80% of heat pump sales in the French market. On the one hand, intended to replace older boilers quickly, "Coup de Pouce Chauffage", implemented by the French government in January 2019, has strongly pushed the heat pump market. On the other hand, air-to-air heat pumps are cheaper and easier to install than others. With the majority of air-to-air heat pump sales of the global sales in residential buildings, we will focus primarily on air-to-air heat pumps in this research.

1.3 Importance of heat pump faults

The faults of heat pumps have been studied extensively since then. According to a survey from Madani and Roccatello [2014] in several heat pump manufacturers, 37000 heat pump fault reports during the warranty period are collected and treated. They are related to the most recent heat pump models during the period from 2010 to 2012. These faults are categorized by different fault types related to heat pump units as faulty components or heating systems as control, electronics, and temperature sensors. For example, Fig.1.4 shows the share of air-to-air heat pump faults.

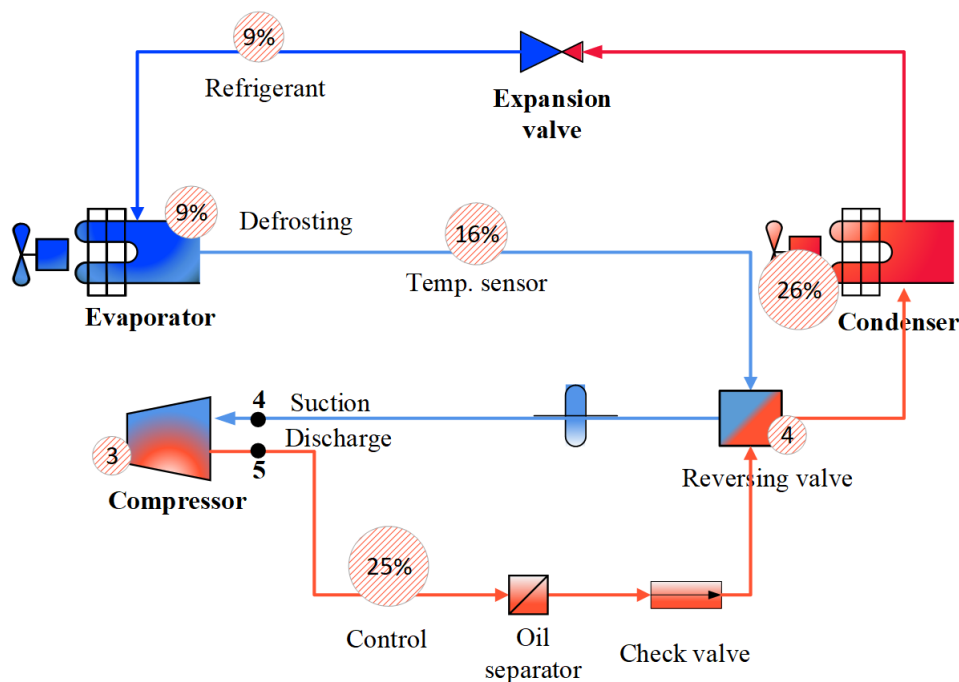


Figure 1.4: The share of different faults in air-to-air heat pumps reported from manufacturers [Madani and Roccatello, 2014]

As can be seen from Fig.1.4, faults such as refrigerant leakage, fan, compressor, valve are related to the heat pump unit; others are related to the heating system as control, electronics, sensors (92%, which are presented in Fig.1.4), and others (8%). These faults can be results along the building lifecycle, which can come from the design process, installation, operation, and maintenance. Those lead to significant degradation of heat pump performance.

Many approaches are proposed to study the heat pump faults with different concerns. First of all, some research learned about heat pump faults to improve the heat pump design. The frequent problems are no heat balance, bad dimension of the pipe diameters, heat exchanger surfaces, wrong material choices, etc. As a result, an undersized heat pump will not supply an adequate energy requirement. In contrast, if a heat pump is too large, the system will use more energy than necessary, increasing running costs and losing efficiency. The European standard NF-EN 14511 is released regarding the heat pump design, which contains specific requirements for nominal and application conditions. The heat pump can be well-designed according to the building type, energy use, and energy demand. Besides, new heat pump designs with high technology have been studied and applied for years, for example, optimized heat exchanger design [Kim et al., 2020], variable speed capacity in compressors [Madani et al., 2011], oil free compressor technologies [Schiffmann and Favrat, 2009], special expansion solutions [Elbel and Hrnjak, 2008; Mader et al., 2010], different cycle layouts [Elbel and Hrnjak, 2004], improved refrigerant flow [Devotta, 1995; Maddah et al., 2020; Xiao et al., 2020].

Secondly, some authors have studied the heat pump faults during the installation and maintenance phase to minimize the installation errors, reduce significant damages, and avoid the overall heat pump performance deterioration. Davis and Robison [2008] monitored seven new high-efficiency residential heat pumps. They diagnosed several installation errors, including a malfunctioning TXV, no heat pump thermostat installed, incorrect indoor unit installed, and incorrect control wiring preventing proper system staging. The authors reported that once the problems were repaired, the systems performed at the expected levels. Another example, Mowris et al. [2004], reported on field measurements of refrigerant charge and airflow. Over three years, 4168 new and existing split heat pumps were tested. The measurements showed that 72% of the tested units had improper refrigerant charge, and 44% had improper airflow. Approximately a 20% efficiency gain was measured after refrigerant charge and airflow were corrected. Besides, Hourahan and Baxter [2015] researched the impact of installation faults on heat pump performance in residential. Faults have a significant increase in energy use. Concerning the refrigerant, the energy use increases 20% at the 30% undercharge. It also increases around 10% to 16% at the 30% overcharge of refrigerant, regardless of the climate and building type. As can be seen from these examples, installation and maintenance play an important role in heat pump performance. To ensure the heat pump efficiency, it requires a proper installation from the indoor unit, outdoor unit, the piping connection between two units, the security functions, defrost system, the leak/pressure test, temperature set point, the refrigerant charge, fan rotation direction of the heat exchanger, sealing and filling of the refrigerant circuit, the lubrication, the electric connection, and voltage supply [AQC, 2019]. Besides, the maintenance should be inspected annually about the tightness of the refrigeration circuit, the bubble control at the sight glass, the cleanliness of the aerualic circuits, heat exchangers and air filters, and the setpoint values. The best service time is at the end of the cooling season before start-

ing the next heating season. Overall, technician competence is essential in installation and maintenance to maintain the initial heat pump performance.

Last but not least, many studies have been concerned about heat pump controls to detect performance degradation during operation, support the maintenance process, and improve the heat pump performance and efficiency. Fault detection and diagnostic (FDD) methods are studied and developed rapidly in recent years. [Kim and Kim, 2005] developed a rule-based FDD model to detect compressor fault, evaporator fault, refrigerant leak, and condenser fault in constant speed and variable speed vapor compression systems. Kim et al. [2008] adopted eight fault detection methods to detect compressor fault, fluid flow rate fault, refrigerant fault, and liquid line fault in a residential heat pump. [Choi et al., 2012] developed an algorithm to determine the refrigerant charge amount of a heat pump using the degree of subcooling. Gasche et al. [2012] developed a non-isothermal two-phase algorithm to detect refrigerant leakage in a compressor. Those FDD algorithms were used to ensure heat pumps perform as designed throughout their lifetime.

As can be seen from the above analysis, numerous research about the new designs, developed equipment, optimization, model predictive controller, etc., have been studied in order to improve heat pump performance, its energy efficiency and to meet the building energy demand and occupant's comfort. A careful reader may observe that each paper presented in the previous paragraph typically focused most on the method of how to improve the heat pump performance. Few studies systematically evaluated the impact of faults on heat pump measurements over a wide range of operating conditions. In the author's opinion, there is still a lack of a global view on heat pump performance in practice during its operation.

As the heat pump is well-designed and the entire installation is valid, the heat pump performance is still not guaranteed. It depends as well on the environmental conditions, energy demand, etc. During its operation, many operating faults can occur. It could be soft faults and hard faults. Soft faults progress undetectably overtime during system operation until they are significant, which leads to a premature failure of components, a loss in comfort, or excessive energy consumption. They could be, for example, dirty filters, dirty coils, refrigerant leakage, etc. These faults result in degraded heat pump performance, energy waste, and shortening equipment life.

In contrast, hard faults happen accidentally without any warning. They can be compressor failure, power supply, wires, and electrical faults. They will stop the machine from working; consequently, heat pump performance cannot be evaluated in these cases. The occurrence of operating faults may affect one or more components of the equipment. This would damage the whole system. Yoon et al. [2011] evaluated an air-to-air heat pump equipped with a thermostatic expansion valve (TXV) under different singly imposed operating faults in environmental chambers. Observations were made during heating and cooling mode. They identified sensitive and insensitive features related to each fault under the heating or cooling mode. The authors concluded that evaporator fouling and condenser fouling caused the most significant performance degradation. Du et al. [2016] has studied a split residential

heat pump in the cooling mode under controlled laboratory conditions. They used different types of expansion valves, compressors, and refrigerants to evaluate some common faults. Their analysis showed that the fault intensities above 15% lead to a considerable decrease in the COP value. The author also cited other publications as Kim et al. [2009] and Cho et al. [2014], which reported similar results. Few studies mentioned the impact of the heat pump operating faults on the residential building, increasing heating and cooling consumption and leading to inadequate thermal comfort for users. Hence, it would be essential to analyze the heat pump operating faults and their impacts on heating and cooling consumption in the building. With this result, we can better evaluate the building energy performance under the operating fault impacts. Then, we can compare it to the threshold of building energy consumption from French building thermal regulation RT2012, limiting the primary energy consumption of the new residential building in France H2b zone to about 50 kWh/m²/year.

Comparing to other fault types, for example, design faults, installation, and maintenance faults, the operating faults are more difficult to control. They randomly appear during normal operations, progress undetectably over time, and affect heat pump performance. However, they have not been considered yet in the design process. Most building simulation tools such as EnergyPlus, TRNSYS, eQuest, COMETH, Buildings, etc., cannot assess degraded performance because of operating faults. These current simulation tools assume that HVAC equipment, particularly heat pumps, performs as rated. Therefore, there is still a need to develop a method to model those faults in design and associate them with a building simulation model. With this approach, we describe the operation of HVAC systems, estimate the system performance and evaluate the causes and consequences of faults in lower levels during the building's lifecycle, for example, from the component level to the system and the entire building.

1.4 Objectives

Despite the huge contribution of heat pump systems in saving energy and cutting global emissions, there is still a potential to improve heat pump efficiency and reliability during its life cycle, particularly during its operation. This research potentially supports assessing the building performance under the heat pump operating faults for new and existing buildings. As can be seen from Table.1.1, among seven out of the 20 top-priority faults that occur in vapor compression systems such as heat pump, nonstandard charging, condenser, and evaporator fouling are the most prominent faults, which have a significant impact on energy consumption. Besides, based on the field data about the service frequency, Breuker and Braun [1998] noted that refrigerant leakage occurs most frequently, followed by the condenser, air handling, evaporator, and compressor faults. Hence, three faults, refrigerant leakage, condenser, and evaporator fouling, which evolve undetectably over time until they start to create serious comfort problems, are considered in this study. To integrate these operating faults into the design process, we propose a methodology that allows us to describe

the evolution of each operating fault and helps us to analyze their impacts on heat pump performance. Operating faults will occur based on the experimental results. We apply a probability notion to take into account different working cases and generalize the fault occurrence model. Then, these various fault occurrence will be regulated by a Petri net. This method drives the occurrence order of each fault, and the combination along the building lifecycle. When operating fault occurs or evolves to a higher level, the Petri net applies this new fault level in the heat pump model, which modified the heat pump performance. Then, Petri net will transfer these new values to a building energy simulation, particularly COMETH, to calculate the annual energy consumption. This method should be developed and tested for a selection of competing technologies. In order to cover all aspects with the above objectives, this dissertation is divided into three chapters, which are described as follows.

Chapter 2 - State of art: This chapter will carry out the state-of-the-art of heat pump systems with their technology. Then, operating faults will be analyzed to show their causes and their consequences with different heat pump models. As mentioned before, operating faults will develop in times; therefore, the fault occurrence models are presented. This part introduces the currently available fault modeling methods, particularly the Petri net model, which shows most of the advantages for the study requirements.

Chapter 3 - Operating fault impact on heat pump performance: This chapter presents two approaches for heat pump modeling, integrating the operating faults: a refrigerant cycle model, and an empirical model from experience. We fix separately each operating fault into this refrigerant cycle model with different fault levels in different temperature conditions. The results are compared to the experimental results, and we analyze their impacts on heat pump performance. Since many operating faults can occur at the same time during heat pump life cycle, we then, combine different operating faults with different fault ratios in order to approach the heat pump performance in reality. Finally, the impact of different fault combinations on heat pump performance are analyzed.

Chapter 4 - Dynamic evolution of coupled building and heat pump simulation taking into account operating faults: This chapter presents heat pump modeling in building energy simulation COMETH, integrating the operating faults. A case study of a residential building in Paris is presented. Different scenarios of operating faults are presented. First of all, a single fault with its evolution during the building simulations is simulated. Additionally, the impact of two and three simultaneous operating faults on the heat pump is considered to study. The Petri net is used in this dynamic fault modeling in order to regulate the fault occurrence in time. It allows finding the variations of the energy consumptions according to the operating faults in the exploitation phase. By analyzing the results, we can evaluate the building energy consumption according to the French building thermal regulation RT2012. We can conclude the system performance and the impact of the operating faults during a life cycle of a heat pump, 15 years in our study.

The results bring observations and generate new issues to be examined. In the **Conclu-**

sions and perspectives, we will draw the highlight of thesis works and present a future outlooks. The latest issues and new hypotheses create the necessity for a new conceptual model and a new investigation.

Chapter 2

State of the art

This chapter will carry out the state-of-the-art of heat pump systems with their technology. Then, operating faults will be analyzed to show their causes and their consequences with different heat pump models. As mentioned before, operating faults will develop in times; therefore, the fault occurrence models are presented. This part introduces the currently available fault modeling methods, particularly the Petri net model, which shows most of the advantages for the study requirements.

2.1 Description of heat pump technology

In order to identify the heat pump operating faults, this section gives an overview of the theoretical heat pump operation.

2.1.1 Heat pump components

The first functioning heat pump was built in 1856 and was developed in the 1930s. It has remained the basic design for nearly a century. In this part, we will focus on the vapor compression heat pump cycle, which is presented in Fig.2.1.

Fig.2.1 shows heat pump cycle diagram, which contains four principal components: the evaporator, the compressor, the condenser, and the expansion valve. Additionally, other parts are mentioned as the suction accumulator, the pressure switch, the reversing valve, oil separator, check valve, dehydrator, and sight glass, which allow the system to operate efficiently.

Heat exchangers

The heat exchanger consists of an evaporator and a condenser. The primary function of the evaporator is to increase the temperature of the liquid refrigerant and change it into the gas state. In contrast, the condenser delivers heat for space heating and transforms the refrigerant from gas to a liquid state. In a reversible air-to-air heat pump, the heat exchanger is a tubular one. It is usually made of copper pipes whose length cannot be changed. Also,

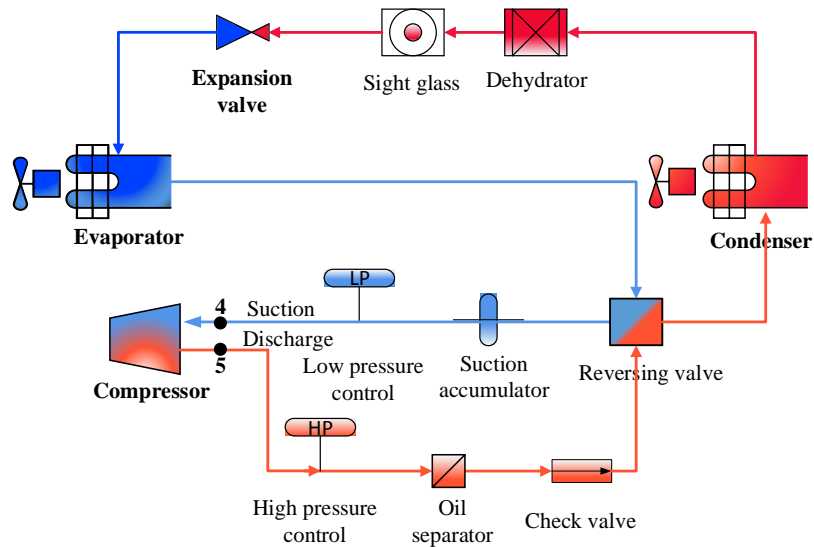


Figure 2.1: Simplified heat pump diagram

it is equipped with a coaxial lamella design matched to the heat source, with the ventilator ensuring air input. Its design makes sure that heat energy must be led directly into the exchangers.

Compressor

The compressor is the heart of the heat pump. Its task is to suck the fluid refrigerant, secondly compress it to high temperature and high pressure, and lastly deliver it to the condenser where the heat is released. Fig.2.2 shows different types of compressor, which are used for heat pump, for example, reciprocating, scroll, rotary screw and centrifugal compressor.

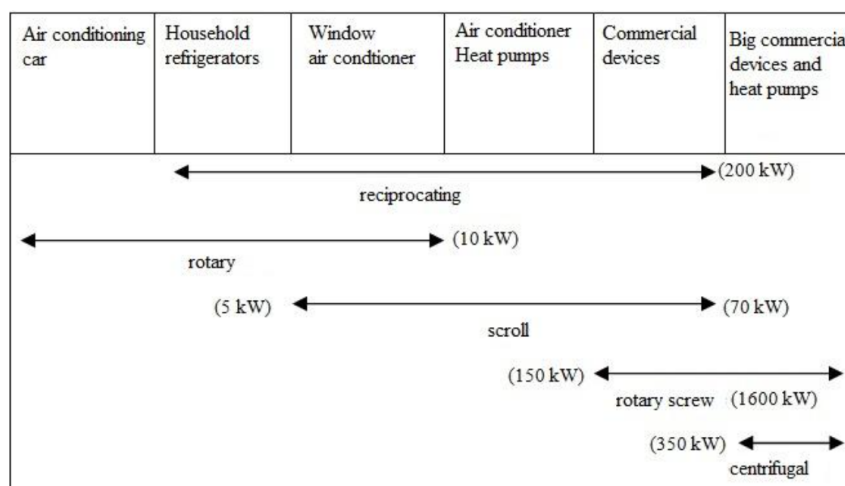


Figure 2.2: Usage scopes of various compressor types [Guzda and Szmolke, 2016]

For the residential applications, the scroll or reciprocating compressors are the most commonly found in domestic heat pumps. Based on the compressor speed, heat pump is divided into inverter system and fixed speed system. A fixed speed system is a system where

a compressor in the outdoor unit operates at a constant speed. In contrast, an inverter system varies motor speed in order to maintain a constant demanding temperature. Inverter systems are more commonly installed nowadays as they are approximately 30-45% more efficient than fixed speed systems [Staffell et al., 2012]. They achieve the set temperature more quickly than fixed speed systems.

Expansion valve

The expansion valve creates a strong pressure drop, so it lowers the pressure and the temperature of refrigerant. Then, the refrigerant state becomes partially a vaporized. There are various designs of expansion valves, for example the fixed orifice expansion valve, the thermostatic expansion valve (TXV - Fig.2.3), and the electronic expansion valve (EEV). If conditions never change as the load on the system is constant and the ambient temperature remains steady, a fixed orifice expansion valve is ideal. However, static conditions are not realistic in real condition, and we do not consider fixed orifice expansion valve in this study.

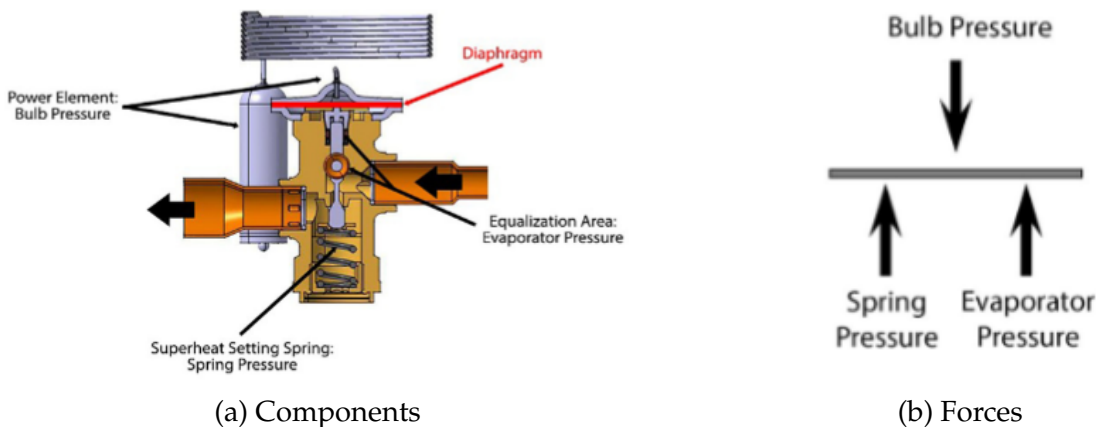


Figure 2.3: Thermostatic expansion valve [Danfoss, 2017]

Fig.2.3a presents a construction of TXV, which contains a diaphragm, a power element, a setting string and an orifice. There are three different forces in a TXV, as bulb pressure, spring pressure, and evaporator pressure, which is showed in the Fig.2.3b. Bulb pressure (P_1) comes from the bulb that is mounted at the outlet of the evaporator. The bulb senses the suction temperature. If the suction temperature increases, the bulb drives the diaphragm down. Spring pressure (P_2) is constant and pushes up against the diaphragm. Evaporator pressure (P_3) comes from the evaporator load on the system. It pushes the diaphragm up when the suction pressure increases. This varies according to different operating conditions, such as room temperature changes. Based on the balance between these three pressures, the valve will open or close to precisely control the flow of liquid refrigerant into the evaporator.

Reversing valve

The reversing valve controls the direction of flow of the refrigerant in the heat pump. It changes the heat pump from heating to cooling mode or vice versa. Fig.2.4 shows how the

reversing valve works in both modes.

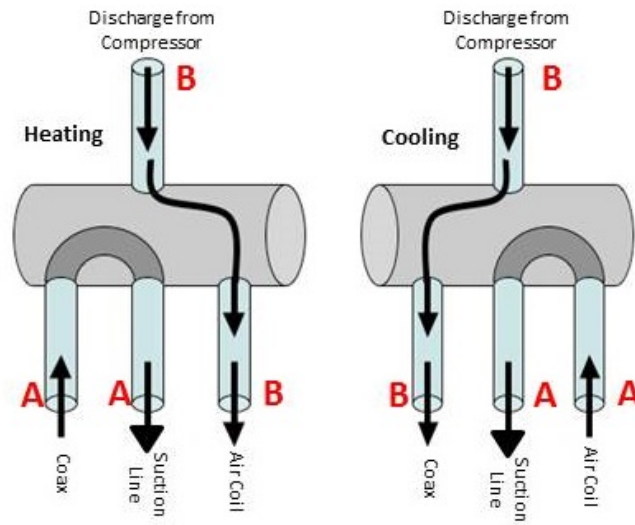


Figure 2.4: A reversing valve

As can be seen in Fig.2.4, a reversing valve has two switch positions. There is no intermediate position. It has four pipe connections, three of them on one side and the fourth on the opposite side. The middle one of the three connectors is permanently on the suction side, and the single connector on the opposite side is permanently on the high-pressure side. Since the remaining two may be on either the suction or the high-pressure side, depending on how the unit is currently switched. A reversing valve also possesses a solenoid pilot valve with a coil that can be powered to change the direction of the flow of the refrigerant.

Other components

To allow the system to operate efficiently, other parts such as the suction accumulator, the pressure switch, oil separator, check valve, dehydrator, and sight glass will be mentioned following.

- Accumulators are necessary for the heat pump to protect the compressor from liquid slugging.
- Pressure switches control the pressure on the low and high-pressure sides in the refrigerant circulation. When the refrigerant pressure has been reached on its limit, they will close an electrical contact.
- The oil loop ensures the lubrication of the compressor's moving mechanical parts. A small amount of oil leaves the compressor with the refrigerant gas. The oil separator removes oil from the compressor's discharge refrigerant and then returns it to its crankcase. This helps to avoid oil circulation throughout the system.

- A check valve located close to the compressor outlet ensures the refrigerant flow is not inverted when the compressor turns off. It avoids liquid from the condenser in the compressor.
- A dehydrator located on the liquid line before the TXV, removes moisture, acid, sludge, and particles from the circulation. It can therefore prevent possible ice formation at the expansion valve. If there are still impurities on the liquid line, the sight glass, which is located close to the dehydrator, will light up to show a risk for circulation.

2.1.2 Refrigerant and regulation evolution

The refrigerant is a chemical compound, which is responsible for the heat exchange from the evaporator to the condenser. It absorbs heat from the evaporator and releases it to the condenser while changing from a liquid state to a gas state and back. The choice of the refrigerant has a great impact on the efficiency of the heat pump system, which depends on several criteria, such as thermodynamic properties (pressure, critical temperature), energy efficiency, and environmental impact. Firstly, for some refrigerants at high temperatures, its pressures become too high, which can stop the heat pump work. Low pressure has another disadvantage that the volume needs to be increased. Secondly, above a certain temperature, a refrigerant reaches its supercritical area where the fluid and gaseous phase of the refrigerant can not be distinguished. Last but not least, in case of leakage, most refrigerants impact strongly to the greenhouse effect.

Over the last decades, researchers investigated the various refrigerants in heat pump uses to improve the performance of heat pump thermodynamic cycles and reduce their negative impacts on the environment, particularly from refrigerant leakage. At the beginning of the twentieth century, the refrigeration industry was restricted to ammonia, carbon dioxide, sulfur dioxide, and water for domestic appliances. Then, the introduction of R12 by Thomas Midgley in 1930 about non-flammable and non-toxic refrigerants kicked off the vast use of CFCs and, later on, HCFCs. In 1973, Sherwood Rowland and Mario Molina presented that CFCs would deplete the ozone layer. This led to the international agreement to phase out the use of CFCs in the Montreal Protocol 1987. Also, later on in the amendments, they include the reduction of HCFCs in heat pump applications. Last but not least, HFC is introduced to the market. Different refrigerant types are showed below.

- Natural refrigerant: Inorganic refrigerant such as CO₂, SF₆, air, water or nitrogen compounds such as Ammonia NH₃. Generally they have negligible global environment drawbacks, but some of them are flammable or toxic.
- CFC (Chlorofluorocarbons): All hydrogen atoms in the molecule are replaced with chlorine and fluorine in various ratios. High chemical stability has proved to be a great disadvantage on the ozone layer. They are prohibited for heat pumps, for exemple R11, R12, R113, R502 and others.

- HCFC (Hydrochlorofluorocarbons): Not all hydrogen atoms are replaced which causes reduced risk of ozone layer. However, these refrigerants are not used at present, as R21, R22.
- HFC (hydrofluorocarbons): The refrigerant contains only fluorine. They do not pose a risk for ozone layer, but they contribute to global warming, for example, R134A, R407C and R410A, R32.

Carl and Marianne [1992] showed that the refrigerants R123 and R134A can replace many CFC refrigerants. Devotta [1995] shared the same results, which showed that the refrigerant R134A is a good replacement fluid. Other authors [Wang, 2014; Fang et al., 2017; Yang and Nalbandian, 2018] compared refrigerants R134A and R1234yf. The results showed that a heat pump optimized with R1234yf might have lower performance than a heat pump optimized with R134A because the thermal conductivity of R134A is higher than that of R1234yf.

Besides, R410A offers excellent performance with no influence on ozone depletion and has been a dominant refrigerant in most domestic heat pumps. However, R410A has a significant impact on the climate due to its high GWP. Thus, the heat pump industry has been focusing on the development of R410A substitutes. R32 represents a promising substitute for residential and light commercial air conditioning and heat pump systems, among valuable alternatives. Its GWP is around 675 (32% of that of R410A) [Fizel, 2019] and has a zero ozone depletion potential (ODP). Its saturation curve is very close to that of R410A, allowing the use of most of the components, being the sizing very close, especially for the compressor. The heat pump coefficient of performance using R32 was increased up to 10% concerning the R410A case when operating under the same conditions [Xu et al., 2013]. The potential reduction of the environmental impact is related to the lower GWP and the performance improvement compared to the other options. That is a reason why R32 is used these days popularly in heat pump applications. According to AFPAC [2020], 60% of the air-to-air heat pumps on the market use R32, against 25% in 2018.

Along with those scientific works and high heat pump sales in the market, public authorities have released different policies about refrigerant uses in residential, for example, the F-Gas. It highlighted three aspects as follows.

- The reduction of direct emissions: by controlling the installation as well as carrying out periodic inspections according to the quantity of fluid used
- The restricted use of certain high global warming potential (GWP) refrigerants in certain types of installations: for example, restriction of R410A in installations containing less than 3 kg of fluid as from 1st January 2025
- The limit of the number of TEqCO₂ sold on the market: by promoting the use of low-GWP HFCs, such as R32 for small and medium power installations, or HFOs for centralized installations of higher power

2.1.3 Heat transfer mechanism

In this part, we describe and analyze the heat transfer process of a reversible air-to-air heat pump, which is shown in Fig.2.5. It shows the refrigerant working cycle in heating mode (Fig.2.5a) and cooling mode (Fig.2.5b).

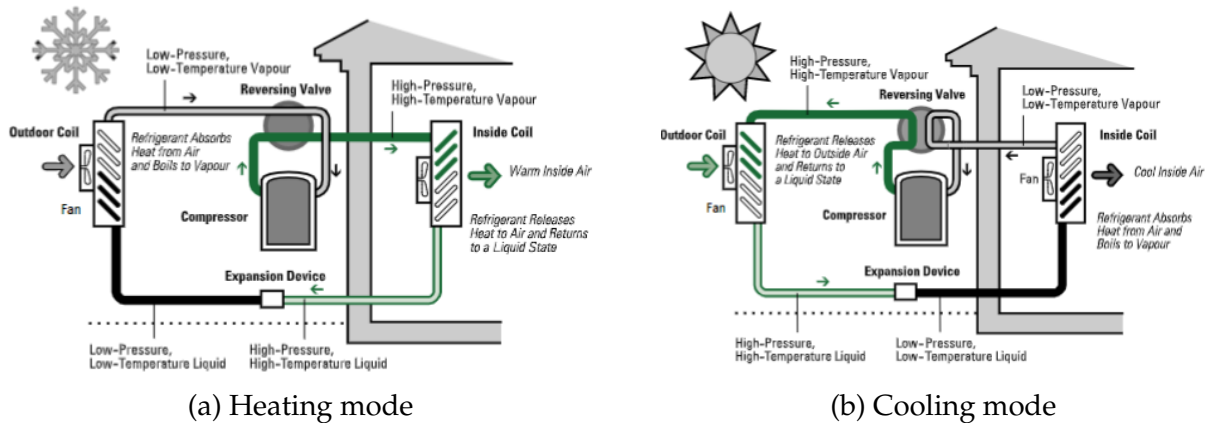


Figure 2.5: A reversible air-to-air heat pump diagram in different working modes

The heating cycle

During the heating mode (Fig.2.5a), heat is taken from outdoor air and released indoors. First, the liquid refrigerant passes through the expansion device, changing to a low-pressure liquid/vapor mixture. It then goes to the outdoor coil, which acts as the evaporator coil. Since the refrigerant temperature in the evaporator is less than the atmospheric temperature, it tends to absorb the heat from the air loop and evaporate progressively, becoming a low-temperature vapor. This vapor passes through the reversing valve to the accumulator, which collects any remaining liquid before the vapor enters the compressor. The vapor is then compressed to high pressure and high temperature. Finally, the reversing valve sends the gas, which is now hot, to the indoor coil, which acts as the condenser. The high temperature allows the condenser coil to deliver the heat to the air loop, causing the refrigerant to condense into a liquid. This liquid returns to the expansion device, and the cycle is repeated.

If the outdoor temperature falls to near or below freezing when the heat pump is operating in the heating mode, moisture in the air passing over the outside coil will condense and freeze on it. This frost build-up decreases the efficiency of the coil. It reduces the heat transfer to the refrigerant. So that the frost must be removed, to do this, the heat pump will switch into the cooling mode by switching the reversing valve. This sends hot gas to the outdoor coil to melt the frost. At the same time, the outdoor fan, which usually blows cold air over the coil, is shut off.

The cooling cycle

During the cooling mode (Fig.2.5b), the process is similar to the heating mode. However, the unit takes heat out of the indoor air and rejects it outdoors. Also, the heat pump dehu-

midifies the indoor air. Moisture in the air passing over the indoor coil condenses on the coil's surface and is collected at the bottom of the coil.

From the above analysis, we can see that heat pumps operate on the principle of heat transfer. It tends to move from a location with a higher temperature to a location with a lower temperature. In the next part, we will discuss how to model an air-to-air heat pump in different approaches as the mathematical models, experimental models, etc.

2.2 Heat pump models without faults

The above analysis clearly shows the heat pump structure with its components, functions, and operation. This part deals with calculation method for heat pump performance, which is characterised by the coefficient of performance (*COP*) and energy efficiency ratio (*EER*). These two parameters show heat pump's efficiency in heating and cooling mode, respectively. They are determined by dividing the heating/cooling capacity of the heat pump by the electrical energy needed to run the heat pump at a specific temperature. The higher the *COP/EER* is, the more efficient the heat pump is. The calculation of heat pump performance will be presented in different modeling approaches under the nominal conditions.

Among the heat pump models found in the literature, there are two main paths for heat pump simulations. The first approach is using experimental data (empirical models). The models are obtained by calculating the heat pump performance in terms of capacity, power input and coefficient of performance to the operating conditions. Based on the experiment reference, the performance can then be interpolated during numerical simulations, or used to produce an equation-fit of the heat pump performance. The second approach, the refrigerant cycle model, uses the fundamental laws of energy - mass balance, with varying detail degree of each heat pump component and inputs collected from the manufacturer's data. These two models are presented as following.

2.2.1 Refrigerant cycle model

This part describes the principles and the equations of the heat transfer in an air-to-air heat pump. The starting point of heat-pump simulation is to describe the operation of a heat pump in terms of mathematical relationships. This is achieved by the modelling of the individual components of the heat-pump system, namely the compressor, condenser, expansion valve and evaporator. The model incorporates mass, momentum and heat-balance equations, thermodynamic and thermo-physical property relationships and heat or work transfer relationships, from where a set of mathematical equations can be derived and solved. All main influencing parameters are explained. The component sub-models, each describing the steady-state performance of the evaporator, condenser, and compressor, which is shown in a diagram of the heat pump in Fig.2.6. It shows the temperature evolution of refrigerant and air in evaporator and condenser.

This refrigerant cycle model is defined as a series of mathematical relationships to obtain

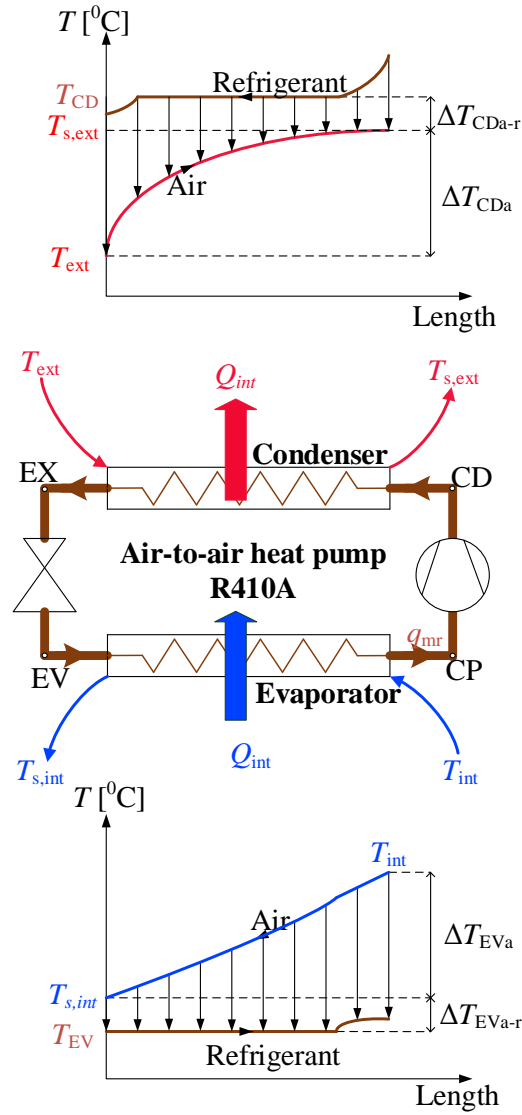


Figure 2.6: Theoretical temperature evolution of refrigerant and air in evaporator and condenser in cooling mode [Jacques et al., 1997]

the time-independent operating cycle for specified constant operation conditions. We call it the steady-state heat-pump model as well. The data input of heat pump dimension, the energy demand and the temperature working conditions are supplied.

- K : Thermal exchange coefficient of heat exchanger [$\text{W}/\text{m}^2\text{K}$]
- S : Heat exchanger surface [m^2]
- Q_{int} : Sensible supplied energy in the building zone [W]
- $T_{\text{int}}, T_{\text{ext}}$: Indoor and outdoor air temperatures [K]
- $\Delta T_{\text{EVa-r}}, \Delta T_{\text{CDa-r}}$: The temperature difference between the outlet air temperature (a) of the evaporator (EV) or condenser (CD), and the refrigerant temperature (r) respectively [K]. These two pinch temperatures are assumed as 5°C [Underwood, 2016]

There are two way to define the overall heat transfer rate Q across a given heat exchanger. On the one side, by using LMTD - logarithmic mean temperature difference from the refrigerant side and based on the heat pump design information as the thermal exchange coefficient K and heat exchanger surface S , the heat transfer rate Q is calculated as follows.

$$\begin{aligned} Q_{EV} &= K_{EV}S_{EV}LMTD_{EV} \\ Q_{CD} &= K_{CD}S_{CD}LMTD_{CD} \end{aligned} \quad (2.1)$$

LMTD is an indicator of the average temperature difference between the hot and cold fluids in a heat exchanger.

$$\begin{aligned} LMTD_{EV} &= \frac{\Delta T_{1,EV} - \Delta T_{2,EV}}{\ln(\Delta T_{1,EV}) - \ln(\Delta T_{2,EV})} \\ LMTD_{CD} &= \frac{\Delta T_{1,CD} - \Delta T_{2,CD}}{\ln(\Delta T_{1,CD}) - \ln(\Delta T_{2,CD})} \end{aligned} \quad (2.2)$$

where

- $\Delta T_{1,EV}, \Delta T_{1,CD}$: the temperature difference between hot and cold fluids at one end of the evaporator and the condenser, respectively
- $\Delta T_{2,EV}, \Delta T_{2,CD}$: the temperature difference between hot and cold fluids at the other end of the evaporator and the condenser, respectively

On the other side, the energy demand Q can be calculated from the air side of heat exchanger as following. These equations are used in case of air condensation. In other cases, the enthalpy diagram is recommended.

$$\begin{aligned} Q_{EV} &= 0.34q_{v,EV}\Delta T_{EVa} \\ Q_{CD} &= 0.34q_{v,CD}\Delta T_{CDa} \end{aligned} \quad (2.3)$$

where

- $\Delta T_{EVa}, \Delta T_{CDa}$: The air temperature drop (a) across the evaporator (EV) and the air temperature rise (a) across the condenser (CD) [K]
- $q_{v,EV}, q_{v,CD}$: The air flow rate acrossing the evaporator (EV) and the condenser (CD) respectively [m^3/h]

Based on the thermo-physical property relationships from Fig.2.6, the evaporating and condensing temperatures in the cooling mode are calculated:

$$T_{EV} = T_{\text{int}} - (\Delta T_{EVa} + \Delta T_{EVa-r}) \quad (2.4)$$

$$T_{CD} = T_{\text{ext}} + (\Delta T_{CD} + \Delta T_{CDa-r}) \quad (2.5)$$

added to the 100% vapor refrigerant, the heat would increase the temperature. The refrigerant moves from point EV_1 to point EV_2 , where the resulting refrigerant is superheated. Then, the fluid is transferred to the compressor. A pressure drop (from EV_2 to CP) is presented as the heat losses in refrigerant pipes.

The compressor is characterized by refrigerant suction (p_{EV}) and discharge (p_{CD}) conditions. The incoming temperature of the compressor, determined by the leaving temperature of the evaporator, is used as the starting point of the compressor, as shown by point CP in Fig.2.7. The compressor then increases the pressure of the refrigerant up to the discharge pressure. Compression occurs at constant entropy, also known as isentropic compression. Therefore, the intersection of the constant entropy line and the discharge pressure line will identify the final condition of the refrigerant gas leaving the compressor, as shown by point CP' in Fig.2.7. For non-isotropic compression, the high-pressure vapor must be brought to a saturated condition (point CD), where its enthalpy is calculated in function of compressor isotropic efficiency η_{CPs} as following.

$$\eta_{CPs} = \frac{h_{CD} - h_{CP}}{h_{CD'} - h_{CP}} \quad (2.6)$$

Compressor isentropic efficiency η_{CPs} varies with the compressor's type and size. A suggested value is proposed for the split residential heat pump $\eta_{CPs} = 0.8$ [Campbell, 1992]. It applies to reciprocating, scroll and rotary compressors which are the main types of compressor currently used in vapor compression heat pumps of small to medium capacity. Then, the fluid is transferred to the condenser.

The refrigerant entering the condenser is now a hot, high-pressure refrigerant gas, corresponding to the compressor discharge pressure. The condenser proceeds from right to left in the following three steps. The superheated gas cools down to saturation temperature (from CD to CD_1). Cooling takes place as heat flows from the hot refrigerant gas to the condenser cooling medium.

Next, the 100% saturated vapor at CD_1 is converted to 100% saturated liquid at CD_2 , which is transformed from the high-pressure vapor to high-pressure liquid. The condensation is performed at constant pressure and temperature, thus follows the isobars. This is the phase in which the fluid transfers the calories to the medium, which is presented as its enthalpy decreases. In an ideal condenser, no sub-cooling occurs. CD_2 is the end of the condenser. However, once the refrigerant is a fully saturated liquid, any additional heat loss results in a decrease in temperature. The 100% saturated liquid is sub-cooled from CD_2 to EX. Then, the fluid is transferred to the expansion valve (point EX).

The expansion device is the counterpart of the compressor. Similarly, the expansion device is characterized by the suction (p_{EV}) and discharge (p_{CD}) pressures. The condenser output conditions determine the input condition of the expansion device. The expansion device expands the high-pressure refrigerant gas adiabatically to a low-pressure liquid-vapor refrigerant mixture by a sudden pressure drop through an orifice. Adiabatic expansion in-

icates that there is no change in enthalpy and is characterized by a downward vertical line. The expansion valve reduces the refrigerant temperature and pressure to the evaporating temperature (point EV). The refrigerant quality has increased at the evaporator inlet. A mixture of saturated liquid and vapor goes through the evaporator.

After the characteristics of enthalpy diagrams are defined, the refrigerant mass flow rate q_{mr} and the compressor power W are calculated as follows.

- The mass flow rate of refrigerant is calculated from the sensible supplied energy entering into an evaporator:

$$q_{mr} = \frac{Q_{int}}{h_{CP} - h_{EX}} \quad (2.7)$$

- Thermal power delivered by the compressor into a refrigerant:

$$W = q_{mr}(h_{CD} - h_{CP}) \quad (2.8)$$

- The coefficient of performance COP , energy efficient ratio EER are as the ratio between the supplied energy, and the electrical power absorbed by the appliance, which includes all the auxiliaries:

$$COP/EER = \frac{Q_{int}}{W + W_{aux}} \quad (2.9)$$

Several factors affect the efficiency of a heat pump, in which auxiliary equipment is one of the most critical factors. In this study, its power is estimated at approximately 10% of energy demand [Underwood, 2016].

The amount of detail used in the model would be dependent on the simulation accuracy required. If broad trends were required, then a relatively simple model could be employed. Alternatively, if the simulation were to be used during the design of heat pump systems, where the effects of varying many design parameters are required accurately, a highly detailed simulation would be needed.

2.2.2 Empirical models

Empirical heat pump models are created based on the standard NF EN ISO/CEI 17025. This standard is mainly dedicated to testing or calibration activities and stipulates organizational quality and control requirements to guarantee the validity of the delivered results.

Full load

The heat pump performance coefficients as COP (heating mode) and EER (cooling mode) are calculated according to an introduction of a matrix. The matrix is built based on a 'core value' at full load, which corresponds to the nominal conditions according to NF EN ISO/CEI 17025 standard, and the efficiency coefficient C_{nn} , which is taken by default or

interpolated from test results. They are adapted to the operating conditions based on the approach presented in Annex D of EN 15316-4-2:2017.

Heating mode

In heating mode, the matrix of the coefficient of performance COP of the air-to-air heat pump is presented in Table 2.1. The matrix depends on the outlet temperature of the condenser fluid and the inlet temperature of the evaporator fluid. We consider as the nominal indoor T_{int} and outdoor T_{ext} temperature, respectively.

Table 2.1: The COP matrix of air-to-air heat pump in heating mode

		Priority	T_{ext}				
			-15	-7	2	7	20
T_{int}	5	5					
	10	4					
	15	2					
	20	1				COP_n	
	25	3					

Table 2.1 shows a core value (COP_n) in heating mode. It corresponds to outdoor temperature $T_{ext}=7^{\circ}C$ and indoor temperature $T_{int}=20^{\circ}C$. It must be supplied from the manufacturers or measured by experiment. Other COP values in the matrix are provided in priority order, from 1-1, 2-2 until 5-5, for example:

- First priority (1-1): $T_{ext}=7^{\circ}C$ and $T_{int}=20^{\circ}C$
- Second priority (2-2): $T_{ext}=-7^{\circ}C$ and $T_{int}=15^{\circ}C$
- Third priority (3-3): $T_{ext}=2^{\circ}C$ and $T_{int}=25^{\circ}C$
- Fourth priority (4-4): $T_{ext}=20^{\circ}C$ and $T_{int}=10^{\circ}C$
- Fifth priority (5-5): $T_{ext}=-15^{\circ}C$ and $T_{int}=5^{\circ}C$

If these above points are not supplied, they can be calculated by default as follows. The matrix is fulfilled by multiplying the core value of COP with a correction coefficient of power at full load. The correction coefficients are presented in Table 2.2 under the condition that the nominal power of a residential air-to-air heat pump is lower 100kW [CSTB, 2012].

Table 2.2: The correction coefficient of COP at full load of heat pump in heating mode

Priority	Between the indoor temperature	Between the outdoor temperature
2	$Cnn_{COP}(15,20) = 1.1$	$Cnn_{COP}(-7,7) = 0.5$
3	$Cnn_{COP}(25,20) = 0.9$	$Cnn_{COP}(2,7) = 0.8$
4	$Cnn_{COP}(10,20) = 1.2$	$Cnn_{COP}(20,7) = 1.25$
5	$Cnn_{COP}(5,20) = 1.3$	$Cnn_{COP}(-15,-7) = 0.8$

Each coefficient in Table 2.2 corresponds to the temperature conditions. For example, $Cnn_{COP}(15,20)=1.1$ is the coefficient correction at interior temperature $T_{int}=15$ comparing to

the one at $T_{int}=20$. By multiplying this coefficient Cnn to the 'core value', we can calculate the values of heat pump performance COP at full load for other operating conditions.

$$COP(T_{int}, T_{ext,core}) = Cnn_{COP}(T_{int}, T_{int,core})COP(T_{int,core}, T_{ext,core}) \quad (2.10)$$

$$COP(T_{int,core}, T_{ext}) = Cnn_{COP}(T_{ext}, T_{ext,core})COP(T_{int,core}, T_{ext,core}) \quad (2.11)$$

An example of COP calculation at indoor temperature $T_{int}=15^{\circ}\text{C}$ and outdoor temperature $T_{ext} = 7^{\circ}\text{C}$, while the core value COP at $T_{int}=20^{\circ}\text{C}$, $T_{ext} = 7^{\circ}\text{C}$ is known, is shown as below.

$$COP(15,7) = Cnn_{COP}(15,20) \times COP(20,7) = 1.1COP_n \quad (2.12)$$

Applying the Eq.2.10 and Eq.2.11, the COP matrix of air-to-air heat pump in heating mode is presented in the Table 2.3.

Table 2.3: The COP matrix of air-to-air heat pump in heating mode

		Priority	T_{ext}				
			-15	-7	2	7	20
			5	2	3	1	4
T_{int}	5	5	$0.52COP_n$	$0.65COP_n$	$1.04COP_n$	$1.3COP_n$	$1.625COP_n$
	10	4	$0.48COP_n$	$0.6COP_n$	$0.96COP_n$	$1.2COP_n$	$1.5COP_n$
	15	2	$0.44COP_n$	$0.55COP_n$	$0.88COP_n$	$1.1COP_n$	$1.375COP_n$
	20	1	$0.4COP_n$	$0.5COP_n$	$0.8COP_n$	COP_n	$1.25COP_n$
	25	3	$0.36COP_n$	$0.45COP_n$	$0.72COP_n$	$0.9COP_n$	$1.125COP_n$

Table 2.3 shows the matrix of heat pump performance at specific operating conditions. If the heat pump operates at other temperature conditions, the heat pump performance is interpolated.

Cooling mode

When the heat pump works in cooling mode, the EER matrix will be used for the building simulation. The manufacturers must supply at least a core value corresponding to outdoor temperature $T_{ext}= 35^{\circ}\text{C}$ and indoor temperature $T_{int} = 27^{\circ}\text{C}$. The other values of the matrix are fulfilled by multiplying the core value with a correction coefficient of power at full load. The correction coefficients of EER is presented in the Table 2.4.

Table 2.4: The EER matrix of air-to-air heat pump in cooling mode

		Priority	T_{ext}				
			5	15	25	35	45
			4	3	2	1	5
T_{int}	22	2	$1.44EER_n$	$1.26EER_n$	$1.08EER_n$	$0.9EER_n$	$0.72EER_n$
	27	1	$1.6EER_n$	$1.4EER_n$	$1.2EER_n$	EER_n	$0.8EER_n$
	32	3	$1.72EER_n$	$1.505EER_n$	$1.29EER_n$	$1.075EER_n$	$0.86EER_n$
	37	4	$1.84EER_n$	$1.61EER_n$	$1.38EER_n$	$1.15EER_n$	$0.92EER_n$

These two *COP* and *EER* matrices are filled once at the beginning of the hourly calculation. At each time step during the annual calculation, heat pump performance at operating points are interpolated based on these two matrices, which corresponds to the indoor T_{int} and outdoor T_{ext} temperatures. Other building simulation tools, such as EnergyPlus, TRN-SYS, eQuest, Buildings, etc., use the same principle of coefficient correction to characterize the heat pump performance. For example, EnergyPlus uses the energy input ratio correction factor in the function of temperature (EIRFT). This is an equation-fit model that resembles a black box with no heat transfer equations.

This approach hypothesizes that the thermodynamic quality of the process stays constant over the whole operating range. The thermodynamic quality of a process is expressed by the efficiency coefficient C_{nn} which is the ratio between the real *COP* of the process and an ideal Carnot *COP*. However, in real processes, the efficiency does not stay constant over the entire operating range. Therefore, the extrapolation of test values provides the best results only near the test points. If more test points are available, closer is the performance to the real results of the heat pump. If only one test value ('core value') is available, the *COP* and *EER* matrix are built from this unique reference value corresponding to nominal conditions of the source temperatures of heat pump types. If additional test data are available, the default coefficients can be replaced by heat pump-specific coefficients. Concerning the simulation process, these matrices are filled once at the beginning of the calculation. During the calculation, at each time step, the coefficient of performance *COP* and *EER* at the actual temperatures are obtained by the linear interpolation method.

Part load

In dynamic conditions, the load, in reality, is mostly at a substantially lower level than the design load. If the heat pump always cycles with the design load, this behavior leads to losses during the stand-by and start-up phases of the equipment, thus reducing its energy performance. French thermal regulation RT2012, therefore, considers the part-load calculation of the heat pump, which is presented as follows.

To take into account part-load operating, the full load performance is corrected. Commonly, the coefficient of performance (*COP* and *EER*) is estimated at part load using a correction parameter PLF, partial load factor, which represents the ratio between the *COP* at partial load and the *COP* at full load:

$$PLF = \frac{COP}{COP_n} \quad (2.13)$$

The heat pump's performance is written in the NF-EN 14825 standard, which is described as following. The NF-EN 14825 standard allows using the equation with a default

value of the energy efficiency $C_c=0.9$.

$$PLF = \frac{COP}{COP_n} = PLF_{min} \frac{\frac{PLR}{PLR_{min}}}{\left(\frac{PLR}{PLR_{min}} - 1\right)C_c + 1} \quad (2.14)$$

where:

- PLR : the part load ratio. It is the ratio between the thermal power used and the thermal power at full load.

$$PLR = \frac{Q_c}{Q_{c,n}} \quad (2.15)$$

- $Q_c, Q_{c,n}$: the thermal power supplied and the thermal power supplied defined for heating and cooling nominal conditions.
- PLR_{min} : The minimum thermal load rate. Below the minimum load rate, the heat pump operates on On/Off state.

The performance of heat pumps at part-load conditions is not given in manufacturers' catalogs. The full-load characteristics with manufacturer's data are used for a single operating point, the part-load characteristics being the default values.

The heat pump is divided into an inverter system and fixed speed system based on the compressor speed. A fixed speed system is a system where a compressor in the outdoor unit operates constantly. In contrast, an inverter system varies motor speed to maintain a constant demanding temperature.

- In the case that heat pump operates on On/Off state where a compressor in the outdoor unit operates at a constant speed. We have $PLF_{min} = 100\%$ and $PLR_{min} = 100\%$. The equation of PLR is as follows.

$$PLF = \frac{COP}{COP_n} = \frac{PLR}{(PLR - 1)C_c + 1} \quad (2.16)$$

- In contrast, for an inverter heat pump, it varies motor speed in order to maintain a constant demanding temperature. By default, values obtained from tests, PLR_{min} is taken equal to 40% and PLR_{min} to 100%

$$PLF = \frac{COP}{COP_n} = \frac{PLR}{(PLR - 0.4)C_c + 0.4} \quad (2.17)$$

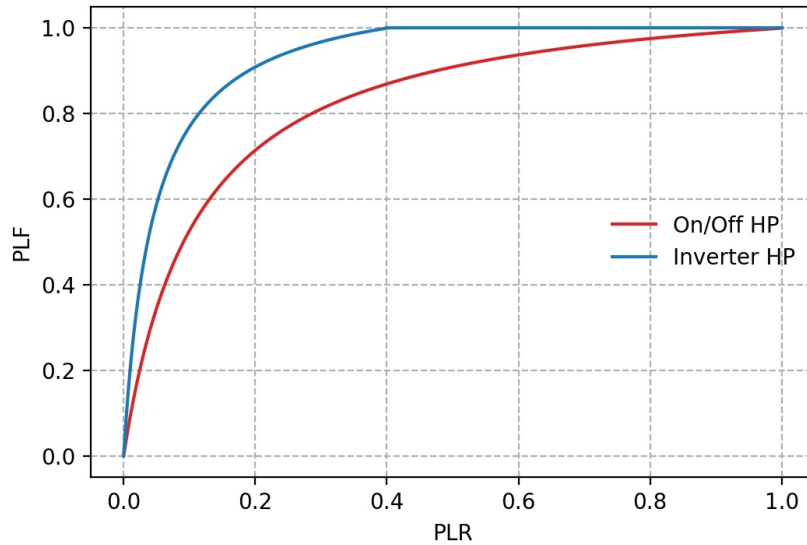


Figure 2.8: Representation of part-load behavior in different types of heat pump

Fig.2.8 shows the part-load behavior of the heat pump with two different modes of compressor: inverter and On/Off. As can be seen, the partial load factor PLF of the inverter heat pump has consistently higher performance than one of the on/off the heat pump. They change the rotational speed of the compressor by a frequency inverter to reduce the efficiency losses caused by the short cycling. This kind of regulation affects the achieved *COP* of the heat pump. It also reduces the range of the on/off regulation but does not eliminate it. Below the minimum power, for example, $PLR = 40\%$, the heat pump operates on an on/Off state.

2.3 Heat pump operating faults

We analyzed the heat pump components and their operation in nominal working conditions in the last two parts, with some heat pump models to characterize its behaviors. If an operating fault occurs, it will deviate the system with its specified behavior and consequently impact the system performance. In this part, we consider analyzing their causes, consequences, fault evolution in time, following by the fault model.

As can be seen from the top 20 priority faults in buildings Kim et al. [2018], vapor compression system faults play an essential part. Among seven out of 20 faults, refrigerant leakage, condenser, and evaporator fouling are the most prominent faults, significantly impacting energy consumption. Downey and Proctor [2002] shared the same findings based on collected data from over 13,000 air conditioners in residential and commercial installations. They mentioned that 65% of the residential units in this survey needed additional refrigerant and/or indoor airflow correction. Besides, based on the field data about the service frequency, Breuker and Braun [1998] noted that refrigerant leakage occurs most frequently, followed by the condenser, air handling, evaporator, and compressor faults. Hence, three

faults, refrigerant leakage, condenser, and evaporator fouling, are considered in this study.

2.3.1 Fault definition

As mentioned in the last chapter, we consider only the operating faults in this research. These faults progress undetectably overtime during system operation. Until they are significant, they lead to a premature failure of components, a loss in comfort, or excessive energy consumption. In this part, the fault level F (%) for each fault will be defined, in which 0% represents no-fault, and 100% represents maximum fault level.

Concerning the compressor faults, faults can arise from various reasons such as gas leakage, improper lubrication, motor failure, etc. They lead to leakage in the compressor. The severity of the compressor leak F_{cpl} is then defined as the reduction of refrigerant mass flow rate compared to a no-fault condition, with 0% indicating the correct mass flow rate and 100% indicating no mass flow rate.

$$F_{cpl} = 1 - \frac{q_m}{q_{m_0}} \quad (2.18)$$

Regarding the liquid line restriction fault, its cause comes from the moisture because of a degradation of tube joinery. Accumulation of these substances will block the filter, dryer and unduly increase the refrigerant flow restriction. The liquid line restriction fault level F_{ll} was the percentage change in the liquid line pressure drop concerning the pressure differential between the condenser exit and the evaporator inlet at the no-fault condition.

$$F_{ll} = 1 - \frac{\Delta P}{\Delta P_0} \quad (2.19)$$

About the fouling in heat exchangers, the cause can be found from the defective fan motor, loose fan belt, and particularly the duct contamination. From the interior side, household articles, like textile goods and carpets, produce chemically reactive dust, and kitchens and baths also generate chemical vapor. If air filters are not maintained in good condition, these particles can flow into the ductwork and stick on the fan coil unit and duct walls. These problems will restrict the airflow to the heat exchanger. Therefore, the fault level of the interior fouling heat exchanger is defined as the percent change in air mass flow rate concerning the reference mass flow rate measured at no-fault conditions, with 0% indicating no fouling, 100% indicating heat exchanger fouled completely.

$$F_{fi} = 1 - \frac{q_v}{q_{v_0}} \quad (2.20)$$

In contrast, the heat exchanger is easily contaminated by dirt or debris from the exterior side and sometimes is surrounded by overgrown weeds or fallen leaves. These problems will reduce the exchange surface of heat exchanger. Therefore, the fault level of the exterior fouling heat exchanger is defined as the percent change in exchange surface concerning the

reference exchange surface measured at no-fault conditions, with 0% indicating no fouling, 100% indicating heat exchanger fouled completely.

$$F_{fe} = 1 - \frac{S}{S_0} \quad (2.21)$$

Last but not least, about the refrigerant leakage, the no-fault refrigerant charge was set in the cooling mode at the AHRI 210/240 Standard A-test condition (AHRI, 2008). The refrigerant undercharges fault was implemented by removing the refrigerant from a correctly charged system. The fault level was defined as the ratio of the refrigerant mass by which the system was undercharged to the no-fault refrigerant charge, with 0% indicating the correct charge, 100% indicating no refrigerant charge.

$$F_{rl} = 1 - \frac{M}{M_0} \quad (2.22)$$

Fouling on heat exchanger

Causes

During operation, fouling is a phenomenon that there is the deposition of any undesired material on heat transfer surfaces, which is presented in Fig.2.9. The Fig.2.9 shows the presence of fouling of a heat exchanger in two different environment (interior and exterior).

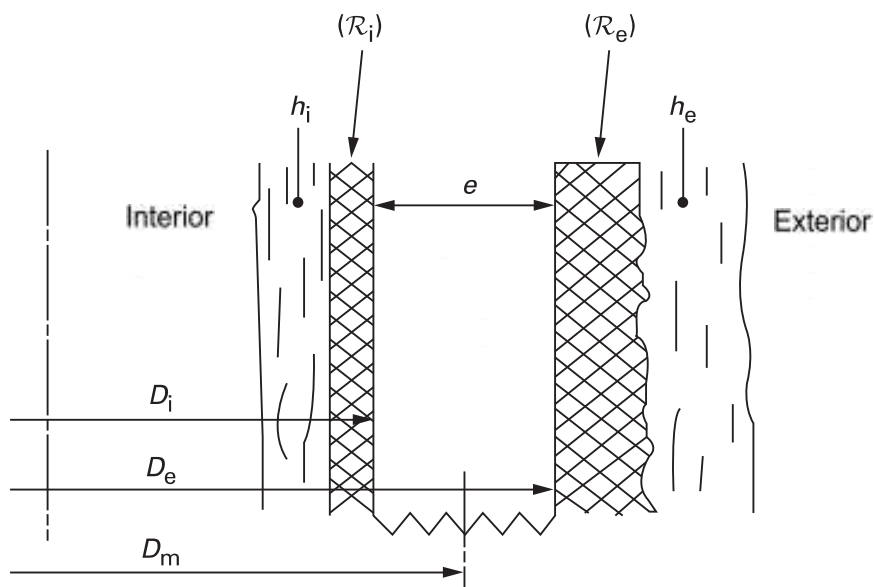


Figure 2.9: Fouling in a heat exchanger

Different types of fouling have been identified, which are listed as follows. They can occur individually but often occur simultaneously.

- **Scaling/Crystallization Fouling:** Scaling is the most common type of fouling. It is commonly associated with inverse solubility salts such as calcium carbonate (CaCO_3) found in water. In case that the temperature increases, reverse solubility salts become less solute and thus deposit on the heat exchanger surface. It is difficult to remove mechanically. The chemical cleaning may be required.
- **Particulate/Sedimentation Fouling:** Sedimentation occurs when particles (e.g. dirt, sand or rust) in the solution settle and deposit on the heat transfer surface. Like scale, these deposits may be difficult to remove mechanically depending on their nature.
- **Corrosion Fouling:** Results from a chemical reaction which involves the heat exchanger surface material. Metal oxides which are corrosion products, exhibit a low thermal conductivity may affect heat exchanger performance.
- **Chemical Fouling:** Fouling from chemical reactions in the fluid stream which result in the deposition of material on the heat exchanger surface. This type of fouling is common for chemically sensitive materials when the fluid is heated to temperatures near its degradation temperature.
- **Freezing Fouling:** Occurs when a portion of the hot stream is cooled to near the freezing point. An example in refineries is when paraffin solidifies from a cooled petroleum product.
- **Biological Fouling:** Occurs when biological organisms grow on heat transfer surfaces. It is a common fouling mechanism where untreated water is used as the coolant. When these microbes taking several millimeters deep may grow across the surface within hours, impeding circulation near the surface wall and impacting heat transfer.

Consequences

The presence of a deposit on the surfaces of a heat exchanger give rise a problem about the efficiency of heat exchanger. The surface of the deposit is rough compared to the original metal surface, which is considered as a layer. The surface of the deposit increases thermal resistance \mathfrak{R} across the heat exchanger, which reduces the efficiency of the heat exchanger. This can be explained by Eq.2.23. It significantly impacts the thermal and mechanical performance of heat exchangers. Furthermore, the rough surface will reduce also the flow area. Reduced heat transfer under fouled conditions consequently contributes to poor heat pump performance. It cannot produce as many as demanded energy. In case that we would like to maintain the energy demand, the system has to work more to meet the requirements.

$$\frac{1}{K} = \mathfrak{R} = \left[\frac{1}{h_e} + \frac{D_e}{D_i} \frac{1}{h_i} + \frac{e}{\lambda} \frac{D_e}{D_m} \right] + \mathfrak{R}_e + \frac{D_e}{D_i} \mathfrak{R}_i \quad (2.23)$$

where

- K : Global exchange coefficient of the heat exchanger [$\text{W}/\text{m}^2\text{K}$]
- \mathfrak{R} : Global thermal resistance [$\text{m}^2\text{K}/\text{W}$]
- h : Heat transfer coefficient [$\text{W}/\text{m}^2\text{K}$]
- D : Hydraulic diameter [m]
- e : Thickness [m]
- λ : Thermal conductivity [W/mK]

Fouling of the heat exchanger reduces its heat transfer parameter. In consequence, the heat exchanger is partially blocked, and only some airflow across the heat exchanger. Fig.2.10 shows clearly the relation between the fouling and airflow rate in the heat exchanger. The more fouling heat exchangers are, the more decrease the airflow is. Besides, the air source mass flow is decreased because of a sudden fault as a malfunction of the circulation pump on the heat source side or of the air fan.

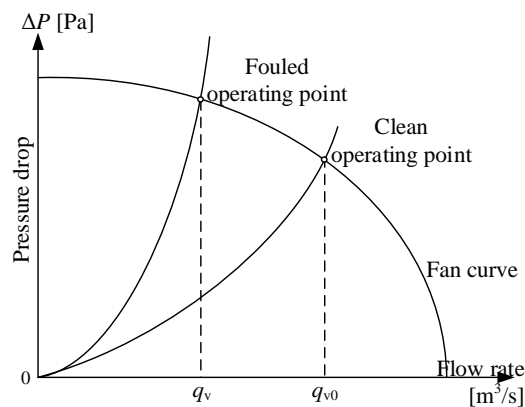


Figure 2.10: The impact of the fouling on the airflow in heat exchanger

Experiments

A significant number of laboratory tests were taken by Kim et al. [2006], Payne et al. [2017] and Cho et al. [2014] to characterize heat pump performance degradation due to faults. The goal of the experiment was to develop the correlations that characterize the heat pump performance operating with the operating faults. They used the same heat pump and test apparatus. Fig.2.11 shows the outdoor section, while Fig.2.12 presents its graphical representation and its dimensions.



Figure 2.11: Side view of the outdoor section with the flow guide

The studied system was an R410A split residential heat pump of an 8.8 kW nominal cooling capacity, Seasonal Energy Efficiency Ratio (SEER) of 13, and Heating Seasonal Performance Factor (HSPF) of 7.8. The system comprised the indoor fan-coil section, outdoor section with a compressor and four-way valve, a thermostatic expansion valve (TXV), and connecting tubing. Both the interior and exterior heat exchangers were of the finned-tube type. The system was installed in NIST's environmental chambers and charged with refrigerant (4,65 kg of R410A) in the cooling mode according to the manufacturer's specifications. The coil had 81 cm x 175 cm of finned area, with 7 fins cm^{-1} of a wavy-lanced type fins.

Fig.2.13 shows the side view of the indoor coil assembly. It comprised two identical slabs and was designed for airflow from the bottom to the top. The two slabs were configured in an A-shape at an angle of 60° . Each slab of the coil had 48.5 cm x 43 cm of finned area with 5 fins cm^{-1} of the wavy-lanced type. Each slab had two inlets from the TXV and two outlets connected to the suction manifold.

Fig.2.14 shows the configuration and outside dimensions of the indoor fan-coil unit. Fin thickness for both the indoor and outdoor coils was 0.12 mm. The indoor blower and system functions were controlled through normal thermostat low voltage wiring, powered by the air handlers low voltage transformer, connected to single-pole single-throw manually activated switches.

At the beginning, a residential heat pump was tested in both heating and cooling mode at

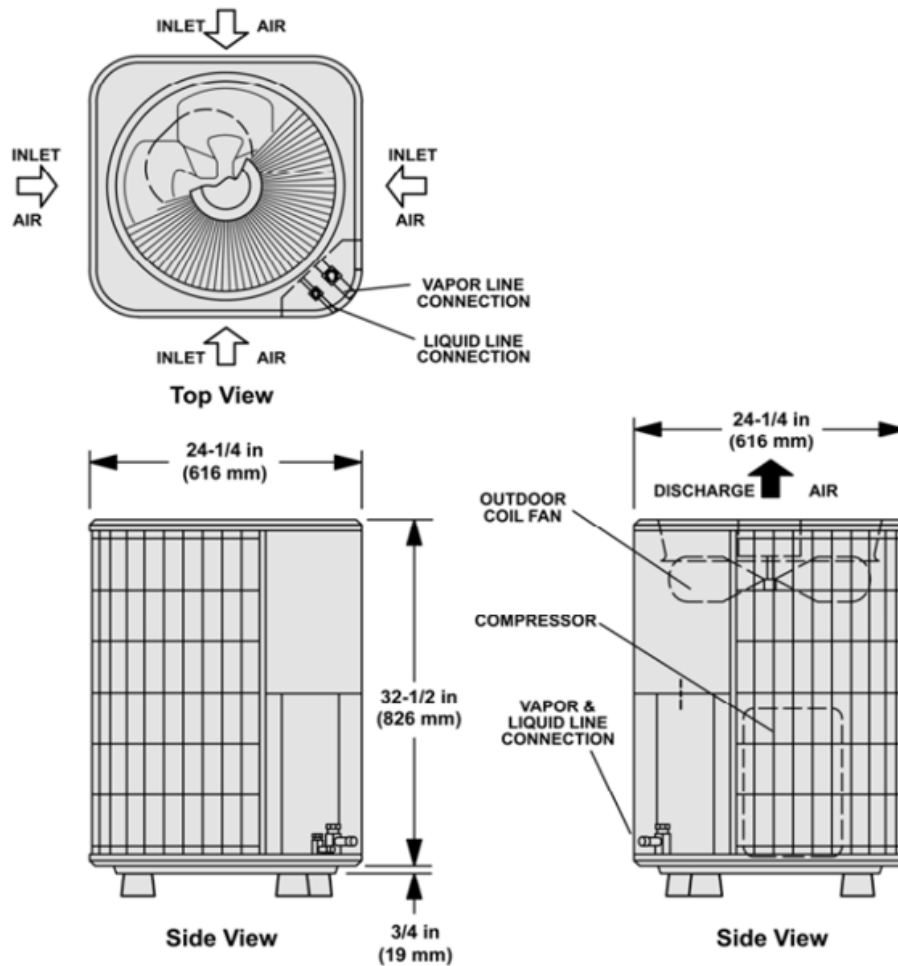


Figure 2.12: Outdoor section dimensions

several indoor and outdoor conditions with no faults. No-fault tests were performed twice to check experimental repeatability, and steady values are the average of these test results. Then, no-fault performance of the system will be used as a reference model of various system features as a function of the independent variables of indoor and outdoor temperature. Before imposing the single fault on the experiment, a constant indoor and outdoor temperature. As presented in the last part, the fault level is defined by the percent change from the reference case.

For the study of the no-fault, the airflow rate through the coil was $1700 \text{ m}^3/\text{h}$ during standard cooling tests. With the same fan speed, heating airflow rate varied from $1650 \text{ m}^3/\text{h}$ to $1675 \text{ m}^3/\text{h}$. Cho et al. [2014] reduced the speed of the nozzle chamber fan at the end of ductwork. By measuring the necessary inputs and outputs of the system under an elementary fault, heat pump performance as COP , EER are presented in a dimensionless, normalized format. They are obtained by dividing the value obtained for the heat pump operating under a selected fault to their value obtained for the heat pump operating fault free. Cho et al. [2014] fit a mathematical function to approximate the operation of a heat pump. An equation of heat pump performance is proposed as following.

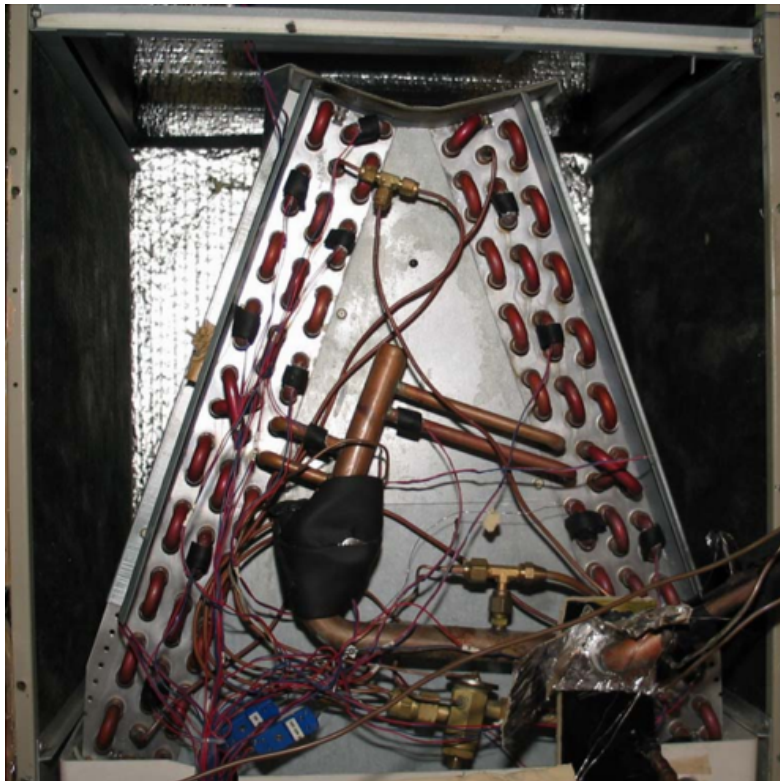


Figure 2.13: Side view of the indoor coil in an up flow configuration

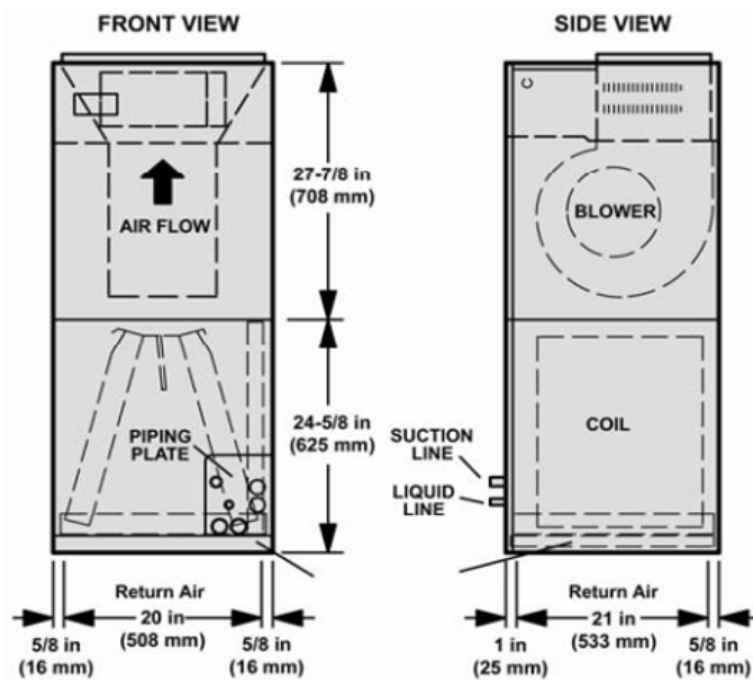


Figure 2.14: Side view of the indoor coil in an up flow configuration

$$\gamma = \frac{X_{\text{fault}}}{X_{\text{no-fault}}} = 1 + (a_1 + a_2 T_{\text{int}} + a_3 T_{\text{ext}} + a_4 F) F \quad (2.24)$$

This Eq.2.24 correlates the dimensionless parameters in both heating and cooling mode as a function of the indoor dry-bulb temperature (T_{int}), outdoor dry-bulb temperature (T_{ext}), and fault level (F) with a_1 , a_2 , a_3 , and a_4 are correlation coefficients, X_{fault} and $X_{\text{no-fault}}$ are

performance parameters for a faulty and fault-free heat pump, and Y is a dimensionless parameter representing the ratio of the faulty performance from that of the fault-free heat pump. Table 2.5 shows correlation coefficients for fouling fault of interior heat exchanger.

Table 2.5: Correlations for non-dimensional performance parameters for interior fouling [Cho et al., 2014]

Fault name	Performance parametre Y	$Y = \frac{X_{\text{fault}}}{X_{\text{no-fault}}} = 1 + (a_1 + a_2 T_{\text{int}} + a_3 T_{\text{ext}} + a_4 F)F$			
		a_1	a_2	a_3	a_4
Fouling interior heat exchanger (fi)	Q_{tot}	1.85×10^{-1}	1.77×10^{-3}	-6.4×10^{-4}	-2.77×10^{-1}
	W_{tot}	1.35×10^{-2}	2.95×10^{-3}	-3.66×10^{-4}	-5.88×10^{-2}
	EER	$Y_{EER} = Y_{Q_{\text{tot}}} / Y_{W_{\text{tot}}}$			
	COP	4.65	-2.12×10^{-1}	1.5×10^{-2}	-6.44×10^{-1}

Concerning the fouling in the exterior heat exchanger, Cho et al. [2014] simulated fouling of the outdoor heat exchanger by blocking the bottom part of its finned area with paper strips. Figure 2.15 shows the outdoor coil with a blockage or fault level of 35% as an example.

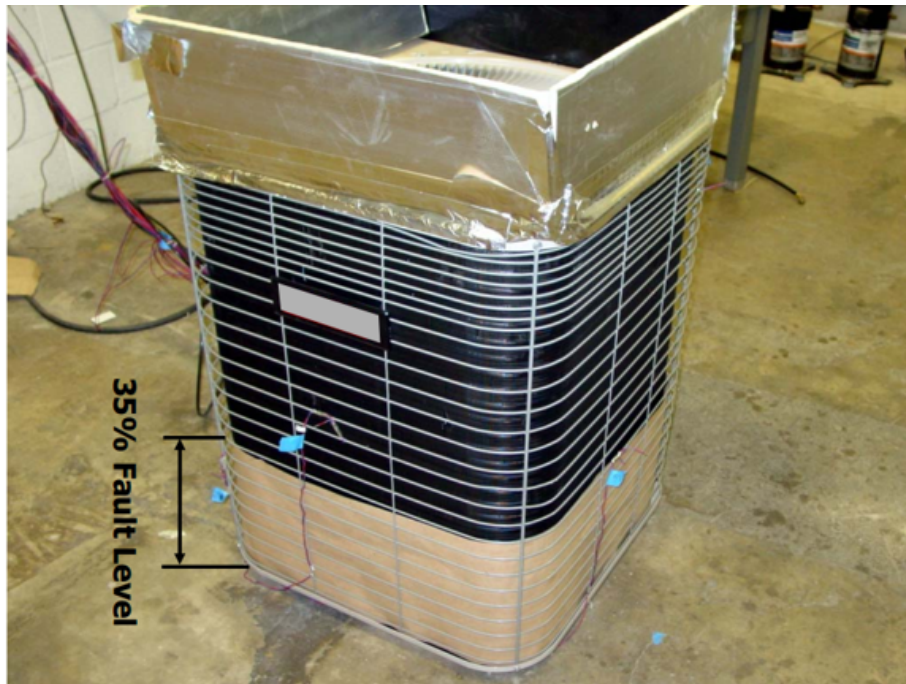


Figure 2.15: Outdoor unit with lower finned area blocked (35% of the entire finned area blocked)

Using the same principles in order to characterize and normalize heat pump performance, the system was measured the necessary inputs and outputs under two conditions of no fault and an elementary fault. Then, the authors fit a mathematical function to approximate the operation of a heat pump with correlation coefficients a_1 , a_2 , a_3 , and a_4 as from the Eq.2.24. Table 2.6 shows correlation coefficients for fouling fault of exterior heat exchanger.

Table 2.6: Correlations for non-dimensional performance parameters for exterior fouling [Cho et al., 2014]

Fault name	Performance parametre Y	$Y = \frac{X_{\text{fault}}}{X_{\text{no-fault}}} = 1 + (a_1 + a_2 T_{\text{int}} + a_3 T_{\text{ext}} + a_4 F)F$			
		a_1	a_2	a_3	a_4
Fouling exterior heat exchanger (fe)	Q_{tot}	-2.39×10^{-1}	8.95×10^{-3}	1.44×10^{-3}	-6.43×10^{-1}
	W_{tot}	1.29×10^{-1}	-5.58×10^{-3}	5.82×10^{-3}	1.15
	EER	$Y_{EER} = Y_{Q_{\text{tot}}} / Y_{W_{\text{tot}}}$			
	COP	-16.5	7.92×10^{-1}	-1.59×10^{-2}	-1.18

Fault evolution

Fouling is a complex phenomenon due to involvement of many variables, for example composition of the fluids, operating conditions in the heat exchanger, type and characteristics of the heat exchanger, location of fouling, and presence of microorganisms. The processes occur simultaneously and depend on the operating conditions. Swan et al. [2018] conducted an experience of different types of heat exchangers, fin, shell and tube. They evaluated heat transfer coefficient and determine the fouling factor to verify if the fans and heat exchange tubes were operating as designed.

In order to estimate the fouling factor and airflow rate during the heat exchanger life cycle, the authors used an ASPEN exchanger design and rating program for heat exchanger design and evaluation [Inc, 2003]. ASPEN's heat exchanger program was used with the input of the exchanger configuration (tubes, fins, rows), the measured duty (average of the process side duty and the air side duty), and the measured process and air temperatures, as well as the process composition. The ASPEN heat exchanger program used the temperatures and exchanger configuration to calculate the area and the corrected log mean temperature difference. The percent of airside flow was determined by comparing the airside data and design data for the exchangers. The daily average data were collected for a three-year period using a process information (data logger) system. The heat transfer coefficient are calculated at every timestep, then, the airflow and fouling factor are determined from ASPEN program, for 25 years.

From the experiment of Swan et al. [2018], the exchangers were found to have lower air flow than originally designed. The evolution of airflow going through the heat exchanger is in time function. As defined in the last section, the fault level of the fouling coil is a function of airflow (Eq.2.20). This fouling fault evolution is presented in Fig.2.16, which was verified from the experimentation during the first three years, and simulated for the total period of 25 years [Swan et al., 2018].

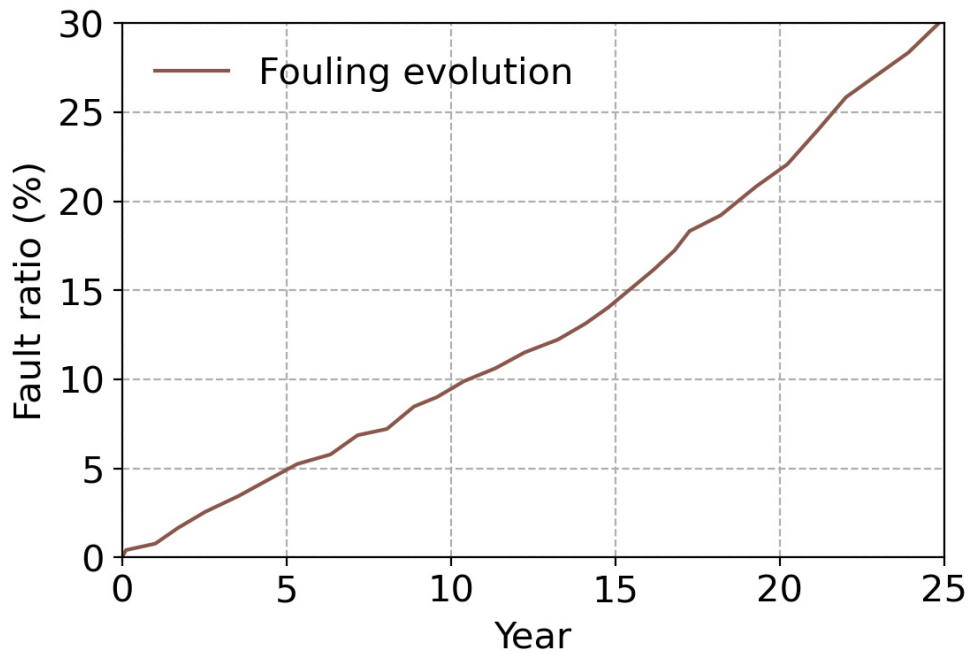


Figure 2.16: Fouling coil evolution

Depending on the working conditions and energy demand, the heat pump works more or less than the one in design conditions. This leads to a variation of degradation level of equipment, which impacts fault occurrence time. An operating fault happens earlier or later as the heat pump works less or more respectively. In this part, an uncertain element of occurrence time is considered. In order to define the dispersion of fouling time of a heat exchanger coil, we based on the experimental results from Siegel et al. [2002]. They did the experiments and simulations to determine coil fouling rate and fouling time. It depends on filter efficiency, indoor dust concentration, coil efficiency, filter bypass, duct penetration, etc. The results are shown in Fig.2.17.

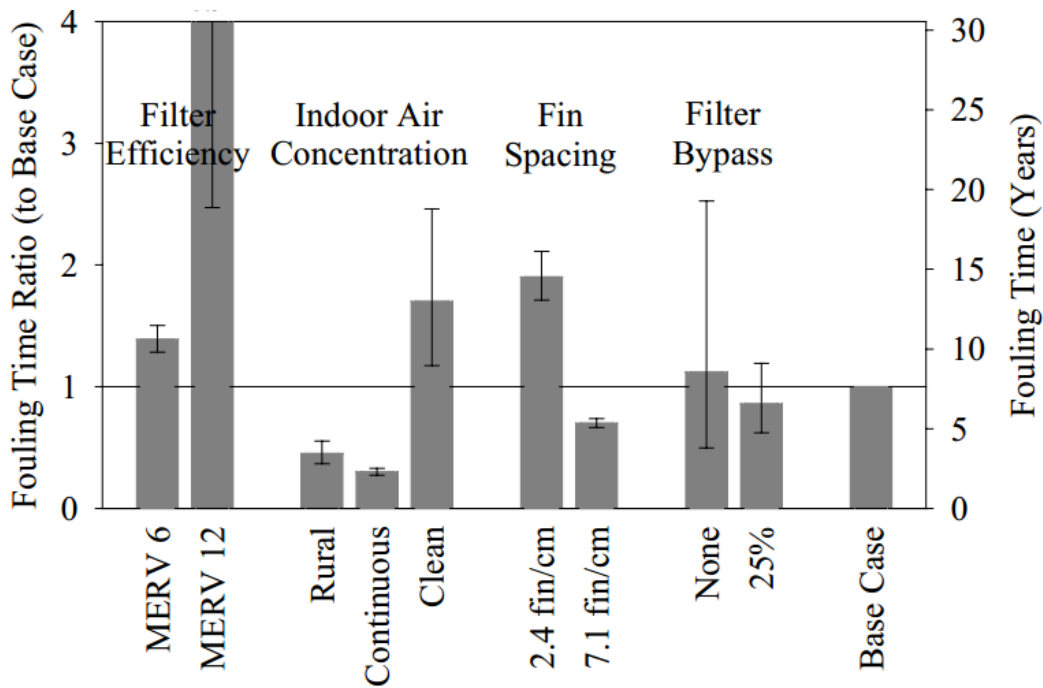


Figure 2.17: Fouling coil evolution

Siegel et al. [2002] considered that the fouling time is the time taken for the pressure drop of the coil to be doubled at a constant flow. The graph shows the fouling time ratio of the heat exchanger coil, which is relative to the base case. Error bars indicate one geometric standard deviation from the mean by varying the all other parameters in the simulation. The fouling time for the base case (MERV-2 filter, urban outdoor concentration, cycling air conditioner, dirty indoor environment, typical coil (4.7 fins/cm or 12 FPI), 10% filter bypass, typical duct penetration) was 7.6 years. Based on this result, the fouling time of a heat exchanger coil varies in a range with a dispersion. Table 2.7 shows the pressure drop and flow of a clean and fouled coil that has deposited enough mass to double the pressure drop at constant flow.

Table 2.7: Flow reduction and pressure drop for different fan curves

Fan curve source	Pressure drop (Pa)		Flow reduction
	Clean	Fouled	
ACCA(1995)	54.0	83.4	5.4%
Parker et al. (1997)	36.1	49.9	5.8%
Siegel et al. [2002]	32.8	41.8	6.5%

As can be seen in Table 2.7, the fractional flow reductions varies between 5.4 – 6.5% for different fan curves between two states of heat exchanger coil: clean and fouled. We take an average value of these three flow reductions to find the fouling time of the heat exchanger coil in our case. The heat exchange coil is fouled if the flow reduction is at 6%, or fouling ratio $F = 6\%$. According to the fault evolution (Fig.2.16), the fouling time is 6.5 (years) at $F = 6\%$. Furthermore, based on the experience of Siegel et al. [2002], from Fig.2.17, if the fouling time is 6.5 years, the dispersion of fouling time is 2.5 years, which can be described in Fig.2.18.

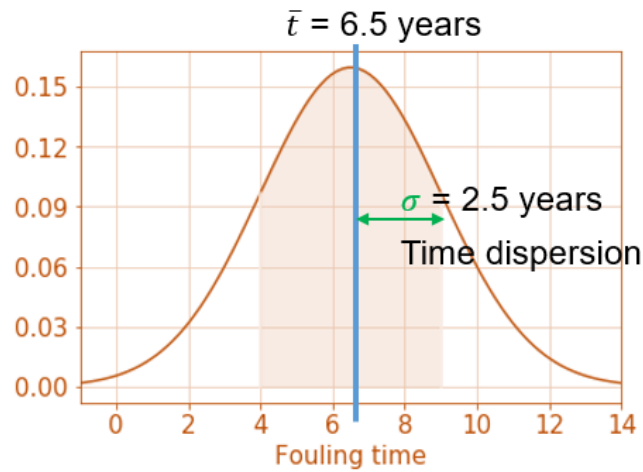


Figure 2.18: The dispersion for fouling time $\bar{t} = 6.5$ years

According to the normal distribution, the parameter fouling time \bar{t} is the mean of the distribution, while the parameter dispersion σ_t is its standard deviation. It represents real-valued random variables whose distributions are not known. For the normal distribution, the values less than one standard deviation away from the mean account for 68.27% of the set; while two standard deviations from the mean account for 95.45%; and three standard deviations account for 99.73%. In our study, we used value of one standard deviation away from the mean to calculate the fouling time. Based on this, the dispersion can be estimated in the function of fouling time as follows. For further study, we can take three standard deviations away from the mean to have a global view of fouling time.

$$\sigma_t = \frac{5}{13}t \quad (2.25)$$

where

- σ_t : dispersion of fouling time t
- t : fouling time

Refrigerant leakage

Refrigerant does not dissipate during normal operation of the heat pump. It remains at the same level of charge, even it changes between liquid and gas states. However, leaks can sometimes develop in heat pumps from corrosion, loose connections, or damage, resulting in a loss of refrigerant. There are 2 types of leakage:

- Permeation leakage is a leak that occurs through a porous wall
- Interfacial leakage is a leak due to a passage (a crack, a scratch, a foreign body creating a passage, under-tightening of 2 assembled components, etc.)

Causes

In general, permeation leakage is neglected in comparison to interfacial leakage, because the migration of a fluid is often much slower. There are two main causes of refrigerant interfacial leakage [Eric et al., 2015].

- Heat stresses (evaporator defrosting period) are the cause of major fatigue and increased risk of leakage at evaporator return bends
- Mechanical stresses are high in refrigerating plants. Liquid hammering or repeated vibration may cause pipe ruptures leading to severe leakage

Consequences

The heat pump performance is influenced by the amount of refrigerant in the system. On the one hand, a rapid leak is easy to detect because it degrades the system performance abruptly. On the other hand, a slow leak is typically difficult to detect, because of the slow and gradual change in performance. Using the same principles in order to characterize and normalize heat pump performance, the authors fit a mathematical function to approximate the operation of a heat pump with correlation coefficients a_1 , a_2 , a_3 , and a_4 as from the Eq.2.24. Table 2.8 shows correlation coefficients for fouling fault of refrigerant leakage.

Table 2.8: Correlations for non-dimensional performance parameters for refrigerant leakage [Cho et al., 2014]

Fault name	Performance parametre Y	$Y = \frac{X_{\text{fault}}}{X_{\text{no-fault}}} = 1 + (a_1 + a_2 T_{\text{int}} + a_3 T_{\text{ext}} + a_4 F)F$			
		a_1	a_2	a_3	a_4
Refrigerant leakage (rl)	Q_{tot}	-5.45×10^{-1}	4.94×10^{-2}	-6.98×10^{-3}	-1.78×10^{-1}
	W_{tot}	-2.54×10^{-1}	1.12×10^{-2}	2.06×10^{-3}	5.74×10^{-3}
	EER	$Y_{EER} = Y_{Q_{\text{tot}}} / Y_{W_{\text{tot}}}$			
	COP	-18.6	8.79×10^{-1}	-1.56×10^{-2}	-2.22

Fault evolution

As the analyse in the last section, refrigerant leakage involves a large number of variables, for example composition of the fluids, operating conditions, type and characteristics of tube. The processes occur simultaneously and depend on the operating conditions. The leakage rate gives information on the refrigerant losses per year. Based on information assembled from Air Conditioning and Refrigeration Technical Institute (ARI) member companies, the maximum residential heat pump annual leak rates of 4% of the charge for 1996 equipment and 2% per year for equipment available in 2005 can be used for the calculations [Andreas et al., 2011]. Therefore in this study, we make an assumption that heat pump average annual leak rate is 2%, which developpes linearly throughout the year. Additionally, according to the report of Armines ERIE [2013] about the Inventory of Refrigerant Emissions from France and overseas territories in 2012, the residential heat pump emission rate varies between 2% and 5%. Therefore, we apply $\pm 2\%$ for the dispersion σ_r of refrigerant leak rate in a residential heat pump in our research.

As the result are nominalized, the result can be applied for every split residential heat pump, which uses the refrigerant R410A, the unit contained the indoor fan-coil section, outdoor section with a scroll compressor, and a thermostatic expansion valve (TXV).

2.3.2 Petri nets, fault occurrence model

As can be seen from the literature, operating faults have been studied for a while. Many researches have studied about the operating faults and analyzed their impacts on heat pump performance under some operating conditions, in which the evolution of operating faults during heat pump life cycle have not been taken into account. To the author's opinion, there is still a lack of a global view on heat pump performance in practice. In this study, we try to model the evolution of each fault, analyze its impact on heat pump performance and building energy consumption in every transition under the graphical and mathematical form. In order to resolve this problem, Petri net is proposed in this study. Petri net was introduced in 1962 by Carl Adam Petri to define a theoretical framework for studying concurrency problems. It has been developed in different areas and systems. They use the flow charts to described graphically parallel or concurrent activities. Additionally, a system of equations is established in order to characterize the evolution of different activities, meeting the requirement of different applications.

Before showing the Petri net in different applications, we will analyze the structure and function of Petri nets. Petri net, as a fault occurrence model, is established based on the observed outputs, to define the system states. Observation and real system must clearly have the same initial state.

Structure

Based on the observed outputs, a Petri net of the system is built by firstly using a conceptual model of Production Flow Schema (PFS) technique [Miyagi & al, 1997]. The aim is to identify the link between different activities, which represent modifications on the flow of items. Then the model is reformed as a bipartite directed graph with three types of objects: places represented by circles, transitions represented by rectangles and directed arcs representing the connection between them. At this step, the model has no dynamic. An example of interior fouling fault modelled by Petri net is illustrated in Fig.2.19.



Figure 2.19: Interior fouling evolution modelled by Petri net

- Place (P): This Petri net composes a set of places $P = \{P_0, P_{1i}, P_{2i}, \dots, P_{ni}\}$ from P_0 to P_{ni} , which characterise the heat pump performance COP . The index of a place corresponds

to fault occurrence order. For example, the place P_0 represents the fault original state, which is clean. The place P_{1i} shows the first fouling state.

- Transition (T): This Petri net composes a set of transitions $T = \{T_{1i}, T_{2i}, \dots, T_{ni}\}$ from T_{1i} to T_{ni} , represent the *COP* diminuation conditions in heat pump. The index of a transition corresponds to fault occurrence order. For example, the transition T_{1i} represents the first fault level, which causes the first fouling.
- Directed arc (\longrightarrow) represents the connection from places to transitions and from transitions to places.
- Token (\bullet) describes the dynamic behavior of a Petri net in terms of state changes. By default, Petri net has one token and the initial marking is at first place P_0 . The presence or absence of a token in a place indicates the actual state of fouling. For example, if the token is located in the initial place P_0 , it represents the proper state of evaporator. In contrast, when the token is located in the place P_{1i} , it represents the first fouling state.

Firing process

The execution of a Petri net is controlled by the number and distribution of tokens in the Petri net. By changing the distribution of tokens in different places, which represents the occurrence or the evolution of faults, the Petri nets define a new fault state of the system. We now introduce the firing process throughout the enabling rules and firing rules of a transition to study the dynamic behavior of the system.

- Enabling rule: A transition (T) is enabled if each input place (P) of (T) contains at least the number of tokens equal to the weight of the directed arc connecting (P) to (T).
- Firing rule: Only enabled transition can fire. The firing of an enabled transition (T) removes the input place (P) the number of tokens equal to the weight of the directed arc connecting (P) to (T). Then, it deposits in output place (P) the number of tokens equal to the weight of the directed arc connecting (T) to (P).

We base on the first part of Fig.2.19. Initially, the place P_0 has one token. The weight of directed arcs in this Petri nets is one. When transition conditions of T_{1i} are validated, transition T_{1i} is enabled. As mentioned before, the weight of directed arcs is one, which is equal to the number of token in this Petri, therefore the transition T_{1i} can be operated immediately. Consequently, the token from the input place P_0 is taken and then distributed to output place P_{1i} , which means the heat pump state is changed. As soon as the token is placed in the place P_{1i} , the equation systems in this place will be activated and finally, the evaporator fouling is characterized.

Petri net examples

Due to their flexibility, the Petri net models are developed and applied in many engineering fields as railway tracks (Andrews 2013), bridges (Le and Andrews 2016), wind turbines (Leigh and Dunnett 2016), and building facades (Ferreira et al. 2018). In this part, we will show two applications among them.

In the building section, Petri net model is proposed to use, for example its application on a facade deterioration is illustrated in Fig.2.18.



Figure 2.20: Petri net about the deterioration of building façade [Ferreira et al., 2017]

This Petri net describes a sequence of possible degradation of a building façade during its life cycle. This Petri net model uses places and transitions to describe the degradation procedure. It is composed of five places P_1 to P_5 representing one state that characterize the degradation condition of external render façades. P_1 means there is no visible degradation and P_5 indicates the presence of extensive damage in the render façade. The transitions T_1 to T_4 represent the time interval required for the façades to progress to a more deteriorated state. Also, the token is used to show the movement through the building façade. This degradation process is delivered in classic mathematical notation, which is shown in Eq.2.26. It expresses the global degradation of façade coatings through the ratio between the degraded area weighted as a function of its condition and a reference area, equivalent to the whole and having the maximum degradation level possible.

$$F_w = \frac{\sum(A_n k_n k_{a,n})}{Ak} \quad (2.26)$$

where

- F_w : the degradation severity of the coating, expressed as a percentage
- k_n : the multiplying factor of anomaly n , as a function of their degradation level
- $k_{a,n}$: a weighting factor corresponding to the relative weight of the anomaly detected; $k_{a,n} = 1$ by default
- A_n : the area of coating affected by an anomaly n
- A : the façade area
- k : the multiplying factor corresponding to the highest degradation level of a coating of area A

In this study, the proposed Petri net model evaluates the performance of rendered façades over time. Their performances are evaluated based on a discrete qualitative scale composed of five condition levels, established according to the physical and visual degradation of these elements. In this study, the author modelled deterioration considering that the transition times between these condition states can be modelled as a random variable with different distributions. For that purpose, a Stochastic Petri Nets model is used, as a formal framework to describe this problem. Based on this example of Petri net for one element, we can apply this type of Petri net for one operating fault modelling. According to the measures and experiences of the fault evolution in time from literature, we can model the degradation performance of heat pump under the operating fault, considering that the transition times between these states are fault evolution time.

However, as mentioned before, there are many operating faults can happen at the same time in reality. Can the Petri net model the numerous elements? An example of Petri net about the degradation of driven train of a wind turbine is illustrated in Fig.2.21, which shows the model of 3 sub-components as bearing, gearbox and shaft.

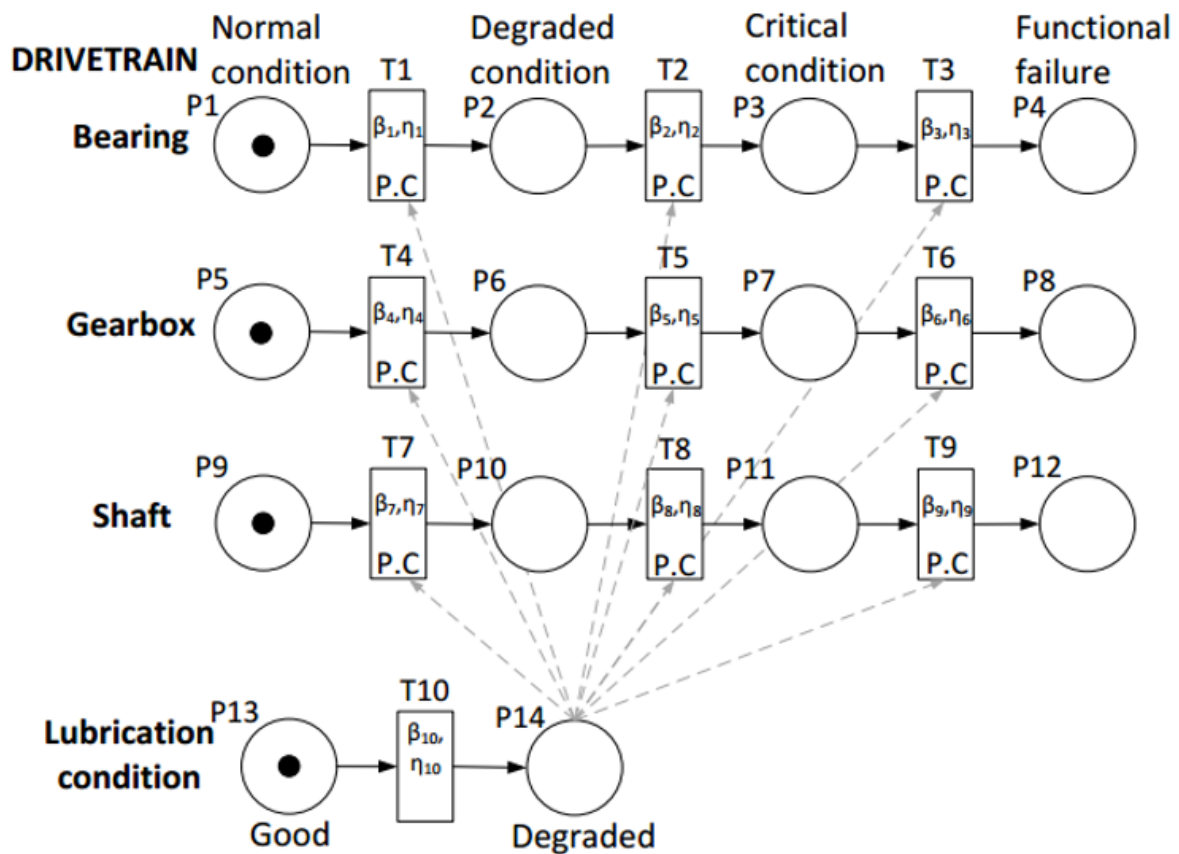


Figure 2.21: Petri net example about the degradation of the drivetrain components of a wind turbine [Le & Andrews, 2016]

Fig.2.21 illustrates the PN modelling the condition degradation of the drivetrain components, as bearing, gearbox and shaft. Their states are represented by places P_1 to P_{12} . The degradation processes between these states are represented by transitions T_1 to T_9 , which contain the transition times between the condition states. As damage accumulates, the characteristic of each component has an increasing failure rate over time. Concerning the lubrication process, it has a significant effect on the degradation process of the whole drivetrain system and therefore it is taken into account in the modelling. While places P_{13} and P_{14} represent the good and the degraded state of drivetrain lubrication oil, transition T_{10} represents the degradation process between these two states. As the lubrication condition degrades – P_{14} is marked, this has effects on all other components, therefore the transition times governed by transitions T_{1-9} are modified. For other wind turbine subsystems and their components, the PNs modules modelling the degradation processes follow similar structure. This paper presents an asset model for offshore wind turbine reliability accounting for the degradation process. The model was developed based on the Petri net which effectively captures the nature of the dynamic processes. The versatility of the method allows the details of the degradation to be incorporated in the model. In particular, in drivetrain system, there are dependent deterioration processes between different components for example the lubrication conditions and other components. The model outputs indicate the performance of the wind turbine components.

As can be seen from these two above examples, Petri nets are applied to model the system operation under the impact of component degradations or operating faults. These examples show how Petri nets combine a well-defined mathematical theory with a graphical representation of the dynamic behavior of systems. The theoretic aspect of Petri nets allows precise modelling and analysis of system behavior, while the graphical representation of Petri nets enable visualization of the modelled system state changes. This combination is the main reason for the great success of Petri nets. Why do we not apply this Petri net approach to model an energy system in the building, such as a heat pump in our research, integrating the operating faults during its life cycle? Using this approach will help us to describe the fault evolution during heat pump's life cycle, analyzes its impact on system performance and building energy consumption.

Conclusion

In this chapter, we carry out the state of the art of the heat pump system with its technology. In order to characterize its behavior in nominal conditions, the refrigerant cycle models and empirical models are presented. Besides, we concern most on the operating faults, which can happen randomly during heat pump's lifecycle, reduce system efficiency and its performance. Their causes and consequences are therefore analyzed in detail. Furthermore, their evolution in time are also taken into account because of their dependence on the working environment, energy demand, etc. With a complexity operation of a heat pump, the issues of taking into account the operating faults during its lifecycle are impor-

tant. In order to model and analyze the impact of heat pump operating faults not only on heat pump performance, but also the building energy consumption, Petri nets are applied in this study.

Chapter 3

Operating fault impact on heat pump performance

This chapter presents two approaches for heat pump modeling, integrating the operating faults: a refrigerant cycle model, and an empirical model from experience. Before considering the operating faults, we show how to use the refrigerant cycle model, which is presented in chapter 2, in order to model an air-to-air heat pump in nominal conditions without operating fault. In order to validate the refrigerant cycle model, and make sure of its accuracy, we then compare the simulation results, such as the heat pump performance COP and EER of this refrigerant cycle model to the results from the standard NF EN ISO/CEI 17025 model.

Then, in order to analyze the impact of operating faults on heat pump performance, we impose separately each operating fault into this refrigerant cycle model. In order to show how this model works with operating faults, we conduct several calculations with different fault levels F , different temperature conditions. In order to show the utilization capacity of the refrigerant cycle model, the simulation results with the operating faults, such as heat pump performance COP and EER are compared to experimental results. The extended experiment study of heat pump faults from Cho, 2014 (section 2.3) are used in this chapter as a reference, and the empirical equations will be used further in chapter 4.

Since many operating faults can occur at the same time during heat pump life cycle, we then, combine different operating faults with different fault ratios in order to approach the heat pump performance in reality. In order to analyze the impact of fault combinations on heat pump performance, we simulate the accumulated operating faults based on the heat pump empirical model.

3.1 Heat pump calculation without faults

In order to compare the heat pump refrigerant cycle model to two empirical models from NF EN ISO/CEI 17025 model (without fault, presented in section 2.2.2) and Cho et al. [2014] (with faults, presented in section 2.2.2), we use the same heat pump type as a reference study from the experiment of Cho et al. [2014]. The reference system was an R410A split residential

heat pump of an 8.8 kW nominal cooling capacity, Seasonal Energy Efficiency Ratio (SEER) of 13, and Heating Seasonal Performance Factor (HSPF) of 7.8 (ARI 2006).

3.1.1 Refrigerant cycle model

To model the heat pump without operating fault, we use the refrigerant cycle model, which is presented in section 2.2.2. As mentioned before, we concern about the broad trends of heat pump performance, therefore a relatively simple model could be employed. In this part, we simplify the heat pump calculation with the following assumptions:

- Heat transfer between the heat exchangers and surroundings is neglected in a simplified approach;
- The superheating and subcooling are neglect in a simplified approach;
- The heat losses in refrigerant pipes are minor (pipes are insulated);
- Pressure drops in the refrigerant pipes between main components are negligible;
- There is no transfer of heat during the compressor works.

With the above assumptions, the enthalpy diagram for the simplified calculation (green line) is presented in Fig.3.1.

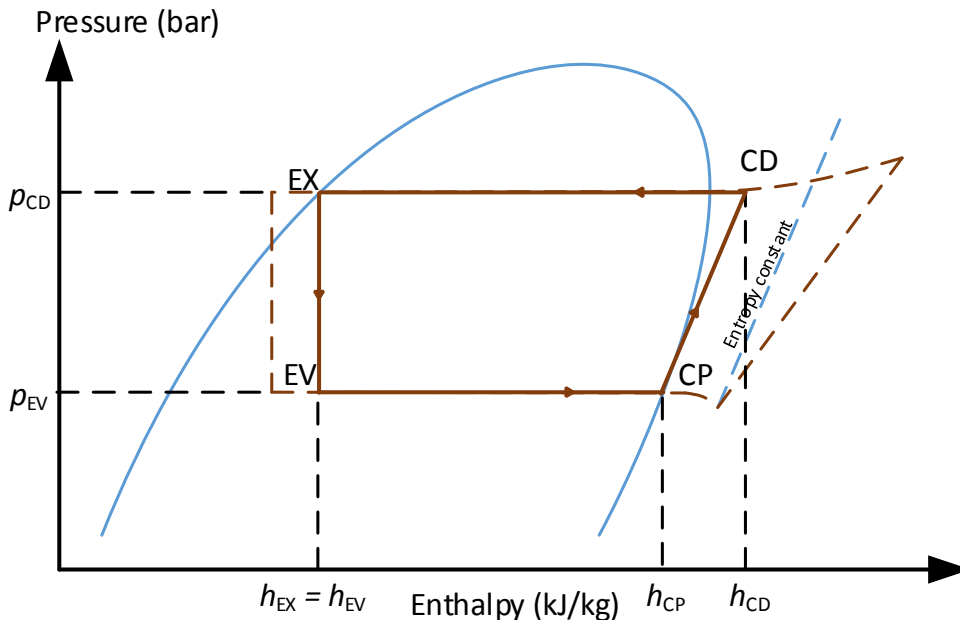


Figure 3.1: Enthalpy diagram for the simplified calculation

Fig.3.1 shows the two thermodynamic cycle representation in enthalpy diagram, one realistic (brown line, which is presented in last chapter), and the proposed simplified cycle

(green line) with the above assumptions. The heat pump is assumed as an ideal heat pump without heat loss. Based on the refrigerant cycle model presented in section 2.2.2, a block-diagram of heat pump model with the simplified approach is presented Fig.3.2. It shows the heat pump calculation process without operating fault.

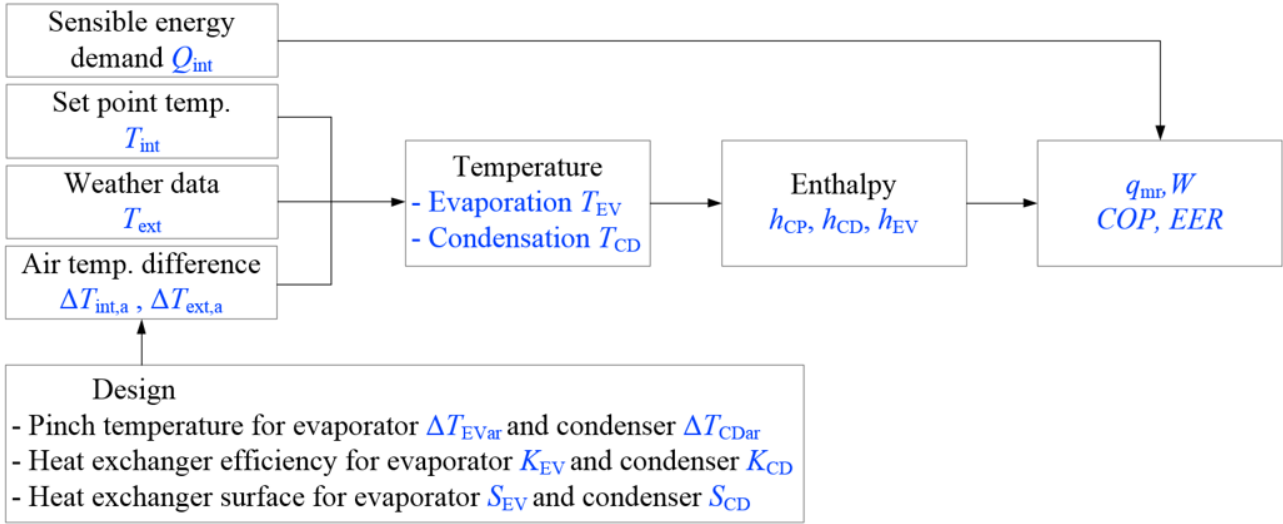


Figure 3.2: Heat pump calculation with the refrigerant cycle model – no operating fault

A heat pump calculation in cooling mode is illustrated following. As presented in section 2.2.2, Fig.3.2 shows input data from the manufacturers about the heat pump dimension KS , the energy demand for cooling Q_{int} , indoor air temperature T_{int} , and outdoor air temperature T_{out} and working conditions. These temperatures are taken hourly from the weather data and the setpoint temperatures. In this calculation, the interior air temperature $T_{int} = 27^{\circ}\text{C}$ and exterior air temperature $T_{ext} = 35^{\circ}\text{C}$ are taken as a operating condition. By using these operating conditions, which are also the nominal conditions of heat pump empirical model in cooling mode (NF-EN ISO/CEI 17025), we can compare the heat pump performance between these two models. In cooling mode, the interior heat exchanger is the evaporator, and the exterior heat exchanger is the condenser.

As presented in section 2.2.2, based on the heat pump design information, we calculate the air temperature drop ΔT_{EV_a} across the evaporator (EV) and the air temperature rise ΔT_{CD_a} across the condenser (CD). Based on Eq.2.4 about the evaporation and condensation process, the evaporating (T_{EV}) and condensing (T_{CD}) temperatures in the cooling mode are calculated. With these two evaporating (T_{EV}) and condensing temperatures (T_{CD}), as presented in section 2.2.2, the refrigerant characteristics (temperature T , pressure p , specific enthalpy h , specific entropy s , vapor quality x) through four principal components are defined. It is based on an enthalpy diagram with a particular refrigerant, for example, R410A, in our research. This process is calculated by Python with the library PropsSI from Cool-Prop. As the enthalpy h_{CP} , h_{CD} , and h_{EX} are defined, the mass flow rate of refrigerant is calculated from the sensible supplied energy Q_{int} entering into an interior heat exchanger (Eq.2.7). Finally, the compressor power and the Energy Efficiency Ratio EER are calculated by Eq.2.9.

Concerning the heat pump calculation in heating mode, using the same principle of calculation process from Fig.3.2, the heat pump calculation at the interior air temperature $T_{int} = 20^{\circ}\text{C}$ and exterior air temperature $T_{ext} = 7^{\circ}\text{C}$ is conducted. Table 3.1 briefly shows the results of heat pump calculation in both heating and cooling modes.

Table 3.1: Enthalpies and heat pump performance in heating and cooling nominal conditions

Mode	Q_{int} (kW)	T_{int} ($^{\circ}\text{C}$)	T_{ext} ($^{\circ}\text{C}$)	T_{EV} (K)	T_{CD} (K)	h_{EX} (kJ/kg)	h_{CP} (kJ/kg)	h_{CD} (kJ/kg)	q_{m_r} (kg/s)	W (kW)	COP EER
Heating	9.9	20	7	270.15	303.15	248.4	420.4	446.5	0.050	1.303	4.53
Cooling	8.8	27	35	290.15	318.15	275.8	425.4	444.2	0.059	1.106	4.43

3.1.2 Benchmark of the refrigerant cycle model with a standard model

Using the simplified refrigerant cycle model, we conduct the heat pump calculation and compare its performance to the results from the standard NF-EN ISO/CEI 17025 model, presented in chapter 2. By applying the same calculation process of the refrigerant cycle model, the heat pump performance COP and EER are calculated in different temperature conditions and presented in the following figures. These two below figures show the performance of the heat pump in heating mode (Fig.3.3) and cooling mode (Fig.3.4) by using two different models: the empirical model from NF-EN ISO/CEI 17025 model and the refrigerant cycle model.

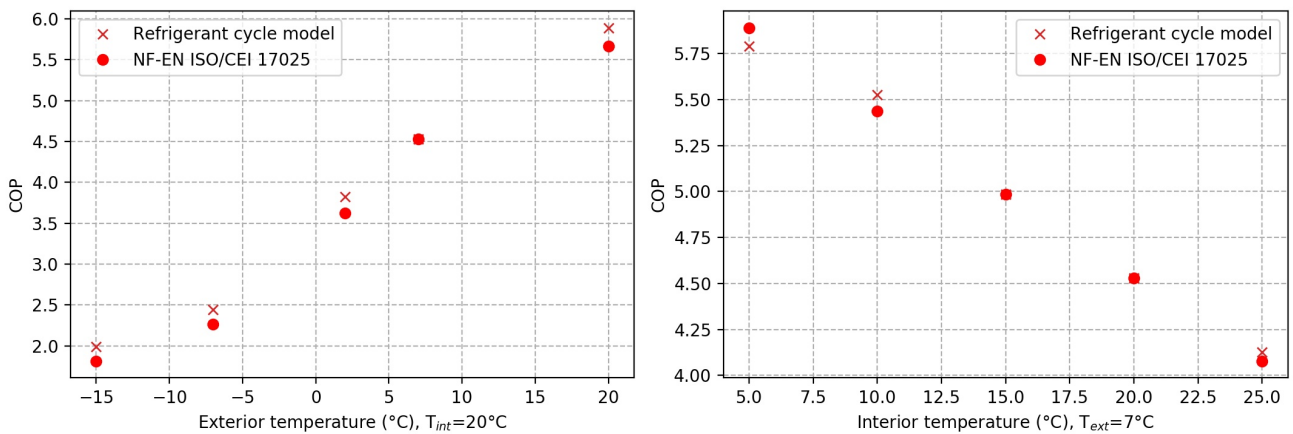


Figure 3.3: Comparison of COP and correction coefficient C_{nn} between the two heat pump models in heating mode, with constant interior temperature $T_{int} = 20^{\circ}\text{C}$ (left) and exterior temperature $T_{ext} = 7^{\circ}\text{C}$ (right)

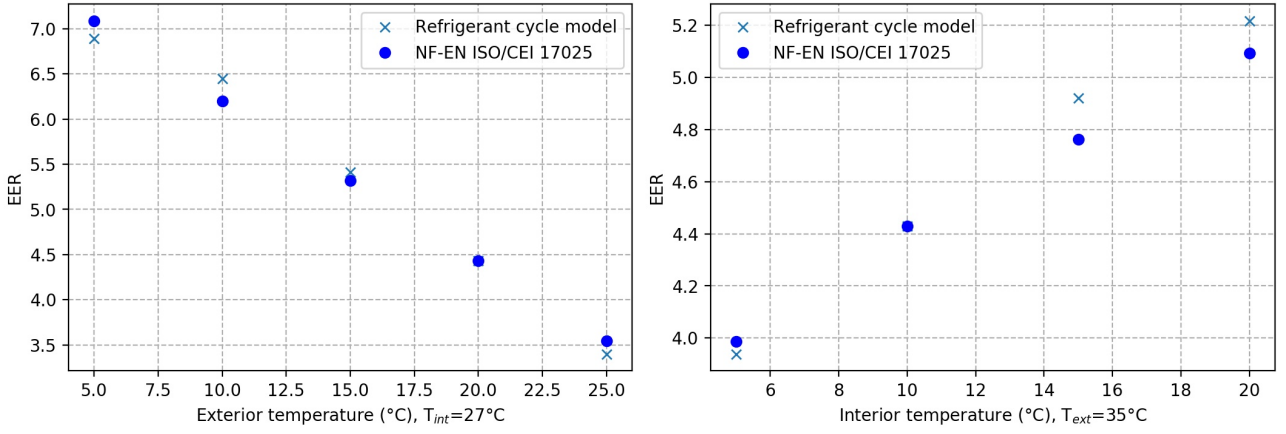


Figure 3.4: Comparison of COP and correction coefficient C_{nn} between the two heat pump models in cooling mode, with $T_{int} = 27^\circ\text{C}$ (left) and exterior temperature $T_{ext} = 35^\circ\text{C}$ (right)

These two figures, show an agreement results of heat pump performance between the refrigerant cycle model and empirical model NF-EN ISO/CEI 17025. As the operation conditions is far from the nominal conditions, where the ‘core value’ is supplied by manufacturers, the difference between two models increase, for example its variation is from 1.2% to 4% in cooling mode and 4.5% to 10% in heating mode. This variation comes from the assumptions of heat pump calculation about the heat transfer and heat loss, the system is assumed to be an ideal system. However, as can be seen from these two figures, the simplified refrigerant cycle model can estimate the heat pump performance, with the maximum difference of 10%, comparing to the empirical model NF-EN ISO/CEI 17025. We can use this simplified model to model the air-to-air residential heat pump and show the performance trends in different working conditions.

With the objective of this study about studying the heat pump performance evolution with different types of operating faults in time, the simplified refrigerant cycle model is proposed. This approach has generalization capabilities, enabling the analysis of different heat pump types and a wide range of operating conditions. Furthermore, as showed in section 2.2.2, there are some parameters from the equation system of heat pump calculation that we can modify. It is presented as an operating fault. Therefore, this simplified model can be used to study also the impact of operating heat pump operating faults. The system of equations helps us to assess the impact of operating on the physics parameters, leading to the degradation of heat pump performance. The heat pump calculation process with the operating fault is presented in section 3.2.

3.2 Heat pump calculation with faults

3.2.1 Refrigerant cycle model

Based on the refrigerant cycle model in section 2.2.2, in this part, we will take into account the operating fault to characterize the impact of operating faults on heat pump performance.

The operating fault of interior fouling is taken as an example. In case that there is an operating fault during the heat pump life cycle, some parameters are modified, which leads to the recalculation of heat pump performance. A heat pump calculation process with a fouling fault is presented following as an example.

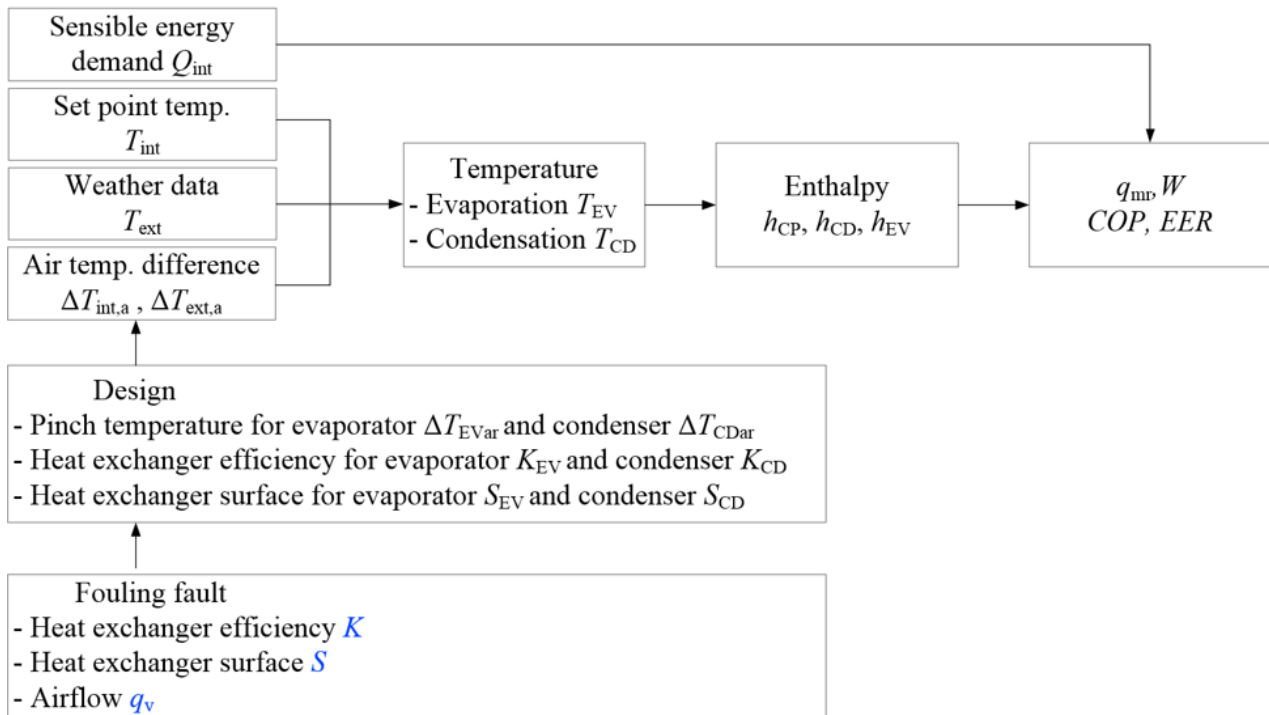


Figure 3.5: Heat pump calculation with the refrigerant cycle model – with a fouling fault

The calculation process with the fouling fault is showed in Fig.3.5. As presented in Eq.2.3 about the heat exchanger from the refrigerant side as well as the air side, the sensible supplied energy entering into an evaporator is a function of airflow rate q_v . In the case of evaporator fouling at the fault ratio $F(\%)$, the airflow q_v decreases, as analyzed in chapter 2. As the airflow rate decreases, following the heat exchange equation Eq.2.3, the sensible energy demand Q_{int} decreases, which leads to the increase of discomfort for user. In order to meet the thermal requirements, we assume that the heat pump still works to supply the same sensible energy demand when an operating fault happens. While the sensible energy demand, Q_{int} is supposedly maintained, the air temperature drop across the evaporator $\Delta T_{CD,ar}$ is, therefore, higher than the one without fault. Because of the increase of air temperature drop across the evaporator $\Delta T_{CD,ar}$, regarding Eq.2.4 about the evaporation temperature and condensation temperature, the evaporation temperature goes down, and the condensation temperature goes up, respectively. As presented in many experiment results [Mehrabi and Yuill, 2018] about the fouling faults, when the evaporator fouling increases, the condensation temperature is approximately constant, and vice versa, when the condenser fouling increases, the evaporation temperature is approximately constant. We take this observation as an assumption for this calculation. Based on the enthalpy diagram of refrigerant R410A, which is shown in Fig.3.6, as the evaporation temperature goes down, the enthalpy h_{CP} decreases. Consequently, the enthalpy h_{CD} is redefined.

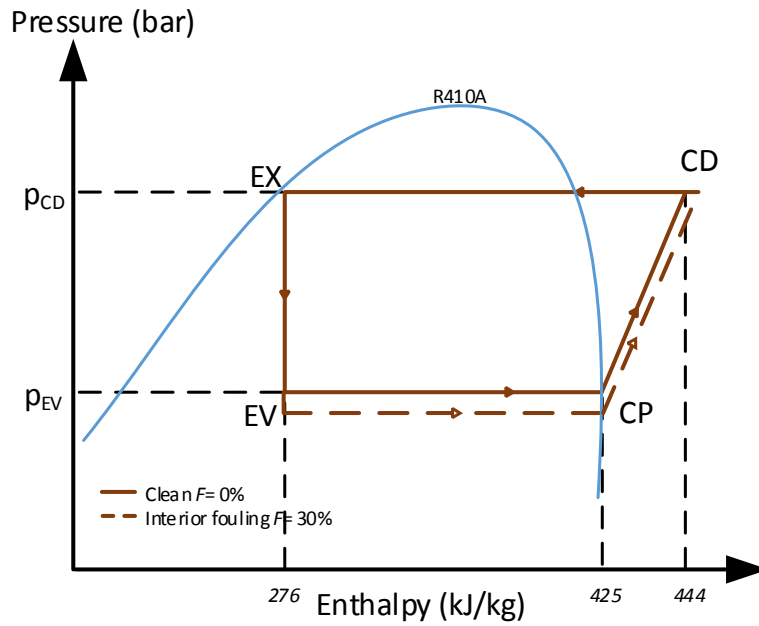


Figure 3.6: The simplified enthalpy diagram of the interior fouling $F = 0\%$ and $F = 30\%$ on an air-to-air heat pump in cooling mode

Fig.3.6 shows the enthalpy diagram of the heat pump in two operating conditions: without fault, $F = 0\%$ (green line), and with interior fouling $F = 30\%$ (blue line) in cooling mode. The enthalpy h_{CD} at the condenser inlet increases from the clean to the 30% evaporator fouled conditions. Then, the compressor consumption increases, which is quantified from our model equations Eq.2.7 to Eq.2.8. As the compressor power increases, the heat pump performance EER decreases, following Eq.2.9. Using the same calculation principle for heating mode, we can analyze the impact of fouling fault on heat pump performance COP. An example of calculation at fault ratio $F=30\%$ is described following in both heating and cooling mode. As the energy demand Q_{int} is supposedly maintained, the airflow q_v decreases by 30%, which leads to the increase of the air temperature drop across the evaporator $\Delta T_{CD,ar}$ by 30%. The heat pump calculation integrating an operating fault using the refrigerant cycle model in both heating mode ($Q_{int} = 9.9\text{kW}$, interior air temperature $T_{int} = 20^\circ\text{C}$ and exterior air temperature $T_{ext} = 7^\circ\text{C}$) and cooling mode ($Q_{int} = 8.8\text{kW}$, interior air temperature $T_{int} = 27^\circ\text{C}$ and exterior air temperature $T_{ext} = 35^\circ\text{C}$) is presented in the table below.

As presented in Table 3.2, since the interior fouling fault happens, some of parameters are modified. We take a case study of interior fouling with fault ratio $F = 30\%$ as an example. In heating mode, the interior exchanger is condenser. When condenser is fouled, the condensation temperature increases by 0.6%, which leads to the increase of enthalpy at point CD and point EX and the increase in compressor power by 7.1%. In consequent, the COP value is decrease of 4%. In contrast, in cooling mode, the interior exchanger is evaporator. When evaporator is fouled, the evaporation temperature decreases by 7.4%, which leads

Table 3.2: Heat pump performance with the interior fouling fault $F=30\%$ and its comparison to the experience case $F=0\%$

Mode	T_{EV} (K)	T_{CD} (K)	h_{EX} (kJ/kg)	h_{CP} (kJ/kg)	h_{CD} (kJ/kg)	q_{m_r} (kg/s)	W (kW)	COP EER
Heating	270.15	305.15	252.1	420.4	448.1	0.05	1.396	4.35
Comparison	-	↑ 0.6%	↑ 1.5%	-	↑ 0.3%	-	↑ 7.1%	↓ 4%
Cooling	288	318.15	275.8	425.04	445.57	0.06	1.211	4.21
Comparison	↓ 7.4%	-	-	↓ 0.1%	↑ 0.3%	-	↑ 9.5%	↓ 5%

to the decrease of enthalpy at point CP and the increase in compressor power by 9.5%. In consequent, the EER value is decrease of 5%. In general, as the interior is fouled, the evaporation and the condensation temperature is impacted, which increases the distance between enthalpy of CP and CD, and increase the compressor power. Since the compressor power increases, the heat pump performance decreases.

3.2.2 Benchmark of the refrigerant cycle model with the empirical model

In order to show the modeling of the refrigerant cycle model, and make sure of its accuracy, we compare the heat pump performance COP and EER between the refrigerant cycle model from previous section, and the heat pump empirical model of Cho et al. [2014]. We conducted different simulations for the air-to-air heat pump in different working conditions. The working conditions are presented in Table 3.3.

Table 3.3: Working conditions for heat pump calculation

Mode	Heating		Cooling			
	1	2	3	4	5	6
$T_{int}(^{\circ}C)$	21.11	21.13	21.1	21.1	26.7	26.7
$T_{ext}(^{\circ}C)$	-8.35	3.10	27.8	37.8	27.8	37.8

The simulation results of two models: the refrigerant cycle model (red line) and the heat pump empirical model of Cho et al. [2014] (blue line) with the fault ratio F varies between 0 and 30%, are shown in Fig.3.7. They show the normalized parameters COP/COP_0 and EER/ERR_0 at a reduced indoor airflow, which presents the fouling fault in the interior heat exchanger.

When the heat pump works at the nominal conditions without fault, the fault ratio $F = 0\%$, the ratio COP/COP_0 and EER/ERR_0 are 1 for both models. As the fault ratio F increases, the difference of heat pump performance between two models increases, for example its variation is until 4.45% for heating mode and 1.37% for cooling mode when the fault increases from 0 to 30%. This variation comes from the assumptions of heat pump calculation about the heat transfer and heat loss, the system is assumed to be an ideal system. At the fault ratio $F= 30\%$ as the maximum fault range in reality, the heat pump performance calculated by the refrigerant cycle model are within an uncertainty of 4.45%, comparing to

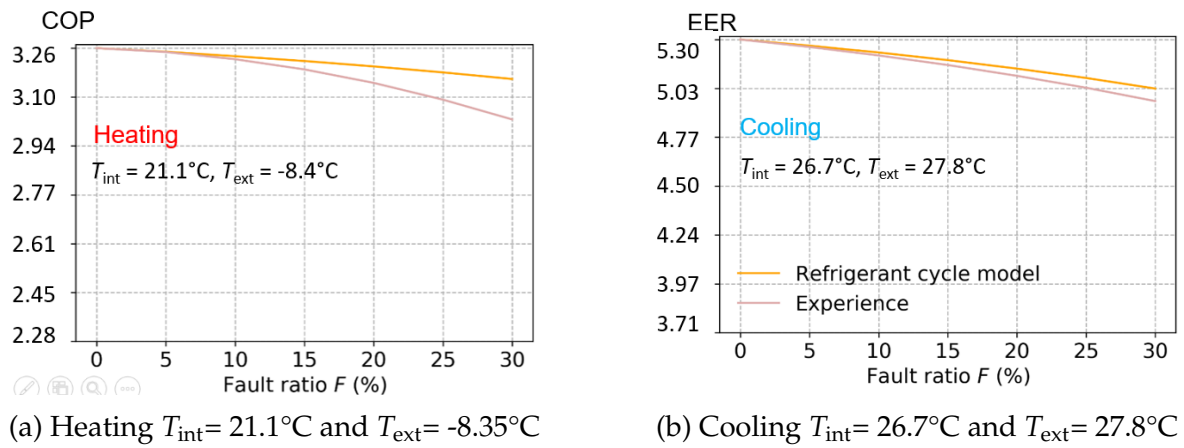


Figure 3.7: Comparison the fault impact of interior fouling heat exchanger on heat pump performance between the refrigerant cycle model and empirical model in two modes

the experience model of Cho et al. [2014]. The simplified refrigerant cycle model can estimate the heat pump performance with the fouling fault, with the maximum difference of 4.45%, comparing to the empirical model from the experience of Cho et al. [2014]. We can use this simplified model to model the air-to-air residential heat pump, when there is an operating fault and show the performance trends in different working conditions. Fig.3.7 shows an agreement results of heat pump performance between the refrigerant cycle model and empirical model from the experience - Cho et al. [2014].

The simplified refrigerant cycle model is proposed to study the operating faults in different operating conditions. It shows the abilities to describe the heat pump performance as close to the one from an actual heat pump. As can be seen, the refrigerant cycle model is developed by understanding the process of physics and underlying principles. To build the physics-based models and determine their parameters, detailed knowledge of the system and its operation processes is necessary. These physical processes are described at as low level as possible. In order to analyze the operating faults, this type of model requires a specific analysis of impacts on thermodynamic diagram with an extensive equation system. It is necessary where we need a model with a high level of detail in the physical processes. In contrast, the experimental approach is quite simple in terms of the equation. It measures the inputs and outputs of the heat pump under different conditions and establishes a relationship. We can use it to analyze the impact of operating faults in different operating conditions as well as different fault ratios. The advantages and disadvantages of each model are briefly presented in Table 3.4.

Table 3.4: Comparison of refrigerant cycle model and experimental model

	Refrigerant cycle model	Experimental model
Require system knowledge	***	No
Physical phenomenal representation	***	No
Possible generalization	***	*
Fault modelling precision	*	***

With the objective of this thesis about the studying the impact of operating faults, we chose the simplified refrigerant cycle model in order to calculate the nominal heat pump performance COP_n and EER_n . As the fault happens, the experience model of Cho et al. [2014] is used to calculate the heat pump performance in consideration of different fault ratios F . The model application in the calculation process is presented in Fig.3.8.

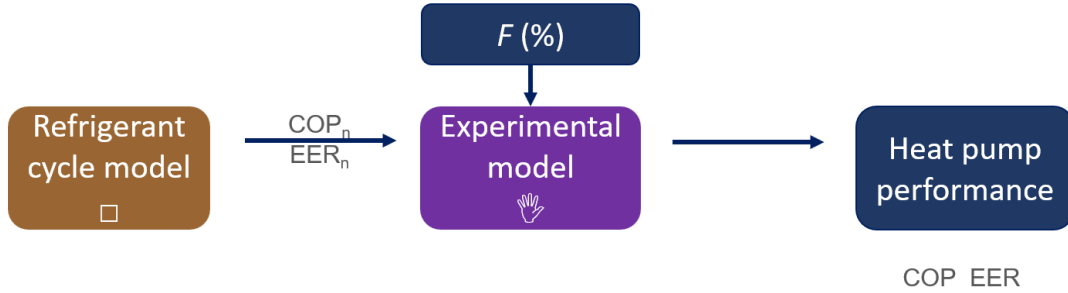


Figure 3.8: Model application

3.3 Combination of operating faults

The last section studied about the single fault and its impact on heat pump performance. However, in the reality, many operating faults can occur at the same time during heat pump life cycle, the impact of these fault combinations should be studied further. We then, focus in this part on the impact of different fault combinations on heat pump performance.

As presented in last section, the heat pump performance under an operating fault is a function of interior air temperature T_{int} , exterior air temperature T_{ext} , fault ratio F_1 and the nominal heat pump performance COP_n and EER_n . It can be expressed as the Eq.3.1 for the first operating fault.

$$\begin{aligned}
 COP_1 &= f(T_{int}, T_{ext}, F_1, COP_n) \\
 EER_1 &= f(T_{int}, T_{ext}, F_1, EER_n)
 \end{aligned}
 \tag{3.1}$$

As there is a second operating fault or more, the heat pump performance will be calculated, based on the interior air temperature T_{int} , exterior air temperature T_{ext} , fault ratio F_2 and the last heat pump performance, for example in this case the value of COP_1 and EER_1 . It can be expressed as the Eq.3.2 as follows. These calculations are presented in Fig.3.9

$$\begin{aligned}
 COP_2 &= f(T_{int}, T_{ext}, F_2, COP_1) \\
 EER_2 &= f(T_{int}, T_{ext}, F_2, EER_1)
 \end{aligned}
 \tag{3.2}$$

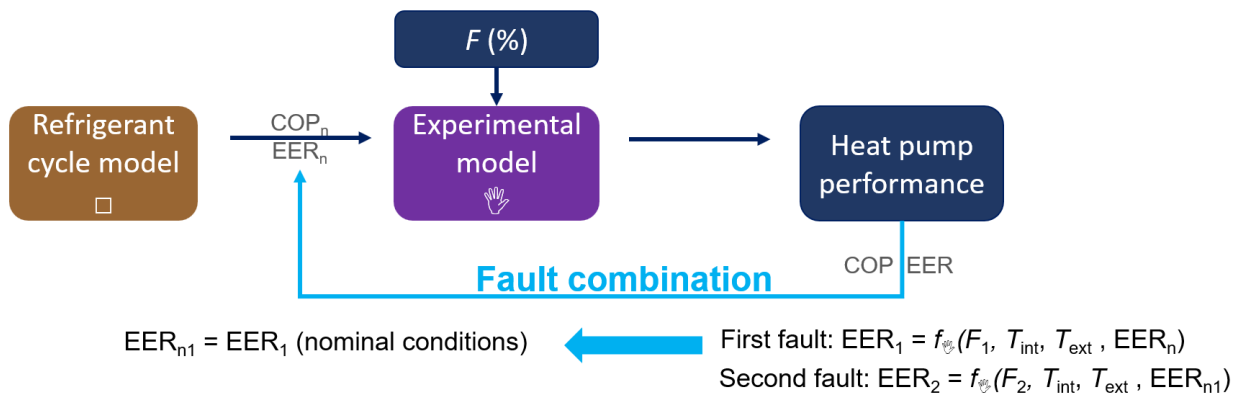


Figure 3.9: Calculation process for fault combination

An example calculation in cooling mode is made in order to analyse the impact of fault appearance order on the heat pump performance, at the same operation conditions - the interior air temperature $T_{int} = 27^{\circ}\text{C}$ and exterior air temperature $T_{ext} = 35^{\circ}\text{C}$. Two considered operation faults with fault ratio $F = 10\%$, are interior fouling and refrigerant leakage, which is shown in Fig.3.10.

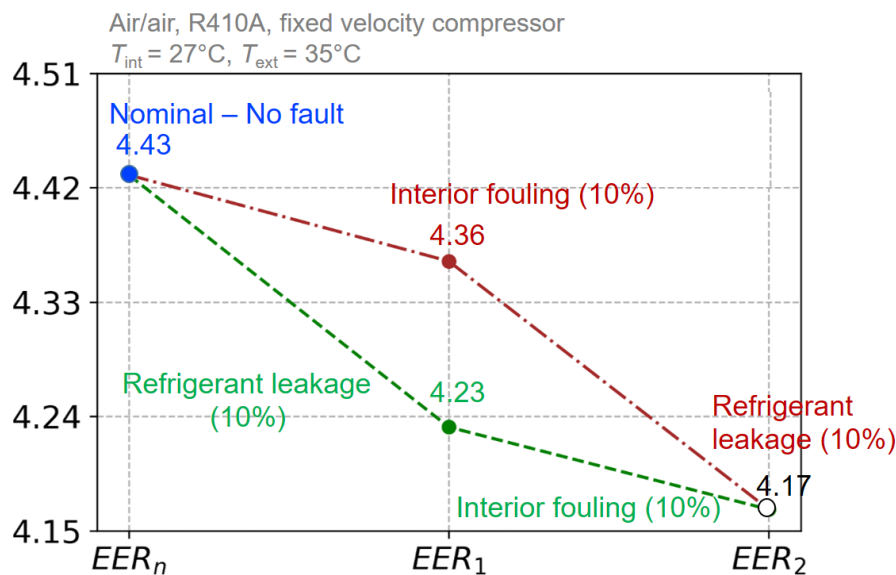


Figure 3.10: Impact of fault appearance order on heat pump performance

There are two scenarios of fault appearance:

- Red line: Interior fouling is imposed before the refrigerant leakage
- Green line: Interior fouling is imposed after the refrigerant leakage

The heat pump performance in cooling mode (EER) is calculated when the fault appears. As can be seen from Fig.3.10, the EER value is the same for two cases. We can conclude that the fault appearance does not impact on the heat pump performance. Therefore, the operating fault combination is a set with no repetition. Based on the combination theory, the possible combinations by selecting objects from a set with no repetition is expressed as following:

- Interior fouling
- Exterior fouling
- Refrigerant leakage
- Interior fouling and exterior fouling
- Interior fouling and refrigerant leakage
- Exterior fouling and refrigerant leakage
- Interior fouling, exterior fouling, and refrigerant leakage

We applied the above calculation process for three operating faults with fault ratios F (%) from 0 to 30%. The simulation is calculated in different conditions for both heating and cooling modes. The heat pump performance in different fault combinations is shown in the following figures.

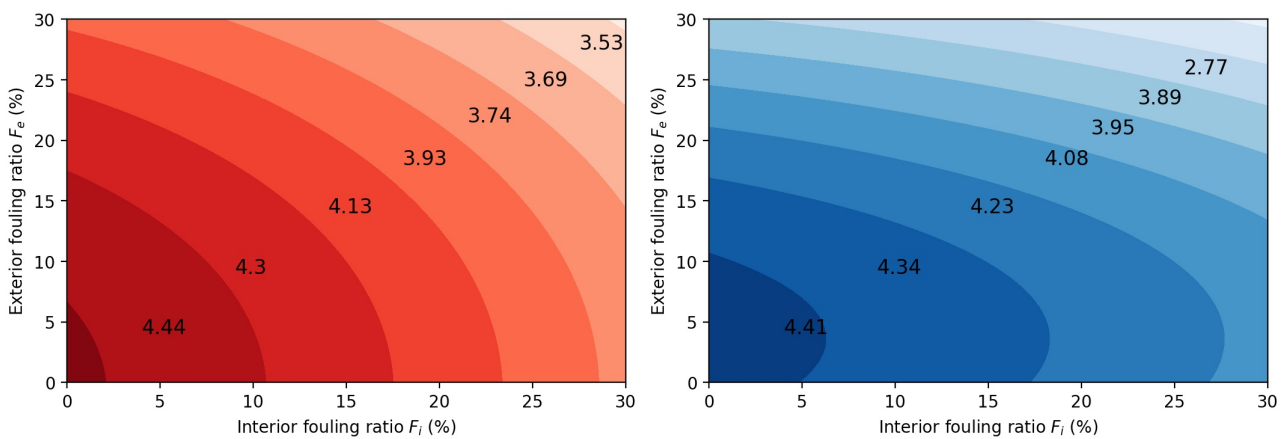


Figure 3.11: Heat pump performance of combination Int-Ext: Interior fouling and exterior fouling

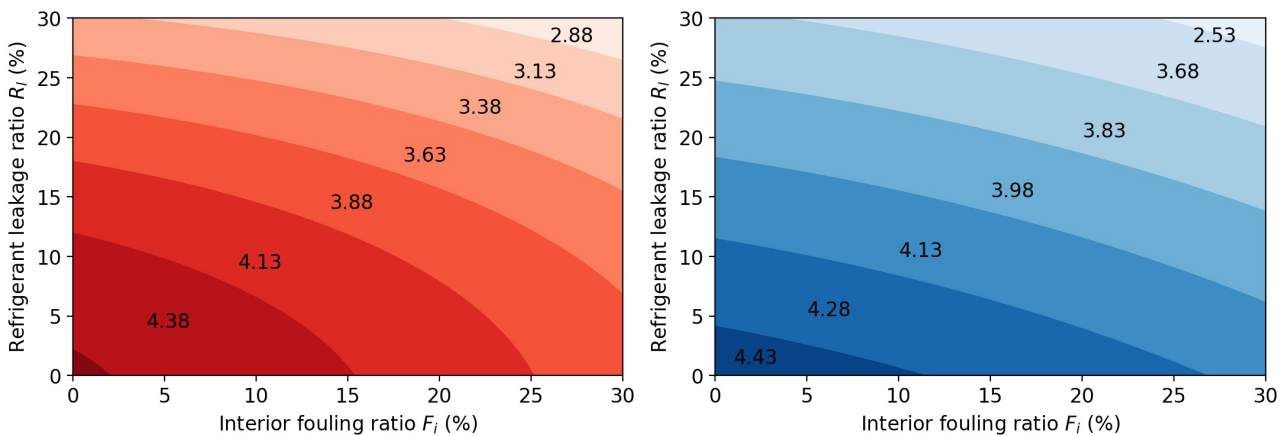


Figure 3.12: Heat pump performance of combination Int-Rleak: Interior fouling and refrigerant leakage

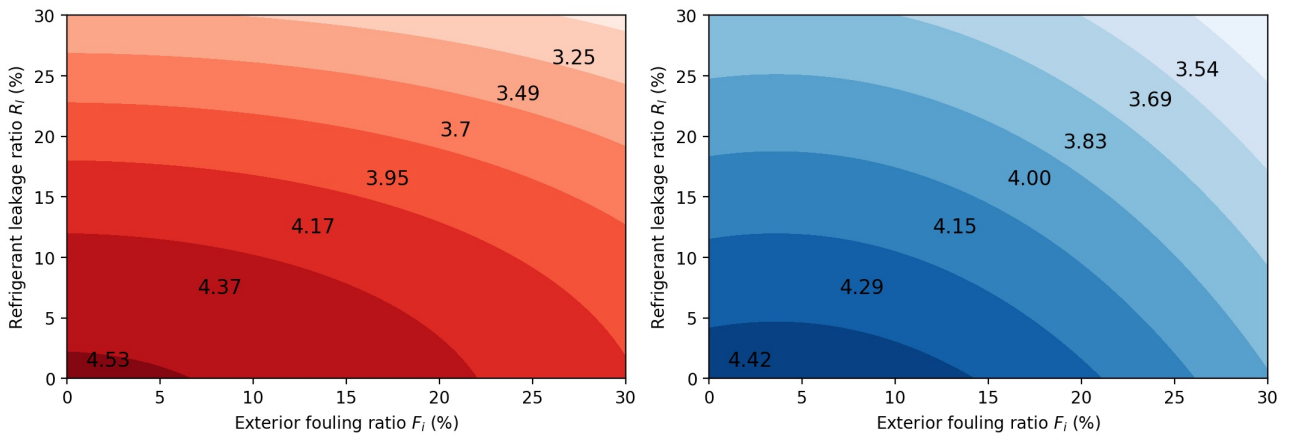


Figure 3.13: Heat pump performance of combination Ext-Rleak: Exterior fouling and refrigerant leakage

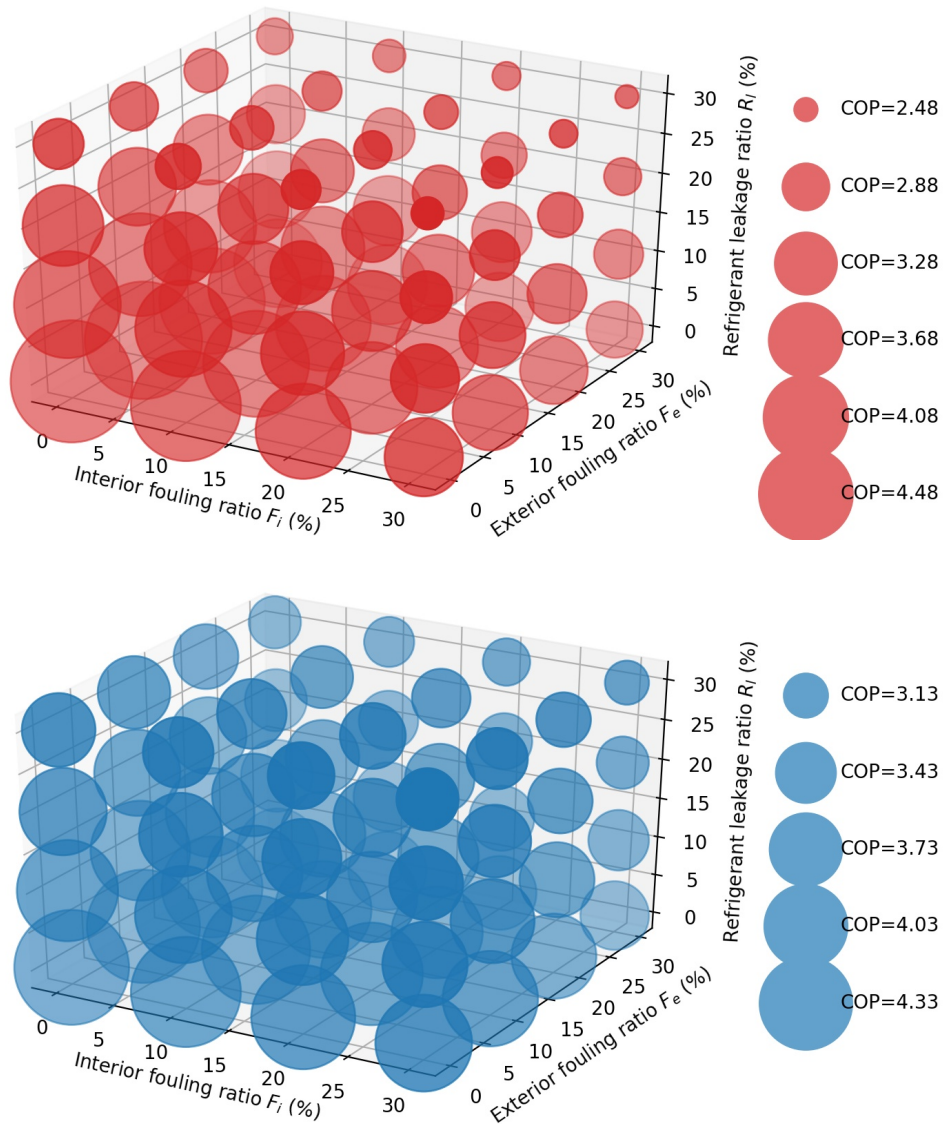


Figure 3.14: Heat pump performance of combination Int-Ext-Rleak: Interior fouling, exterior fouling and refrigerant leakage

These figures shows the impact of operating faults on heat pump performance COP and EER in heating (red graph) and cooling (blue graph) respectively. As the color is plus dark, the heat pump performance is better. Simulations were performed for 4 fault combination sets, with different operating conditions. Because of similarity between the obtained results, we show only four diagrams in the nominal working conditions, for example in heating mode (interior air temperature $T_{\text{int}} = 20^{\circ}\text{C}$ and exterior air temperature $T_{\text{ext}} = 7^{\circ}\text{C}$) and cooling mode (interior air temperature $T_{\text{int}} = 27^{\circ}\text{C}$ and exterior air temperature $T_{\text{ext}} = 35^{\circ}\text{C}$).

Fig.3.11 shows the accumulate impact of the interior and exterior fouling on heat pump performance. In heating mode, the interior fouling has more impact on the COP value than the exterior fouling. For example, for the first decrease of COP value between 4.35 and 4.5, the interior fouling fault F_i is 2.4%, while the exterior fouling fault F_e is 6.3%, and so on. When the fouling fault has a fault ratio which is higher a threshold, for example $F_i = 10.7\%$ and F_e is 17.5%, the distance between each layer of heat pump impact is nearly the same, which represents that if the fouling fault increases from 4 to 8%, the heat pump performance has the same decrease. Besides, in cooling mode, for the first 10% of fouling fault, the interior fouling has more impact on EER value, comparing to the exterior fouling. For example, at the first impact on heat pump performance where EER value varies between 4.4 and 4.5, the interior fouling fault F_i is only 4.9% while F_e reaches to 10.7%. However, from over fault ratio $F = 17.3\%$, the exterior fouling shows the greater impact than the interior fouling on EER value. For example, F_e is from 17.3% to 20.9%, which create the same impact on EER value when F_i is from 17.5% to 27%.

Fig.3.12 and Fig.3.13 shows the accumulate impact of the interior or the exterior fouling and the refrigerant leakage fault on heat pump performance. As presented in section 2.2.2, the refrigerant leakage fault has the important impact on heat pump performance, comparing to the fouling fault. Indeed, in heating mode, for the first decrease of COP value between 4.25 and 4.5, interior fouling fault F_i is 2.4%, exterior fouling fault F_e is 6.3%, while the refrigerant leakage fault F_r is 2.1%, and so on. When the refrigerant leakage fault increases around 4 to 5% increase in fault, it shares the same impact on COP value while the interior fouling increases about 7-10%, and the exterior fouling increases about 10-20%. Besides, in cooling mode, at the first impact on heat pump performance where EER value varies between 4.35 and 4.5, the interior fouling fault F_r is only 4.8% while F_i , F_e reaches to 11.1% and 14.3% respectively. Furthermore, the impact of these two fault combinations is higher than the first combination of two fouling faults. Indeed, the color of impact diagram is brighter, which means the heat pump performance has more degradation.

Fig.3.14 shows the accumulate impact of three operating faults on heat pump performance. As fault increases, the impact on heat pump performance is important. Comparing to the last three combinations, more faults occur, more impacts on heat pump performance in both COP and EER.

In conclusion, the refrigerant cycle model is used in this chapter to analyze the impact of operating faults on the heat pump performance. In the nominal conditions without fault, the

simulation results of the refrigerant cycle model show a good estimation of the heat pump performance, with the maximum difference of 10%, comparing to the empirical model NF-EN ISO/CEI 17025. This approach has generalization capabilities, enabling the analysis of different heat pump types and a wide range of operating conditions. We can use this refrigerant cycle model to simulate and analyze the air-to-air residential heat pump performance trends in different operating conditions without fault. As the simplified refrigerant cycle models is developed based on the equation system of heat pump calculation, we can modify some parameters, which describes an operating fault. Therefore, this simplified model can be used to study also the impact of operating heat pump operating faults. The system of equations helps us to assess the impact of operating on the physics parameters, leading to the degradation of heat pump performance. This simplified model shows a good estimation of the heat pump performance for the fouling fault, with the maximum difference of 5%, comparing to the experience results. We can use this simplified model to model the air-to-air residential heat pump, when there is an operating fault and to show the performance trends in different working conditions. At this stage, we only study this model with a fouling fault. In the future research, the next step is conducting a further study and a validation for the rest of the operating faults.

As the refrigerant cycle model is developed by understanding the process of physics and underlying principles. To build the physics-based models and determine their parameters, detailed knowledge of the system and its operation processes is necessary. In order to analyze the operating faults, this type of model require a specific analysis of impacts on thermodynamic diagram with an extensive equation system. It is necessary where we need a model with a high level of detail in the physical processes. In contrast, the experimental approach is quite simple in terms of the equation. We use it to analyze the impact of operating faults in different operating conditions as well as different fault ratios. With the objective of thesis about the studying the impact of operating faults with different fault ratios F on the heat pump performance trends, we chose the empirical model of Cho, 2014 instead of using the simplified refrigerant cycle model. This model is then combined with the refrigerant cycle model, if there is no information about the heat pump performance from the manufacturers. It is then integrated into the building model, to analyze hourly the evolution of operating faults and their impact on building energy consumption. It will be described in next chapter.

Chapter 4

Dynamic evolution of coupled building and heat pump simulation taking into account operating faults

This chapter presents heat pump modeling in building energy simulation COMETH, integrating the operating faults. It is a software developed by CSTB, is used in this research. It is a dynamic energy simulation with hourly time steps. It enables the calculation of envelope requirements and energy consumption for heating, cooling, domestic hot water, lighting, and auxiliaries such as pumps and fans. The simulation process in COMETH is described after we model the case study - a residential building in Paris with the building envelope and HVAC systems. Based on these information, we perform a dynamic energy simulation and analyze the energy consumption in a typical day and typical year. These results without operating fault are considered as the reference results, which helps us to characterize the impact of operating faults on the building consumption in the next step.

In order to analyze the impact of operating faults of the air-to-air heat pump on building energy consumption, we impose separately each operating fault into this model. As presented in last chapter about the operating fault impact on the heat pump performance, we used and added these new values COP and EER to the heat pump performance matrix in COMETH. At the beginning, the operating fault ratio is fixed. We then compare the heating and cooling energy consumption C_{ep} of the building with the reference results without operating faults in order to see the fault impact on building energy consumption. Then, as operating faults occur at any time and develop throughout the building life cycle, the operating faults with a dynamic fault ratio is presented. The dynamic fault ratio is calculated based on the statistic of fault evolution from the experiments, presented in section 2.3. Additionally, the Petri net is applied in this dynamic fault modeling in order to regulate the fault occurrence in time. The simulation process integrating the Petri net is described. Based on that, we conduct a one-year simulation of three operating faults with their fault evolution. The impact of operating faults on heat pump performance and building energy consumption at every time step during 15 years are presented and analyzed.

4.1 Coupled building and heat pump models – static fault ratio

4.1.1 The simulation process without fault illustrated for the reference case study

Description of the case study

The case study is about a 112m² residential three-bedroom building for four people located in Paris. The surrounding residential neighborhood contain mature trees and no other buildings. The plan of the building is shown in Fig.4.1, and its characteristics are presented in Table 4.1.



Figure 4.1: The reference residential building plan

Table 4.1: Building characteristics

Description	Parameter	Unit
Dimensions: Length/Width/Height	12.9/8.7/2.8	m
Roof (200 mm insulation + 25mm brick) U-value	0.24	W/(m ² .K)
Ground floor (240 mm concrete + 20mm insulation) U-value	0.24	W/(m ² .K)
Exterior wall (300 mm concrete + 12.5 mm exterior insulation)	0.35	W/(m ² .K)
Interior wall (20mm brick) U-value	1.13	W/(m ² .K)
Door U-value	2.5	W/(m ² .K)
Window (double glazing) U-value	1.5	W/(m ² .K)
Permeability	0.6	m ³ /(h.m ²)
Thermal bridge between 2 verticals facades	0.2	W/(m.K)
Thermal bridge between facades and ceiling	0.72	W/(m.K)
Thermal bridge between facades and floor	0.646	W/(m.K)
Thermal bridge between wall and window	0.51	W/(m.K)

The thermal transmittance of exterior wall U-value is $0.35 \text{ W}/(\text{m}^2.\text{K})$, of floor/roof U-value is $0.35 \text{ W}/(\text{m}^2.\text{K})$ which follow the regulatory level, depending on the climate zone. For example, the thermal transmittance of exterior wall and floor/roof in Paris (H1A region) must be less than or equal to the regulatory level of $0.5 \text{ W}/(\text{m}^2.\text{K})$ and $0.37 \text{ W}/(\text{m}^2.\text{K})$ respectively. The lower the U-values, the lower the affection of outdoor conditions to space heating or cooling. Besides, in order to avoid the heat loss throughout the windows and doors, they must be insulated so that the thermal transmittance U-value must be less than or equal to the given maximum level of 1.9 and $2 \text{ W}/(\text{m}^2.\text{K})$. The building airtightness of the envelope and driving forces, such as wind, inside/outside temperature differences, and air pressure differences resulting from mechanical ventilation is $0.6 \text{ m}^3/(\text{h}.\text{m}^2)$.

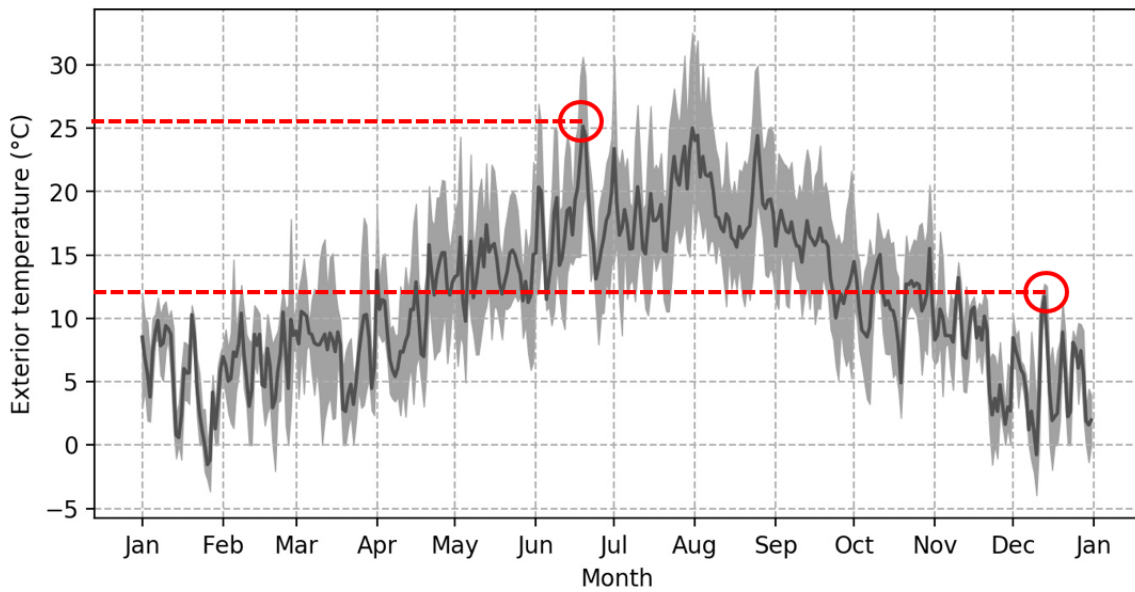


Figure 4.2: Daily exterior temperature in the conventional weather data for H1A region

The studied building is located in Paris (H1A region), which experiences mostly mild weather across four distinct seasons. We chose the conventional weather data from the French thermal regulation RT2012, which is presented in Fig.4.2. The black line shows the daily average exterior temperature, and the grey area shows its daily variation. The maximum daily temperature is around 12.3°C in the winter, and 25.6°C in the summer. July is the hottest month of the year with an average temperature of 19.4°C , and January is the coldest month, with an average temperature of 3.3°C .

When the building is occupied, the heating and cooling setpoints are given from the RT2012 standard, respectively 19°C and 26°C . Additionally, these setpoint temperatures are 16°C and 30°C when the building is unoccupied. Between both temperatures, the building is in free floating conditions. The occupation profile is referred to the residential occupancy RT2012, in which the building is occupied from 17:00 to 9:00 of the following day during the week and whole weekend. Based on the above information about the building structure, the weather data and setpoint temperatures, an analysis of building energy demand is conducted and shown below. Fig.4.3 shows that the studied building is heated from September to April and cooled for the rest of the year, from June to September.

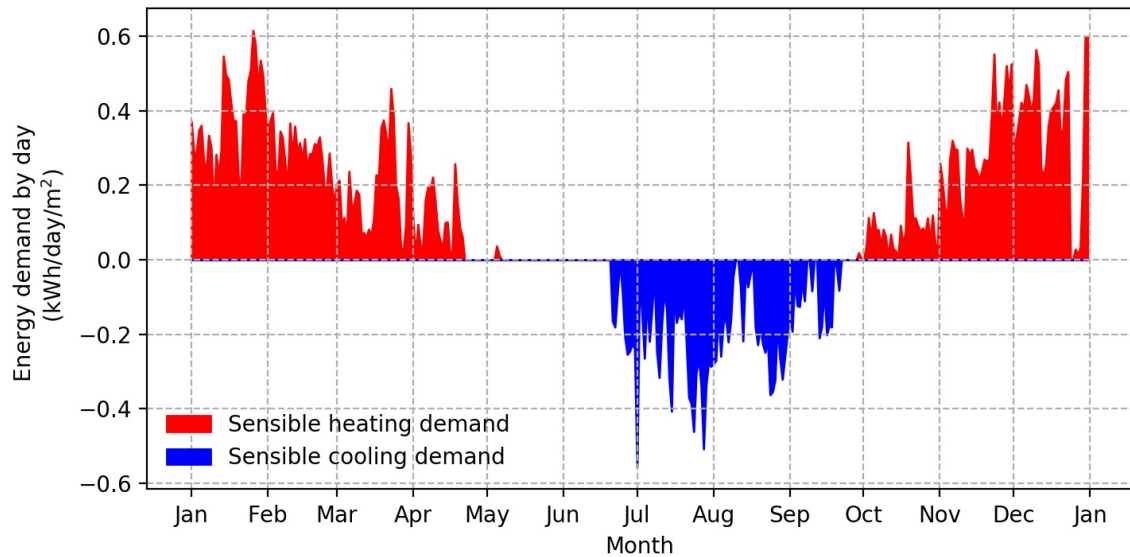


Figure 4.3: Sensible energy demand of the studied building (kWh/m²/day) for heating (red) and cooling (blue)

As presented in Fig.4.3, the maximum heating and cooling demand per day are respectively 0.62 kWh/m² (January 26) and 0.56 kWh/m² (July 1). The peak-power demand of the building for the heating season and the cooling season is 4637 W (interior air temperature $T_{ai}= 19^{\circ}\text{C}$ and exterior air temperature $T_{ae} = -0.7^{\circ}\text{C}$), and 5859 W (interior air temperature $T_{ai} = 28^{\circ}\text{C}$ and exterior air temperature $T_{ae} = 30^{\circ}\text{C}$), respectively. Regarding the heating and cooling system, a reversible heat pump air-to-air FVA71A with the refrigerant R-410A is used. Its dimension Height x Length x Width are 1800 x 600 x 270 mm. Its performance are supplied from the manufacturers, for example COP=3.64 and EER = 3.37 , and compressor power $W = 2.06$ kW and 2.02 kW (Daikin, 2019) at the nominal temperatures $T_{int}=20^{\circ}\text{C}$ and $T_{ext} = 7^{\circ}\text{C}$, and $T_{int}=27^{\circ}\text{C}$ and $T_{ext} = 35^{\circ}\text{C}$, respectively. Concerning the domestic hot water, the individual boiler is equipped. The average domestic hot water demand is assumed as 28 l/person/day at 60°C. Concerning the ventilation, the natural ventilation by opening the window is concerned generally. However, in order to eliminate odors and remove the moisture, mostly in kitchen and bathroom, the minimum ventilation requirements for dwellings consisting of one living room, one kitchen, three bedrooms, one restroom and one bathroom, the specific volume airflow in the nominal condition and at peak point are $Q_{v,base} = 90$ (m³/h) and $Q_{v,peak} = 165$ (m³/h), respectively. Based on the current building envelopes and HVAC systems features described above, there is still a lack of information for a whole building simulation. Some of the parameters were assumed as follows, for example the lighting is assumed as 1.4W/m², the internal heat gain is 10 W/m².

Simulation process

The above information about the building construction records, local climate data, occupancy, internal load, HVAC, and lighting equipment in the last section are considered as the input data in COMETH . They are presented in different blocks in Fig.4.4 as envelope,

weather data, scenario and energy systems respectively. Fig.4.4 generally shows the input and output for a dynamic building simulation in COMETH.

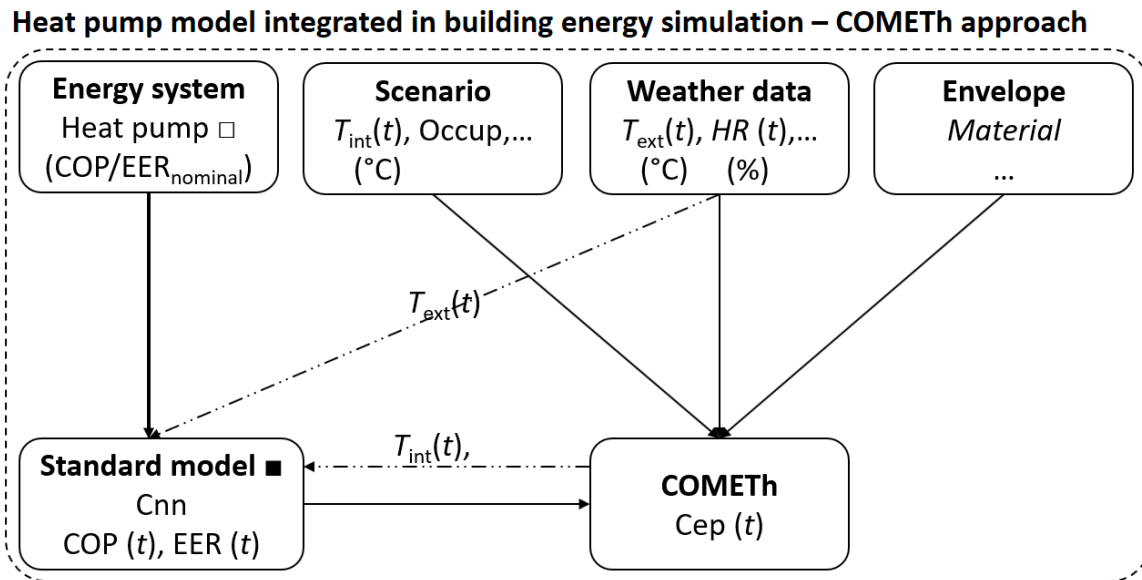


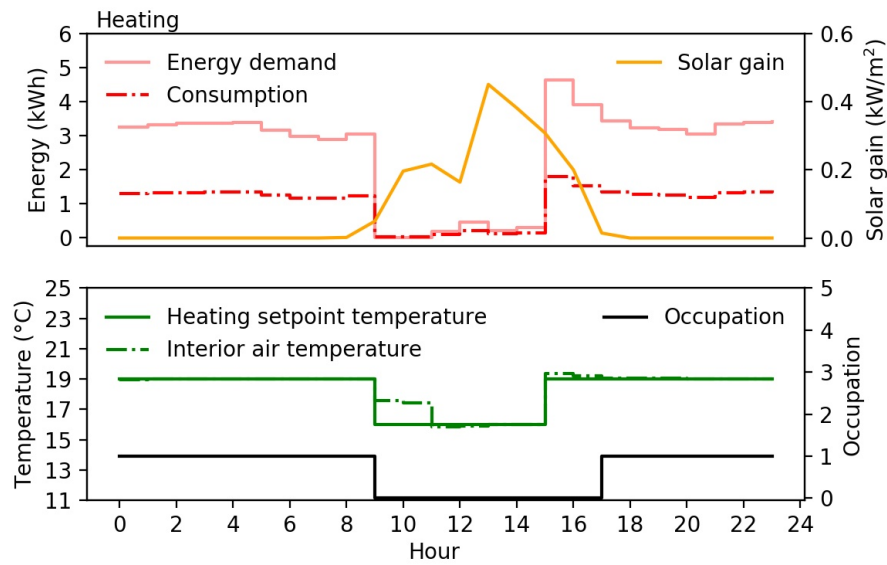
Figure 4.4: Simulation process in COMETH

Concerning the energy system, we focus on the heat pump model. The heat pump simulation in COMETH uses the empirical model from standard EN 15316, presented in chapter 2. As the outdoor temperature T_{ext} from weather data and the interior temperature T_{int} from COMETH evolve in times, the heat pump performance $COP(t)$, $EER(t)$ are therefore calculated at every time step. With all input data and the performance of HVAC systems, we perform a building performance analysis. Among three performance indicators, for example, the annual overall primary energy consumption Cep , the energy demand related to the building envelope, and the summer comfort [CSTB, 2012], we focus only on the first indicator in this study. The reference case as the building simulation without operating fault of the heat pump is presented below to show an energy consumption analysis in COMETH during one typical day and one year.

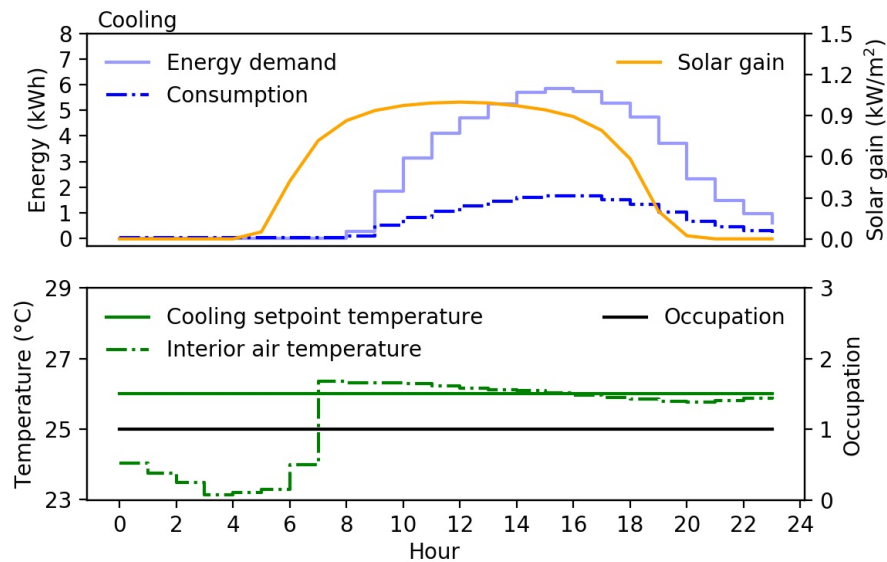
Results of the reference case study

As presented in Fig.4.3 about the energy demand in the studied building in Paris, January 26 and July 1 are two days with the highest energy demand for heating and cooling, respectively. Fig.4.5 shows the energy demand and energy consumption evolution during highest heating demand day (January 26) and highest cooling demand day (July 1) in Paris.

As presented in last chapter, the heating/cooling demands of the building, which is presented as the solid line (red for heating and blue for cooling), are calculated based on the building physics characteristics, the occupant scenario (black line) and the weather data as the exterior temperature, the solar heat gain (yellow line). Concerning the heating/cooling consumption, the heat pump operates adapting to the setpoint temperatures (green line) in order to reach occupant thermal comfort in the building. The energy consumption, such



(a) Highest heating demand day (January 26)



(b) Highest cooling demand day July 01

Figure 4.5: Energy demand, energy consumption of the studied building

as heating and cooling load quantities, is resulted, which is presented in the red and blue dash-dot line, respectively, in Fig.4.5.

Regarding the highest heating demand day (January 26, Fig.4.5a), the heating setpoint is 16°C from 9 am to 5 pm (no occupancy), and 19°C for the rest of the day (occupancy period). Because of thermal losses through building envelopes, the heat pump has to work more in order to reach the demand temperatures. Or, it has to work before to ensure the demand temperature for occupants. Based on the heat pump design standard NBN EN 12831:2003, as the building insulation is average ($U = 0.35 \text{ W/m}^2\text{K}$), the expected drop in interior temperature is 2°C, so the dwell time tolerated of heat pump to reach the occupant comfort can be chosen as 2 hours. It means, the heat pump will start 2 hours before the arrival of occupants. Or, the heating setpoint is set at 19°C at 3 pm. During the period from

9 am to 3 pm, the building is unoccupied, the heating setpoint is 16°C. As the interior air temperature is still over 16°C, heat pump does not work. During the day, the solar heat gain (yellow line) increases thanks to the increase of the incident solar irradiance. In the midday, the total solar heat gain decreases, from which the interior air temperature is lower at 16°C. The heat pump therefore starts to work in order to maintain the interior air temperature is at least 16°C. This leads to a small peak of energy demand and energy consumption at midday.

Regarding the highest cooling demand day (July 1, Fig.4.5b) which is the weekend, according to the occupation profile, the cooling setpoint is therefore 26°C for the whole day. From 5 am, sun rises and the total solar heat gain (yellow line) starts increase up to 0.92 kW/m², which leads to the increase of the air interior temperature. Before 7 am, since the interior air temperature is still below 26°C, for example, it varies between 23°C and 26°C during the night, the building has therefore no cooling demand. As soon as the air interior temperature is over 26°C because of the increase of the total solar heat gain, the heat pump begins cooling the building and maintain the air interior temperature at the 26°C cooling setpoint. For example, at 7 am, the air interior temperature increases up to 26.36°C, the heat pump starts working until midnight to reach the thermal comfort for occupants. As the solar heat gain decreases, the cooling demand decreases, which leads to the decrease of cooling consumption. Fig.4.6 shows the energy consumption of the building in Paris throughout the conventional year.

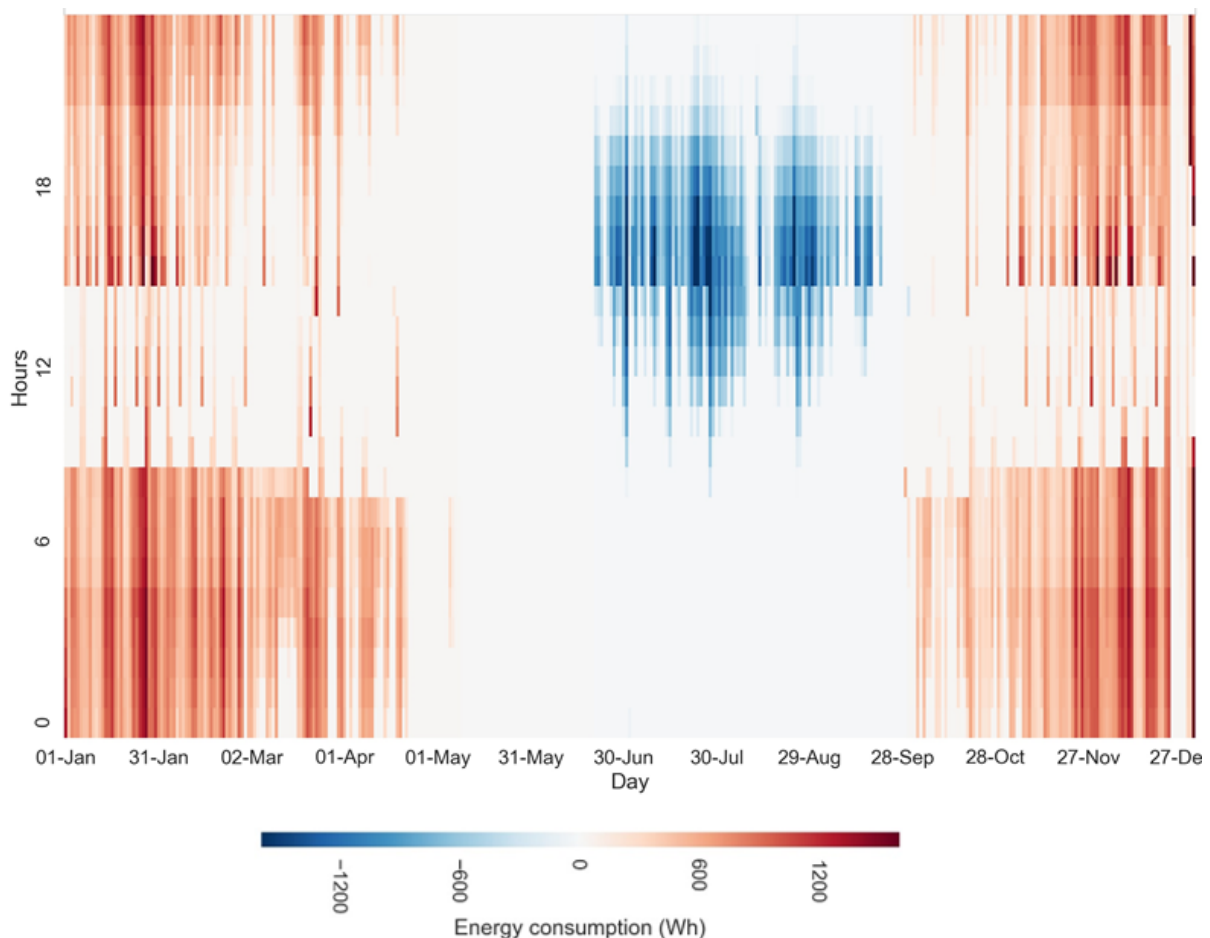


Figure 4.6: Energy consumption of building in Paris throughout the typical year

Heat pump works in heating mode from October to April and in cooling mode for the rest of the year, from June to September. As can be seen in the typical year analysis Fig.4.6, the building occupancy is clearly visible from the heating and cooling consumption during week days, which corresponds to the occupancy scenario from evening (17:00) till the early morning (9:00). Weekends are also clearly identified as the heating or cooling setpoint is set for a full day occupancy. However, we can also notice heating and cooling consumption sometimes during unoccupied periods between 9 am and 3 pm. This energy consumption corresponds to high heating or cooling loads, when the minimum or maximum setpoints are exceeded. This is more often the case during summertime, due to the high solar gains during the daytime unoccupied periods. Also, we can notice there are two periods, for example, the first week of August (during summer) and two middle weeks of December (during winter), the building is not cooled and heated. This corresponds to the occupation profile, which is the vacation week. The heating and cooling consumptions are one part of building energy consumption, which covers also the lighting, ventilation, hot water production, and auxiliaries (pumps and fans). Fig.4.7 shows the energy consumption share of the studied building in two seasons, winter (October to April) and summer (June to September).

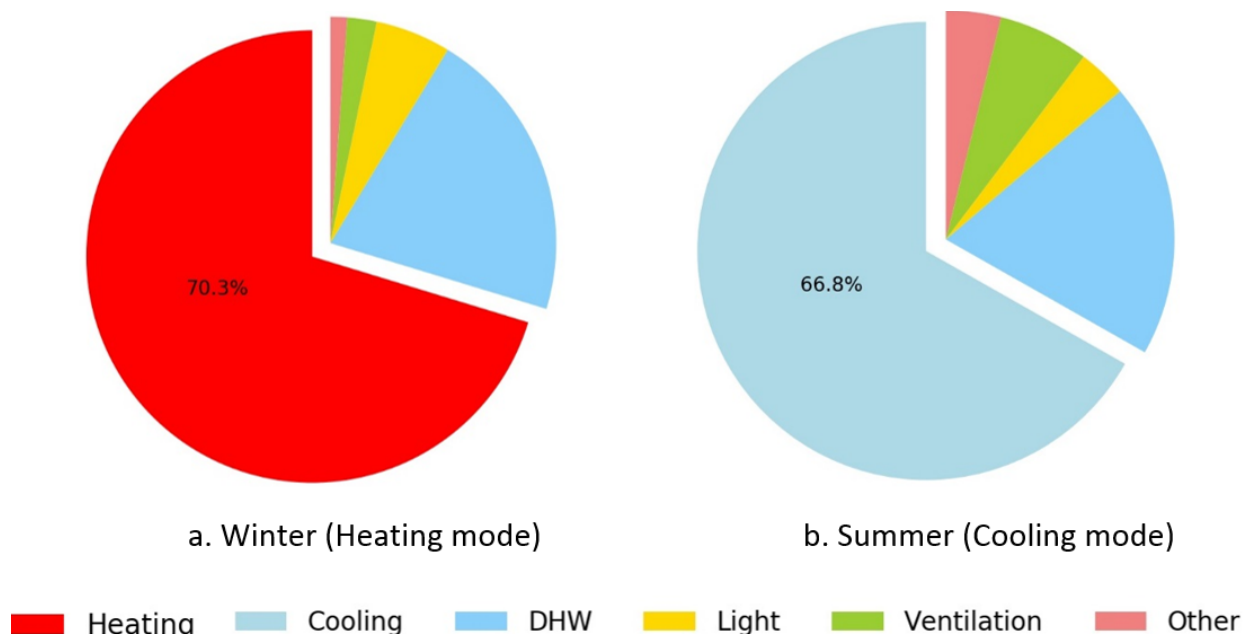


Figure 4.7: Share of energy consumption in the case study in two seasons

The heating and cooling consumption accounts for nearly 70% of the total energy consumption in the studied building during the winter and the summer, respectively. If there is any change in heating and cooling consumption, the energy consumption in building will be impacted considerably. In fact, COMETH conducts a building analysis for one year and it considers that HVAC systems are ideal. They always work in a good state during their life cycle, for example, 15 years – the average lifespan of a heat pump. However, in reality, during its lifecycle, the heat pump operates differently because of operating faults, the change of working environment, the energy consumption, therefore, evolves differently. In its current form, COMETH does not take into account the operating faults. In the next part,

we show how to model an operating fault in COMETH.

4.1.2 The simulation process with a static fault ratio

In order to integrate the operating faults in COMETH, we initially impose the operating fault with a static fault ratio in the heat pump model, which is presented in the top right box of Fig.4.8.

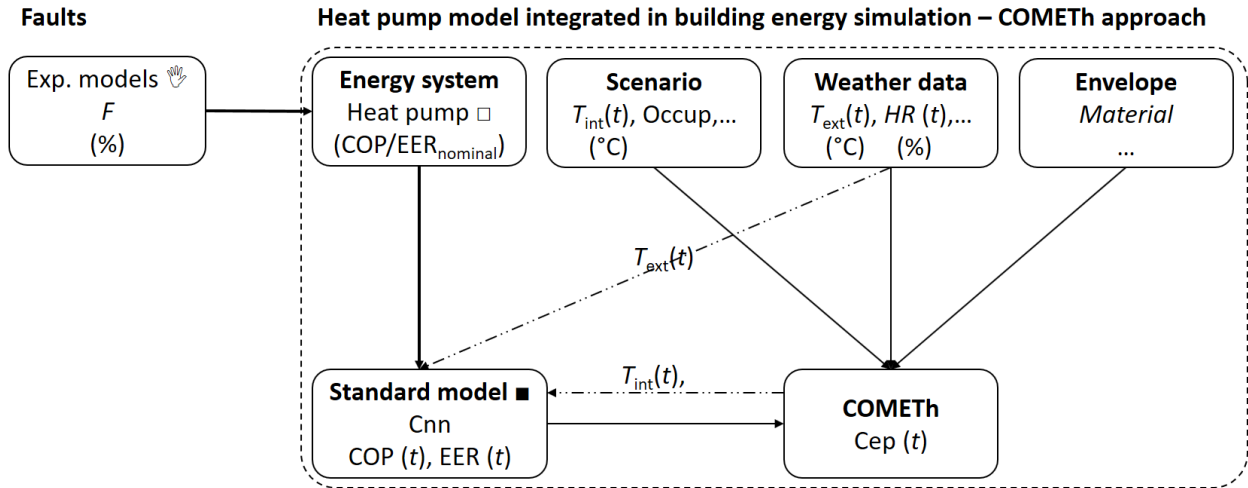


Figure 4.8: Integration of fault in COMETH

The simulation process in COMETH in Fig.4.8 is nearly the same as the one in the simulation without fault. There is only one difference in the nominal performance of the heat pump. COP/EER_{nominal} is modified when an operation fault appears. As discussed in the chapter 3, the refrigerant cycle model recalculates the heat pump performance when there is an operating fault with a static fault ratio F (%). Using the same simulation process as before, we conduct an energy consumption analysis during one typical day in summer and winter with an operating fault. We analyze different scenarios of operating faults. For example, three fault ratios F of 10% - 20% and 30% are imposed on the simulation. Then, we conduct a simulation by combining three studied faults, with different fault ratios F . This simulation helps us to analyze the impact of fault individually and collectively on the building energy consumption. Finally, a one-year simulation with operating fault in COMETH is conducted.

Impact of fault on energy consumption during 1 hottest and coldest day

Three operating faults as interior fouling, exterior fouling, and refrigerant leakage, are intentionally introduced into the refrigerant cycle model. Based on the reference case without fault, each operating fault with three different fault ratios F is added and simulated individually. Heat pump performances COP and EER under the fault operations are compared with those in the normal operation. From this comparison, we can discover the evolution of some parameters. The simulation results of three studied faults are presented in Fig.4.9.

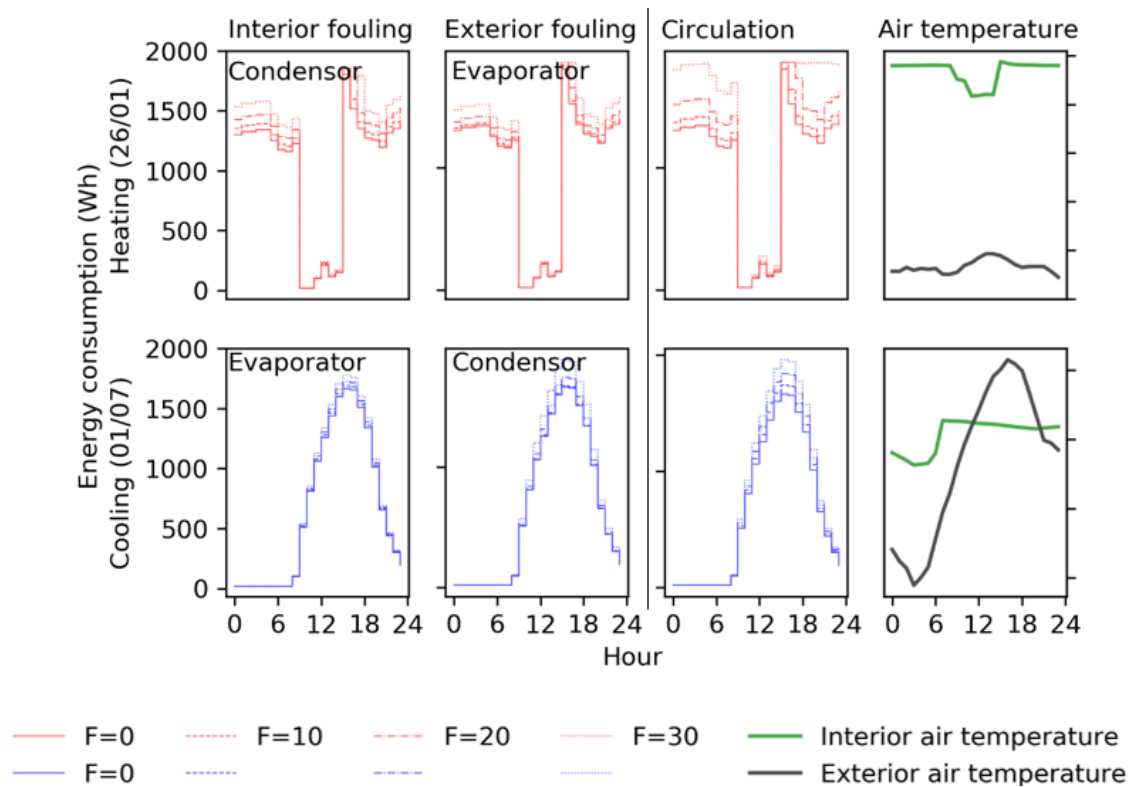


Figure 4.9: Impact of operating faults on building energy consumption during one hottest and coldest day in Paris

Fig.4.9 shows the impact of three operating faults on the energy consumption during one hottest and coldest day under different fault levels F from no-fault (continuous line) to 10% (long dash line), 20% (dot-dash line), and 30% (dash line). Obviously, in order to reach the setpoint temperature, the building energy consumption increases with the increase of the fault level. However, the heat pump has more severe effects in winter than in summer. As presented in the last chapter, as the COP is more affected than EER at the same fault ratio F (%), the heating load increases more than the cooling load. The evolution of energy consumption is not linear with the increase of fault level of each 10%. Regarding the interior fouling, the heating load increases 3.79%, 5.40%, and 7.33%, respectively, when the fault increases from 0 to 10%, 10% to 20%, and 20% to 30%. As the fault ratio increases, the component is impacted physically, which leads to the degradation of its performance quickly.

Among three faults, refrigerant leakage shows the most critical impact on the energy consumption of the building. On the one hand, concerning the heating consumption increase during one day at the same fault level of 30%, the impact of exterior fouling, interior fouling, and refrigerant leakage is respectively 12.60%, 17.41%, and 37.87%. On the other hand, at the same fault level of 30%, refrigerant leakage increase by 16.40% the cooling consumption, followed by 12.36% from exterior fouling and 5.92% from interior fouling. The refrigerant plays an essential role of refrigerant in circulation. As the fault level increases, which means there is a lack of refrigerant in the circulation, it results in improper operating refrigerant pressures, particularly too low, loss of cooling capability, overheating of the

compressor motor, as presented in chapter 2. Additionally, it also impacts the efficiency of other components, which leads to the excessive degradation of heat pump general performance and energy consumption of the building. Concerning the heat exchangers, as we can see from Fig.4.9, the impact of the condenser is more critical than the one of the evaporator. When the coil fouls by 30%, heating and cooling load increases respectively by 7.33% and 12.36% if the coil is the condenser and by 6.85% and 5.92% if the coil is the evaporator. The fault impacts on building energy consumption during one typical day are presented. We now take a look on their impact during one typical year, which is shown in Fig.4.10.

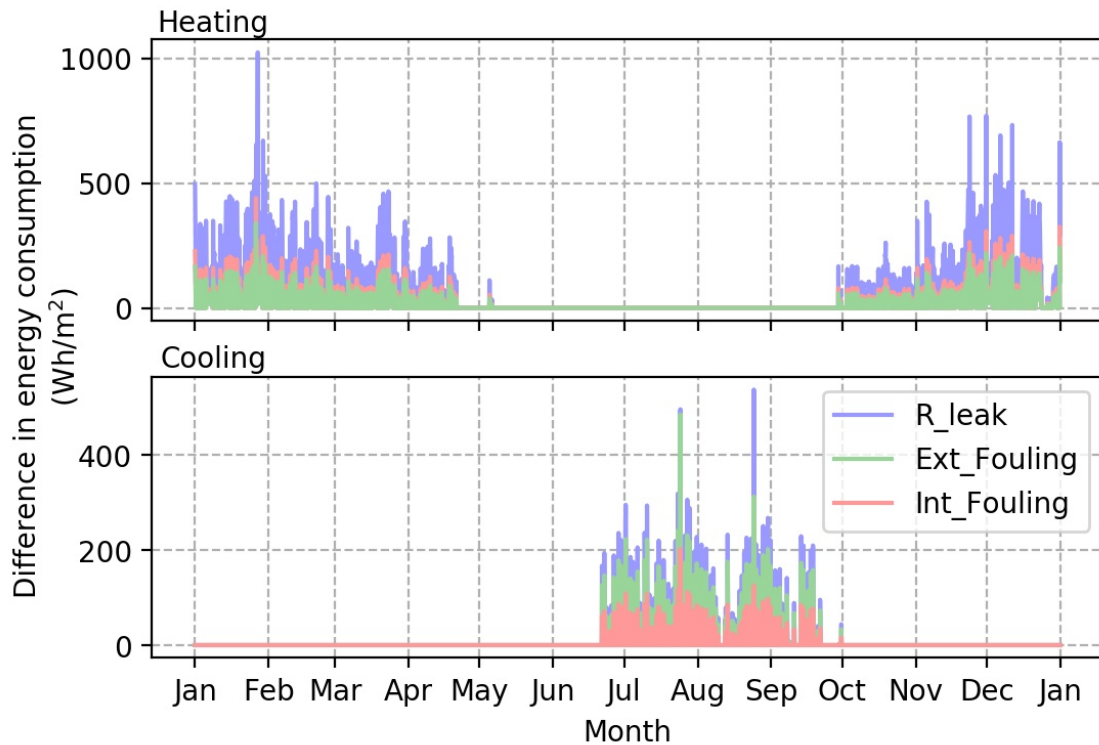


Figure 4.10: Building energy consumption difference between two cases $F=0\%$ and $F=30\%$ for three operating faults during one year

Among three operating faults, the refrigerant leakage always has the greater impact on the building energy consumption than the fouling faults, which leads to the greater difference between two cases: fault ratio $F = 0\%$ and $F = 30\%$. In conclusion, singly operating faults are imposed in the heat pump model. According to the results of this study, a refrigerant leakage of about 30% can result in an average 32% increase in heating consumption and 5% rise in cooling capacity. For interior and exterior fouling, a 30% reduction in airflow increased the average heating consumption by 15% and 10%, respectively. They make heat pump parameters deviate from the design values, which contribute to the decrease of heat pump performance and increase energy consumption.

Fault combination during 1 summer and winter day

Based on the above analysis of three separate studied operating faults, we now study the impact of these three faults if they occur simultaneously. We combine these three faults with

an imposed fault ratio F from 0 to 30%. For three operating faults, there are four combinations as following:

- Combination Int-Ext: Interior fouling and exterior fouling
- Combination In-Rleak: Interior fouling and refrigerant leakage
- Combination Ext-Rleak: Exterior fouling and refrigerant leakage
- Combination Int-Ext-Rleak: Interior fouling, exterior fouling and refrigerant leakage

We simulate the study case with different scenarios of operating fault during the coldest day in winter (January 26) and the hottest day in summer (July 01) in Paris. The results are presented in Fig. 4.10.

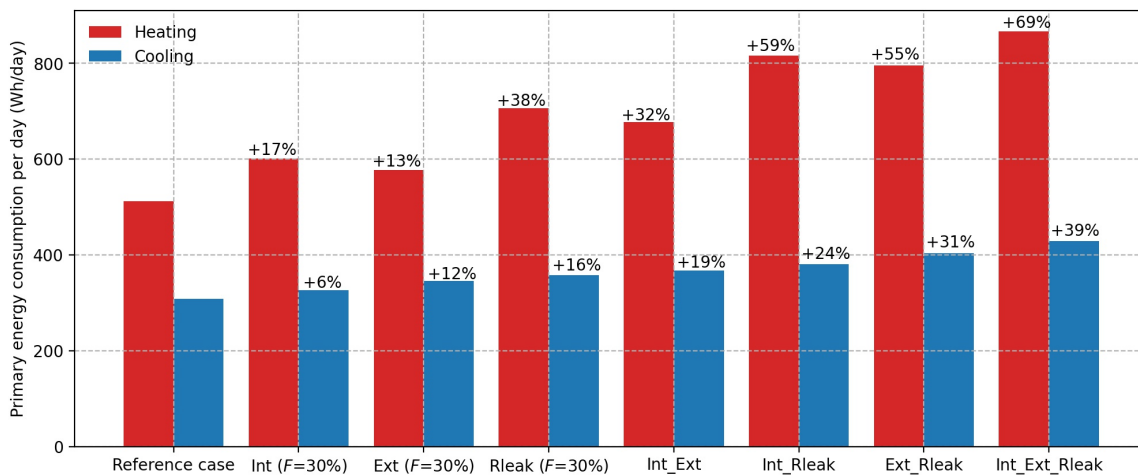


Figure 4.11: Impact of different combinations of three studied operating faults ($F=30\%$) on building energy consumption during one hottest and coldest day in Paris

Fig.4.11 shows the impact of three separate operating faults and four fault combinations on heating and cooling consumption during one hottest and coldest day in Paris. As expected, the collective impact of simultaneous faults on energy consumption varies and depends on the faults considered. In most cases, the collective effect can be described as exceeding additive. Indeed, it is approximately a little higher than the sum of each fault effect. For example, concerning the first fault combination of interior fouling and exterior fouling, the heating and cooling increases by 32% and 19% respectively, which is higher than the sum of each fault impact 17% (interior fouling) + 13% (exterior fouling) =30% and 6% (interior fouling) +12% (exterior fouling) = 18%. This can be explained by the fact that operating faults from one component can affect the efficiency of other components.

4.2 Integration of fault evolution with Petri net model

In order to integrate the dynamic fault ratio in COMETH, Petri net is used. We consider the fault evolution during the heat pump life cycle, around 15 years, and applied it in the Petri net model. It is shown in the top right box of Fig.4.12.

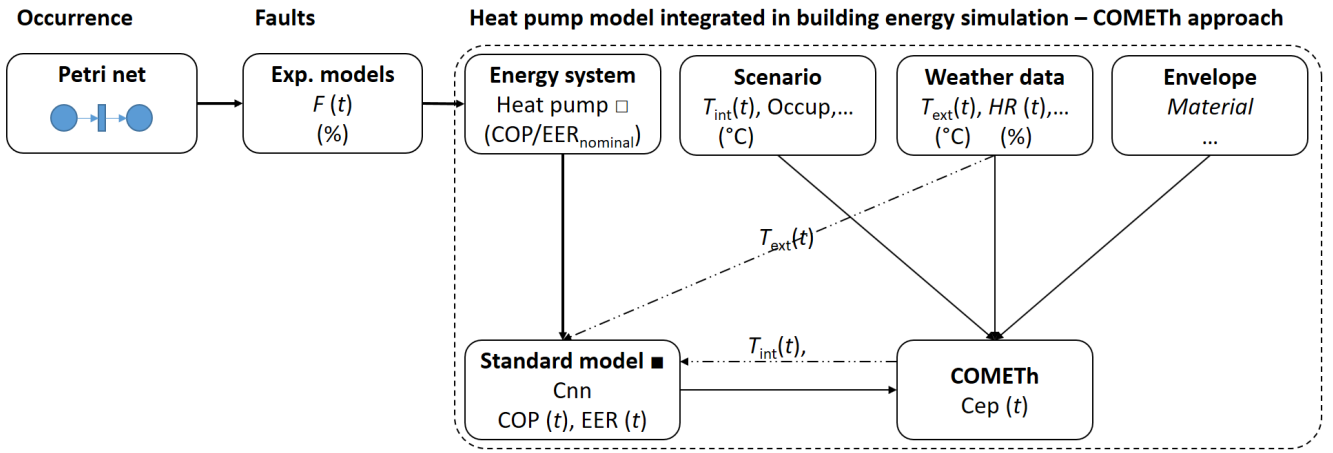


Figure 4.12: Simulation process in COMETH with the integration of Petri net

Fig.4.12 shows the simulation process with the integration of the dynamic fault ratio. This simulation process is nearly the same as the one in the simulation without fault and with a static fault ratio. One difference in this process is that the operating fault evolves in time, regulated by the Petri net. Based on the operation time of the heat pump and the characteristics of Petri net's components, particularly places and transitions, Petri net has different ways to model an operating fault, integrated the fault occurrence time. In this study, three relations of places and transitions are described below.

Firstly, as the heat pump works, the fault develops in time. The relation between time and fault evolution is presented in the Petri net model as below. The place characterizes the fault ratio in function of time, while the transition shows transition conditions ($\Delta t > \Delta t_0$) from one fault ratio to one higher fault ratio.

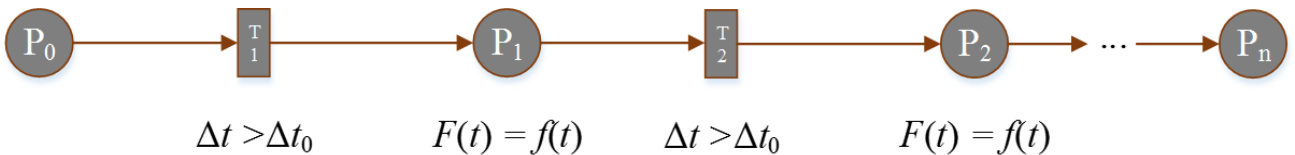


Figure 4.13: Petri net shows the relation between fault evolution and time

In this case, Δt_0 is defined as 0, one month, every two months, and one year. If the time step Δt_0 is too small (as 0, one month, every two months), the fault does not develop much, as presented in the experiments in section 2.3.1. The impact on the heat pump performance is less remarkable, and the building energy consumption is therefore not recognized. Besides, with this type of transition condition, the size of the Petri net will be bigger. In contrast, if time step Δt_0 is one year, the impact on heat pump performance and the energy consumption can be distinguished. However, this transition condition leads to a fault occurrence problem. Operating faults happen at any time during the building life cycle. The fault ratio cannot be updated at the right occurrence time. The heat pump performance and the energy consumption are therefore wrong evaluated.

Secondly, as the heat pump works, the fault develops in time, resulting in the degradation of heat pump performance. The relation between fault evolution and heat pump

performance is presented in the Petri net model as below. The place characterizes the heat pump performance (in this example, we consider the COP value) in the function of fault ratio, while the transition presents a transition condition ($\Delta F > \Delta F_0$) from one COP value to one degraded COP value.

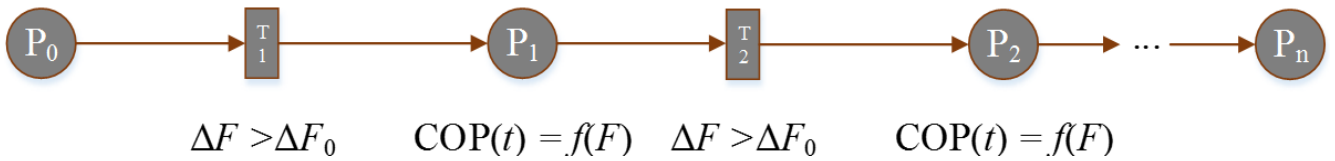


Figure 4.14: Petri net shows the relation between heat pump performance and fault evolution in time

In this example, ΔF_0 is defined as 1%, 2%, till 10%. If the fault ratio is considered every 1-2%, the heat pump performance does not develop much, as shown in section 2.3.2. Therefore, the building energy consumption is not recognized, and the size of the Petri net can be huge. In contrast, if the fault ratio is considered every 5-10%, the impact on heat pump performance and the energy consumption can be distinguished. However, this transition condition also leads to an evaluation problem of simulation results.

Last but not least, as the heat pump works, the fault develops in time, the heat pump performance degrades, the building energy consumption will increase in time, while maintain the setpoint temperature. The relation between heat pump performance and the building energy consumption is presented in the Petri net model below. The place characterizes the building energy consumption in the function of heat pump performance, while the transition presents a transition condition as $\Delta COP > \Delta COP_0$.

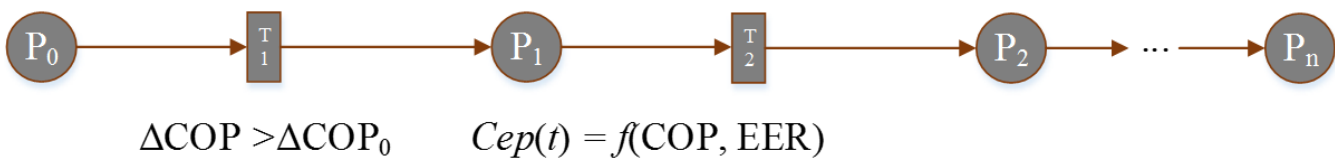


Figure 4.15: Petri net shows the relation between energy consumption of building and heat pump performance in time

In this example, ΔCOP_0 is defined as 1%. Considering the disadvantages of these two above transition conditions, we chose the difference of 1% of heat pump performance for this Petri net model. With this transition condition, we found that the energy consumption in the building can be distinguished, which resolves the disadvantage of these two above transition conditions. It helps us to see the relation between the theoretical occurrence time of the fault, fault ratio, heat pump performance, and energy consumption of the building. Based on the heat pump model, the fault ratio is calculated as the heat pump performance difference of 1%. Then, the occurrence time of fault can be defined using the relation of fault and occurrence time in experiments in section 2.3.1. We use the calculated value of fault occurrence time Δt_{ref} as a transition condition, which is more explicit. An example of the simulation process regulated by Petri net is presented in Fig.4.16 as following.

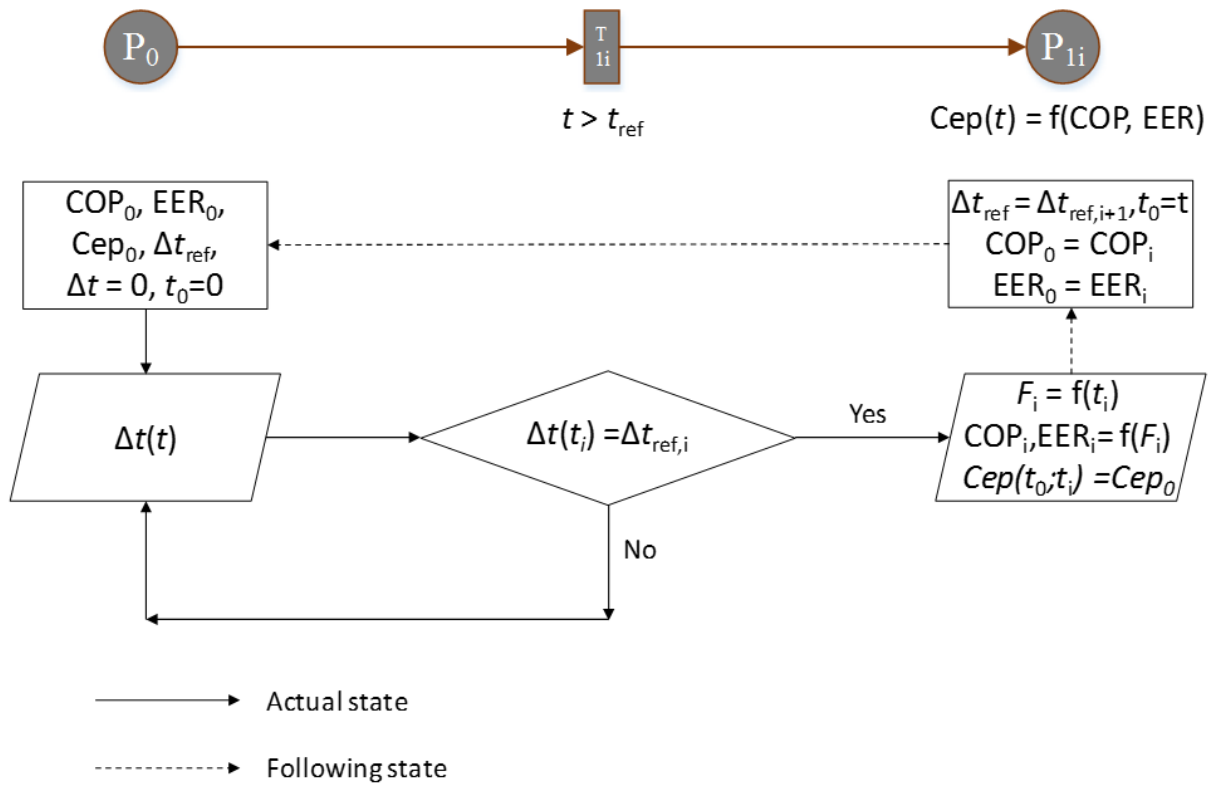


Figure 4.16: Petri net coupling with refrigerant cycle model and COMETH simulation

Fig.4.16 shows the Petri net model, which regulates the occurrence time of the operating fault. It is then integrated into the simulation process in COMETH in Fig.4.16. At the initial state $t_0 = 0$, the heat pump has no-fault $F = 0\%$, the nominal performance of the heat pump is COP_0 and EER_0 , and the building consumption is Cep_0 . The transition of Petri net as theoretical occurrence time t_{ref} is calculated before in chapter 2. In the beginning, the place P_0 has one token. As soon as the heat pump works, the fault evolves in function of time. However, as presented before, we consider the fault only when the difference COP is 1% or the occurrence time Δt_{ref} is reached out. At this step, the values of heat pump $COP(t)$, $EER(t)$ are calculated based on the nominal values COP_0 and EER_0 . When the occurrence time t_{ref} is reached, the transition condition is validated, and transition T_{1i} is enabled.

Consequently, the token from the input place P_0 is taken and then distributed to output place P_{1i} . At this moment t_i , the fault ratio F_i is taken into account to calculate the heat pump performance COP_i and EER_i and energy consumption of the building Cep in the next state. From t_0 to t_i , there is no fault, and the heat pump works normally. After t_i , the heat pump works under the fault condition F_i . These all simulations are coded with Python scripting language on the pyCOMETH platform. Using the same simulation process integrating fault with a defined fault ratio $F(\%)$, we calculate the heat pump performance at the nominal conditions, then the one-year simulation in COMETH is conducted.

4.2.1 Impact of an elementary operating fault

Three studied operating faults with a dynamic fault ratio F (%) are imposed individually in the building simulation. The dynamic fault ratio F (%) is defined based on the fault evolution, which the Petri net model regulates. A 15-year simulation of building energy consumption in COMETH is then conducted and analyzed.

Interior fouling

We assumed that there is only one interior fouling fault that can happen during 15 years. The Petri net regulates the occurrence time of interior fouling as follows.

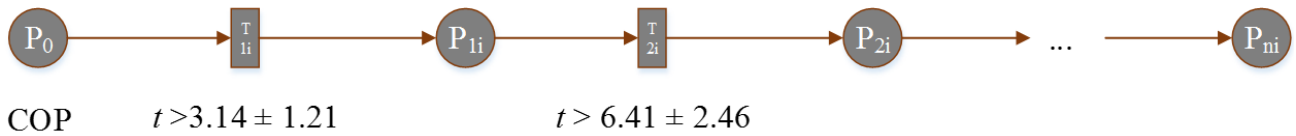


Figure 4.17: Petri net modelling for interior fouling during 15 years

Fig.4.17 shows the evolution of interior fouling fault during 15 years. The transition conditions are the occurrence time of the fault, which theoretically decreases the COP value by 1%. The number in each place and transition represents the status order of each fault. For example, T_{1i} represents the condition, which occurs before the T_{2i} . The fault occurrence time varies based on the dispersion of each fault, which is described in section 2.3.1. For example, as described in Fig.4.17, the interior heat exchanger can be fouled at 3.14 ± 1.21 years, which covers 68% all cases. Following the regulation process of the Petri net in the building simulation in Fig.4.16, a 15-year building simulation with the interior fouling is conducted, which is resulted in Fig.4.18.

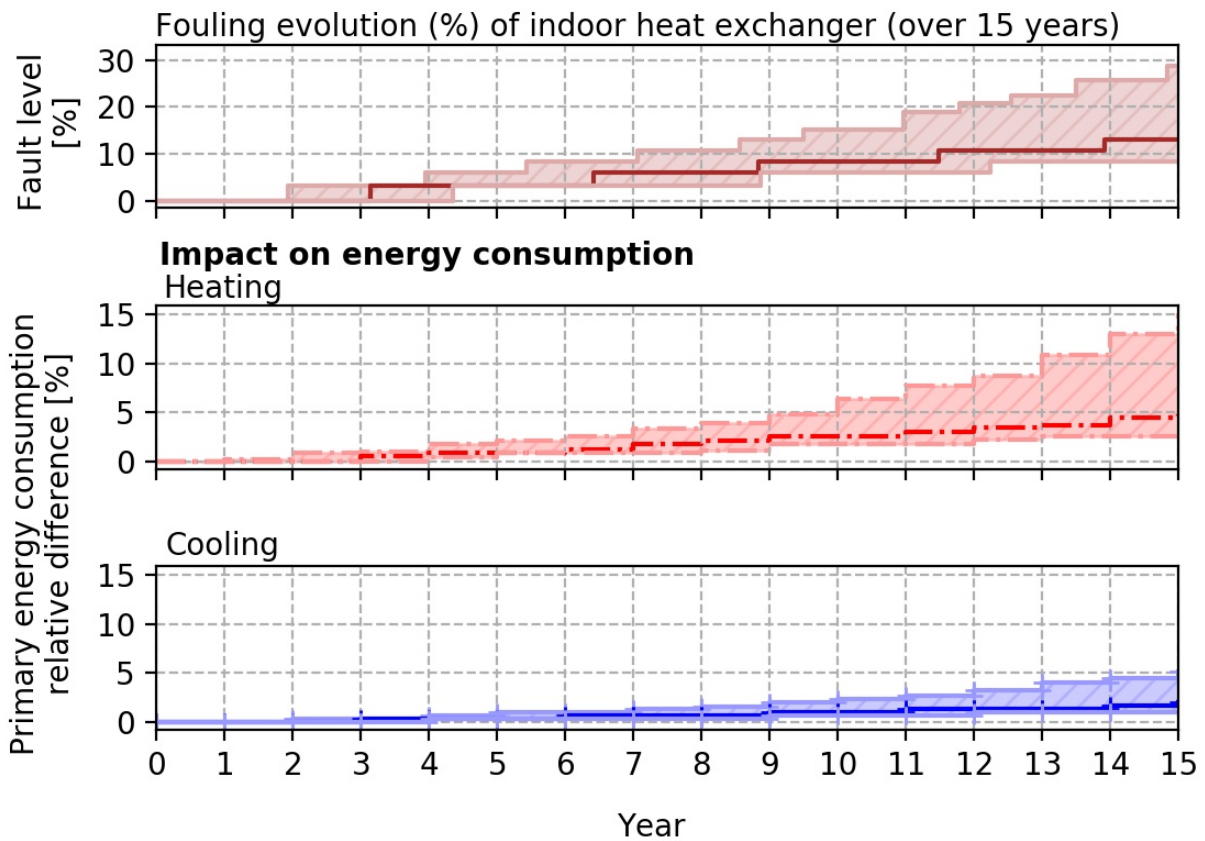


Figure 4.18: Impact of interior fouling on energy consumption during 15 years

Fig.4.18 shows the impact of interior fouling on energy consumption during 15 years. The upper figure shows the interior fouling fault ratio evolution with its range, while the two lower figures describe operating fault impacts on heating and cooling consumption in buildings. The Petri net model regulates the operating fault occurrence. As the fault ratio is changed, the heating and cooling energy of the building is recalculated from that moment. However, the Cep of heating and cooling is only calculated at the end of each year. Therefore, in Fig.4.18, we can only see the impact on heating and cooling consumption at the end of every year. Regarding to the normal distribution of fault evolution, the time dispersion $\sigma = 2.5$ years away from the fouling time $t = 6.5$ years, which represents 68.27% of the set. Fault can occur any time, between 4 years (as soon as possible) and 8 years (as late as possible), with different probabilities. In case that the fault happens at early as possible, for example 4 years, the probability is low. As the time evolves, the fault occur with higher probability. At the 15th year, in case that the interior fouling fault occurs as early as possible (lower probability), the energy building consumption in heating and cooling under the interior fouling is 14%-5% more than the reference case without fault.

The fault regulation of the Petri net model on the exterior fouling and the refrigerant leakage and their impact on building consumption are presented from Fig.4.19 to Fig.4.22.

Exterior fouling

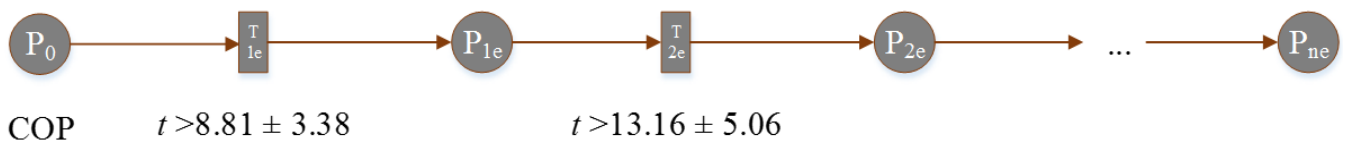


Figure 4.19: Petri net modelling for exterior fouling during 15 years

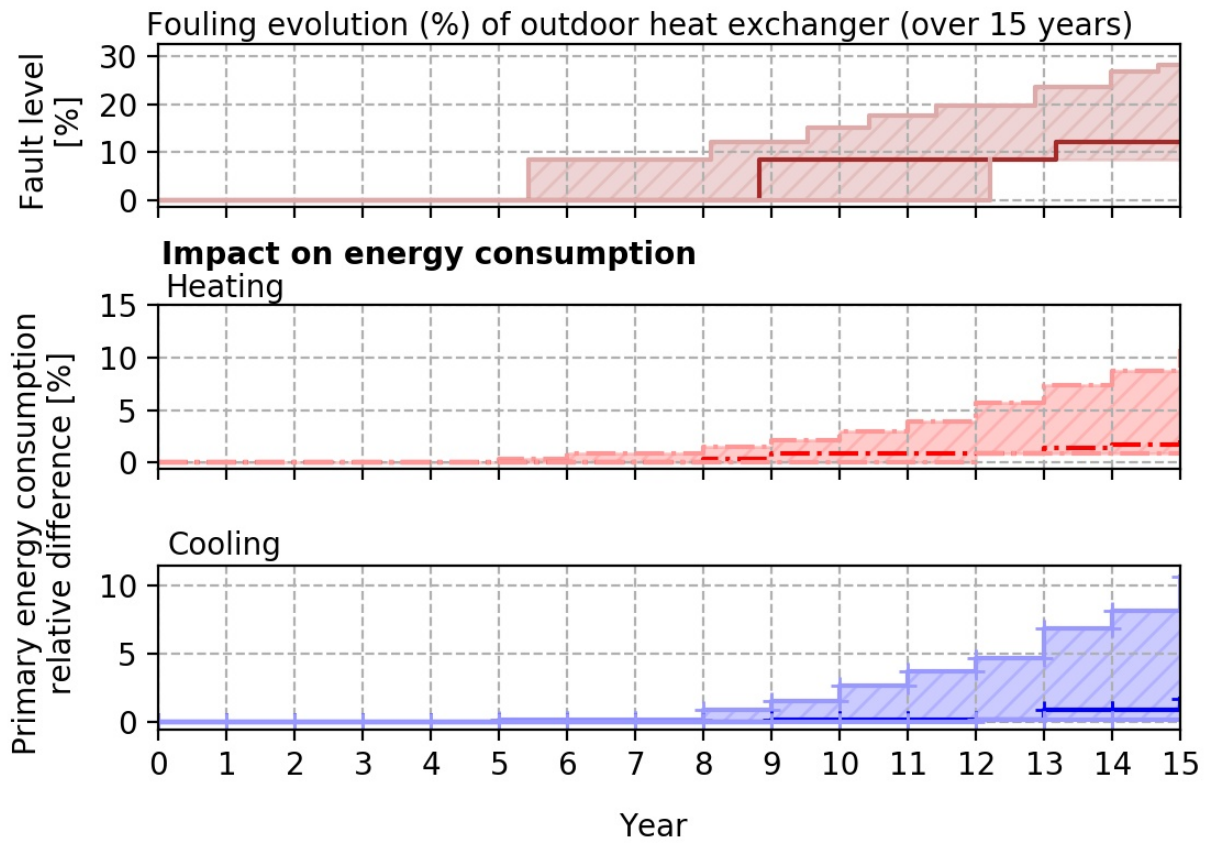


Figure 4.20: Impact of exterior fouling on energy consumption during 15 years

Refrigerant leakage

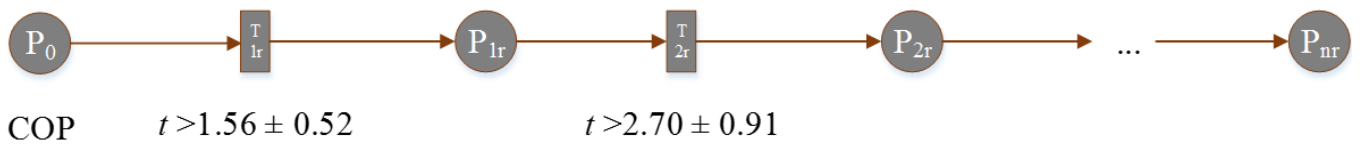


Figure 4.21: Petri net modelling for refrigerant leakage during 15 years

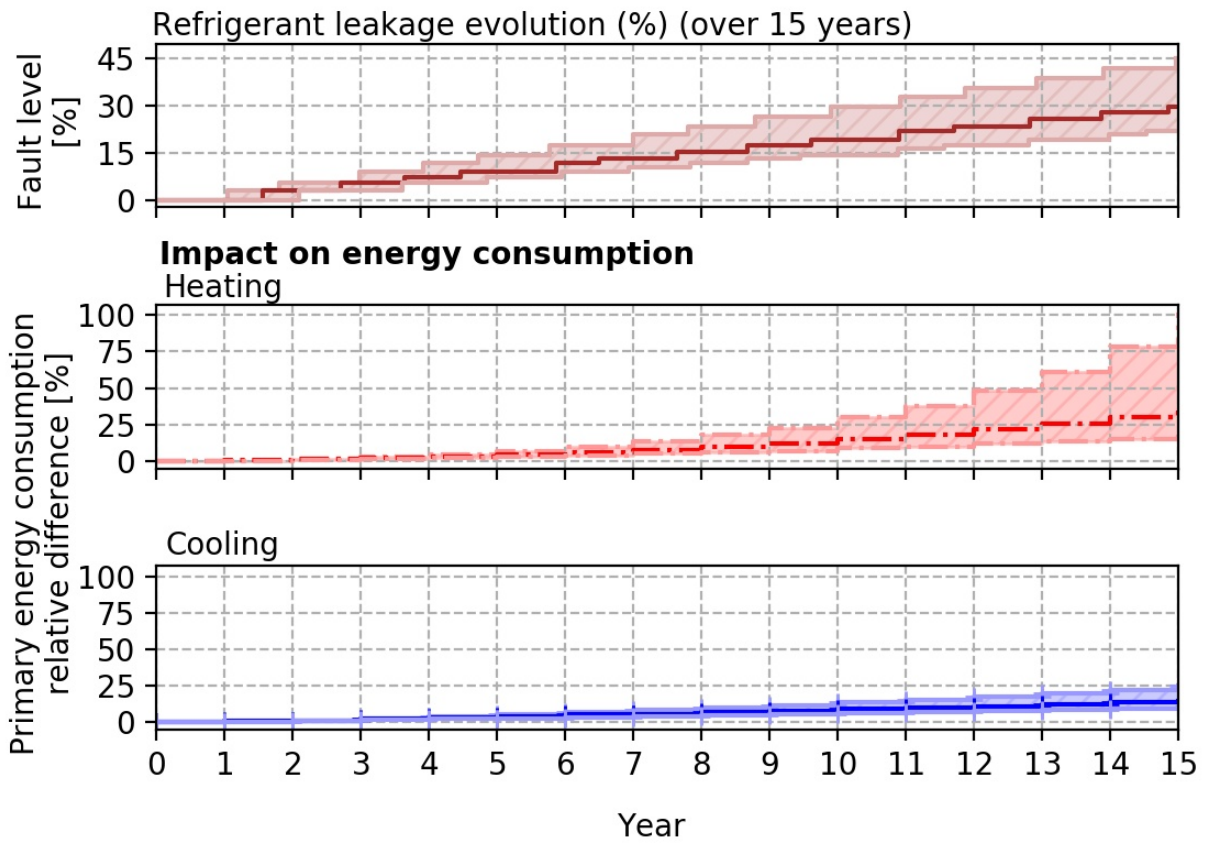


Figure 4.22: Impact of refrigerant leakage on energy consumption during 15 years

Fig.4.18, Fig.4.20, and Fig.4.22 present the impact of three operating faults on building energy consumption. There is a significant difference impact between the three faults. For example, at the same fault level, $F = 10\%$, the impact on heating and cooling consumption compared to the reference case of interior fouling, exterior fouling, and refrigerant leakage is 4%-2%, 2%-1.5%, and 10%-8%, respectively. At the 15th year, the energy building consumption in heating and cooling under the exterior fouling is 10%-9% more than the reference case without fault, followed by 14%-5% of the interior fouling, 80%-25% of the refrigerant leakage.

Besides, the air-to-air heat pump in our research has a more severe effect during long operations in winter. Mainly, if the operating fault is not prepared on time, the fault lasts longer, the impact on building energy consumption is more important.

4.2.2 Impact of fault combination

From the above analysis of three separate studied operating faults, we now examine the impacts of these three faults during 15 year-simulation. We consider if two or more faults occur during the heat pump life cycle. In this part, we can see all occurrence time abilities of operating faults regulated by the Petri net model.

Interior fouling and exterior fouling

We consider only two operating faults of the heat pump, which can happen during 15 years. For example, we take two operating faults of the heat exchanger: interior fouling and exterior fouling. The Petri net model regulates the occurrence time of these two faults, which is shown in Fig.4.23.

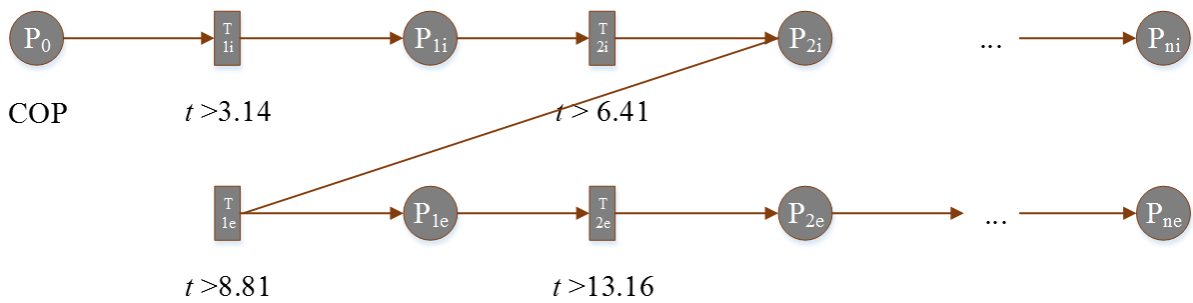


Figure 4.23: Petri net modelling for interior and exterior fouling during 15 years

Fig.4.23 shows the fault occurrence regulation of Petri net for interior fouling (i, upper line) and exterior fouling (e, lower line). Petri net takes into account the operating time t and shows the occurrence order of each operating fault. For example, as described in Fig.4.17, the interior heat exchanger is fouled at $t > 3.14$ years before the exterior heat exchanger is fouled at $t > 8.81$ years. At each state change of an operating fault, the fault ratio is recalculated and used for building energy simulation.

As discussed in section 2.3.1, the occurrence time of fault is varied, which is characterized by the dispersion of each type of fault. The operating fault can occur earlier or later than the fault experiment occurrence time, which means the occurrence time can be less or more than the average value. With the above example of two operating faults as interior fouling and exterior fouling, the Petri net model can show different scenarios of fault occurrence order, which is presented as follows.

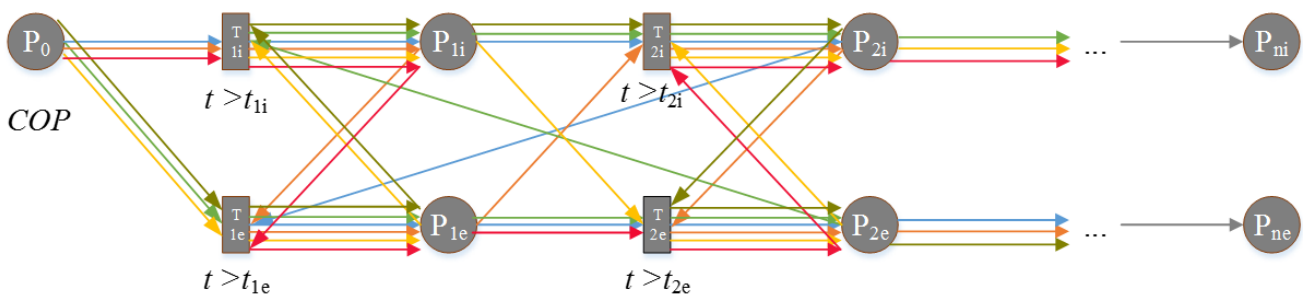


Figure 4.24: General Petri net graph of both fouling faults in heat exchanger of an air-to-air heat pump

Fig.4.24 shows the general Petri net graph regulating the occurrence time of fouling faults in heat exchangers, with two fault states P_1 and P_2 . Each color represents one scenario of fouling evolution and their combinations. Indeed, Fig.4.25 shows different scenarios of fault occurrence order of both fouling faults.

The Petri net in Fig.4.25 shows six possible fault occurrence orders for two operating faults with two fault states. With the multiple fault states during the heat pump operation, the Petri net is a good way to control its dynamic. With the average occurrence time t and its dispersion (section 2.3.1), we conduct a 15-year simulation in order to see how the Petri net model regulate the occurrence time of operating faults. The simulation results are shown in Fig.4.26.

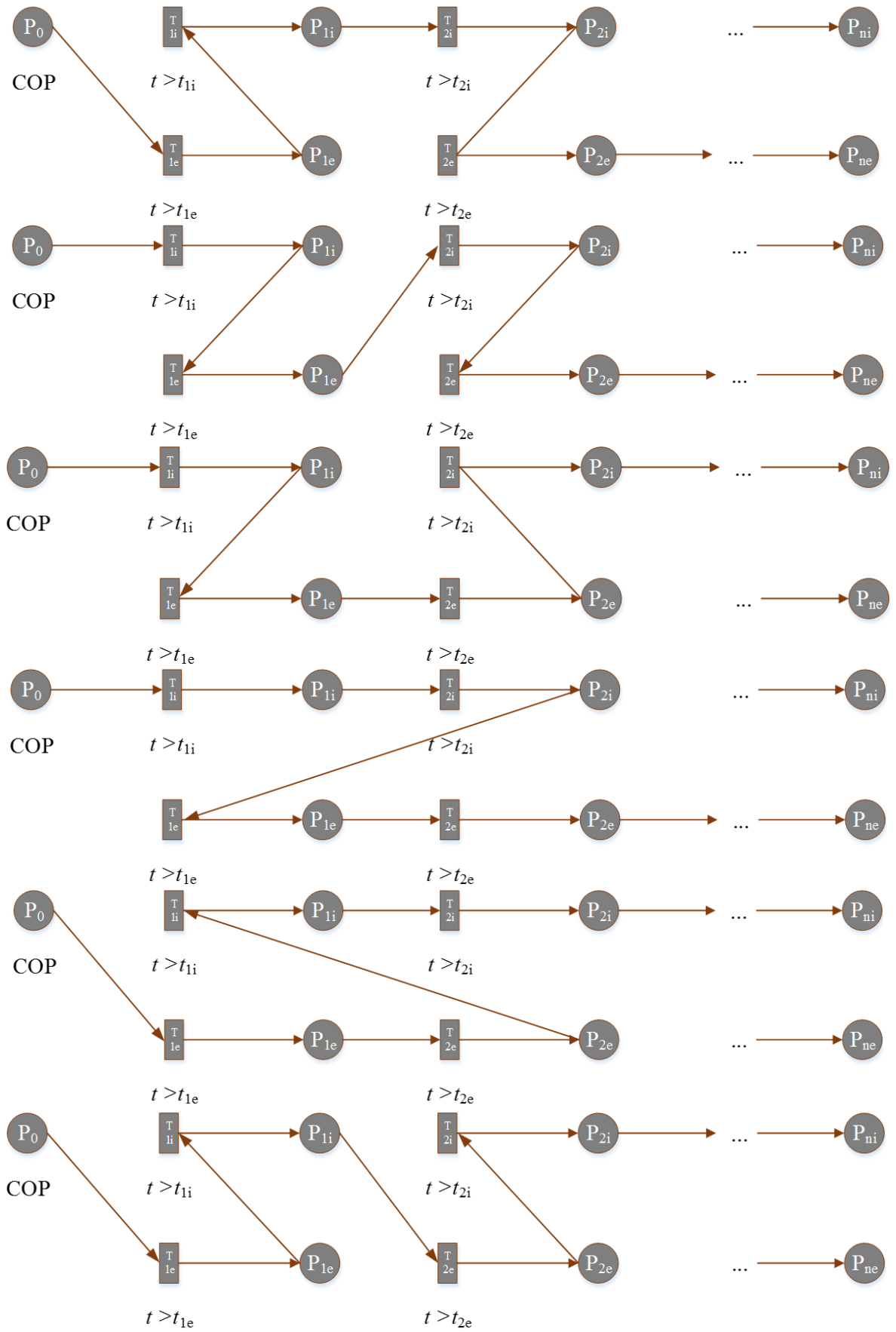


Figure 4.25: Detail Petri net graph of both fouling faults in heat exchanger of an air-to-air heat pump

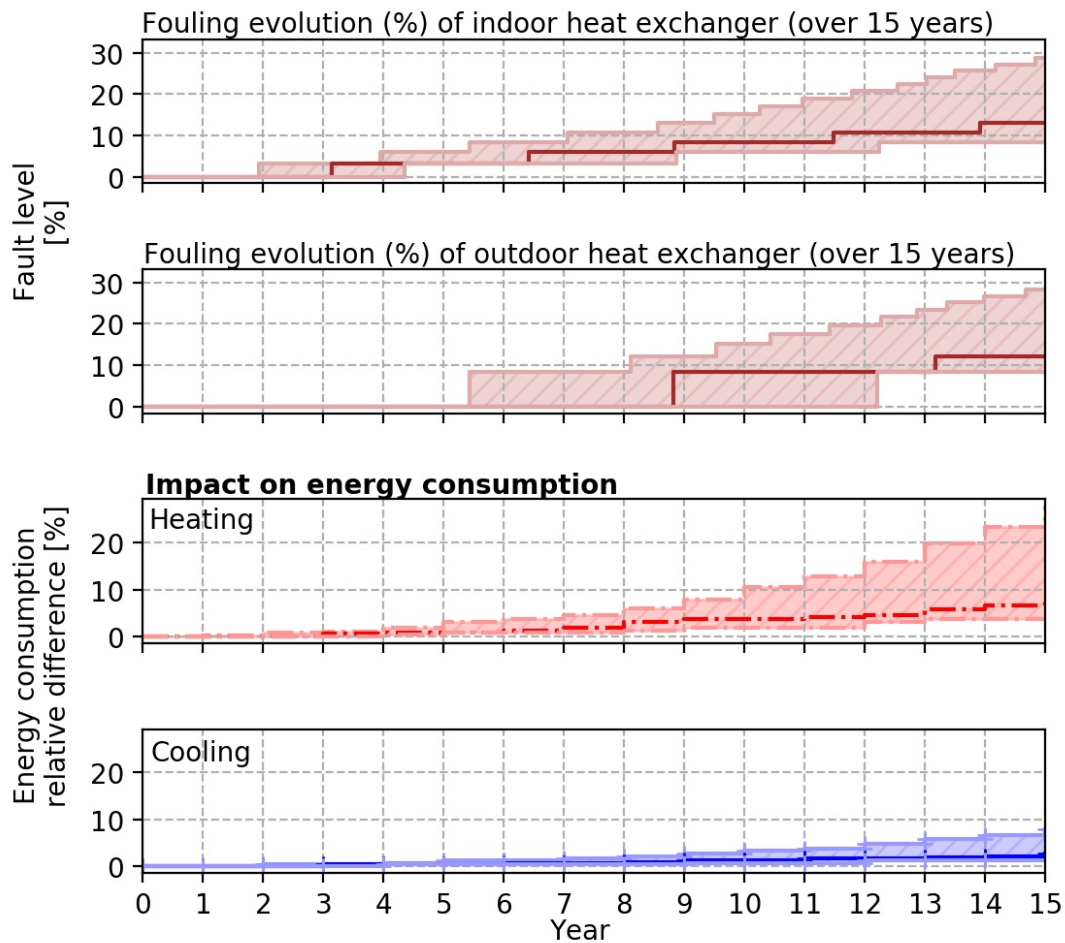


Figure 4.26: Impact of interior and exterior fouling faults on energy consumption during 15 years

Fig.4.26 shows the impact of the fault combination (interior fouling and exterior fouling) on heating and cooling consumption in buildings, corresponding to fault levels during 15 years. The first two upper figures show the dynamic fault ratio evolution with their dispersion, while the two lower figures describe the impact of fault on primary energy consumption. Concerning the fault evolution in the first two upper figure, there are difference scenarios of fault occurrence order of two operating faults. We take two extreme examples. The first one is when the faults occur as early as they can (Fig.4.27), while the second one occur as late as they can(Fig.4.28). These two cases with Petri net model are shown as below.

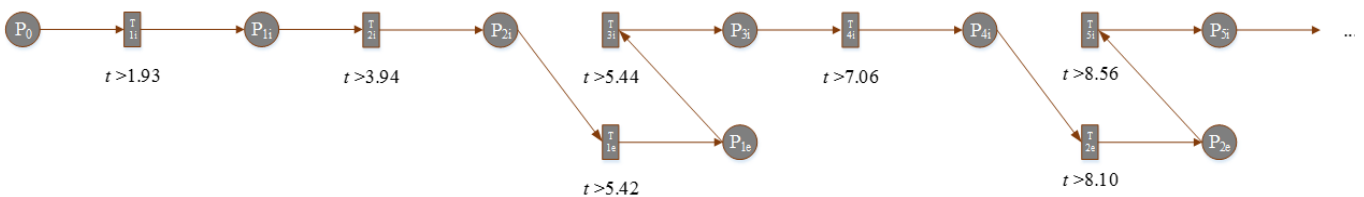


Figure 4.27: Petri net regulation for the earliest occurrence time of two faults combination

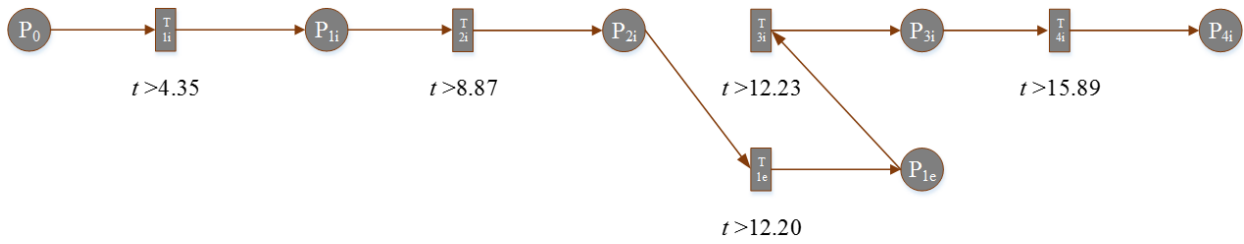


Figure 4.28: Petri net regulation for the latest occurrence time of two faults combination

At each state change of an interior fouling, the fault ratio F (%) is recalculated, which is then used for building energy simulation, which leads to the increase of the energy consumption. The simulation results of other fault combinations are presented in the Fig.4.28 to Fig.4.31.

Regarding to the normal distribution of fault evolution, we consider that the probability of the fault occurrence in two cases: fault combination and single fault is the same. As can be seen from Fig.4.26, at the 15th year, the energy building consumption in heating and cooling is 22%-8% more than the reference case without fault. However, the probability of this result is lower than the single fault occurrence case, which is presented in Fig.4.18 and Fig.4.20.

Interior fouling and refrigerant leakage

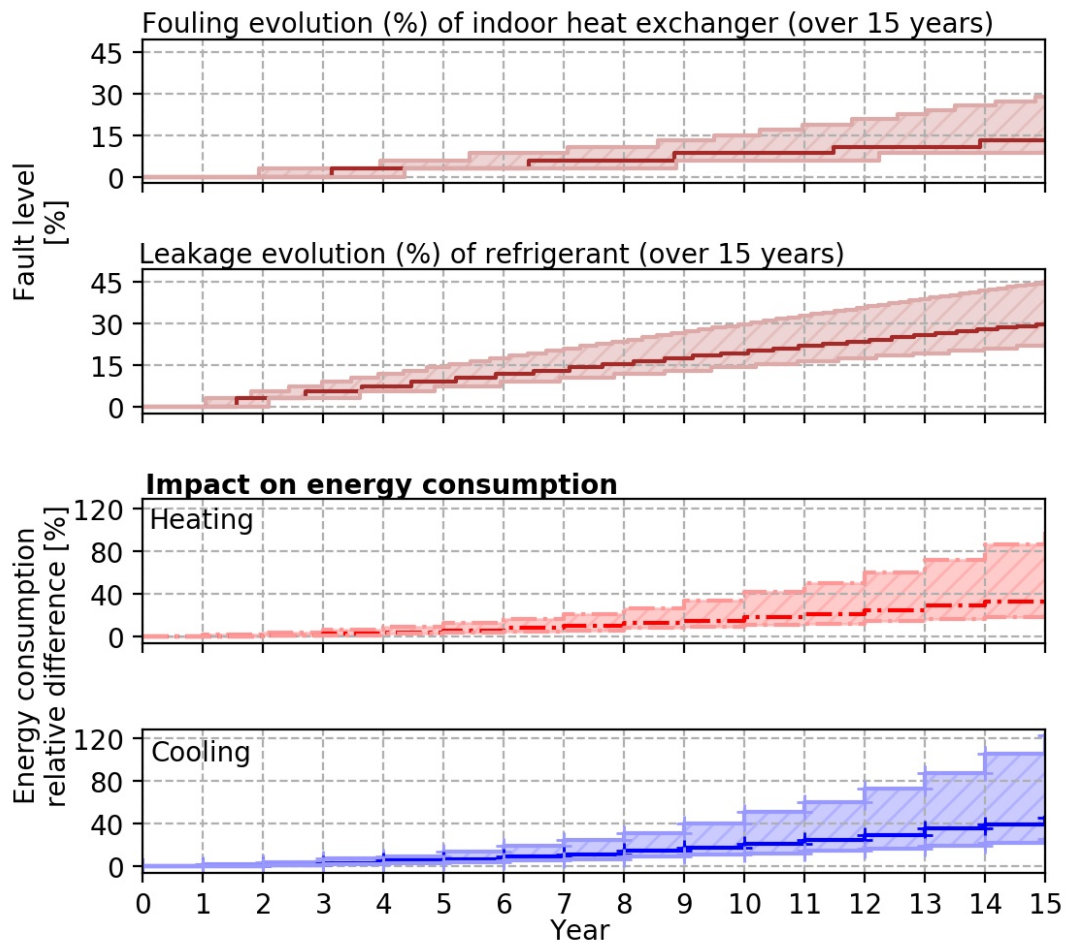


Figure 4.29: Impact of interior fouling and refrigerant leakage faults on energy consumption during 15 years

Exterior fouling and refrigerant leakage

Interior fouling, exterior fouling and refrigerant leakage

Suppose we consider three operating faults with two fault states during the heat pump life cycle, such as the interior and exterior fouling and refrigerant leakage. In that case, the Petri net model shows 54 scenarios of fault occurrence order. One scenario of Petri net regulation is presented in Fig.4.28. With the average occurrence time t and its dispersion (section 2.3.1), we conduct a 15-year simulation in order to see how the Petri net model regulate the occurrence time of operating faults. The simulation results are shown in Fig.4.31.

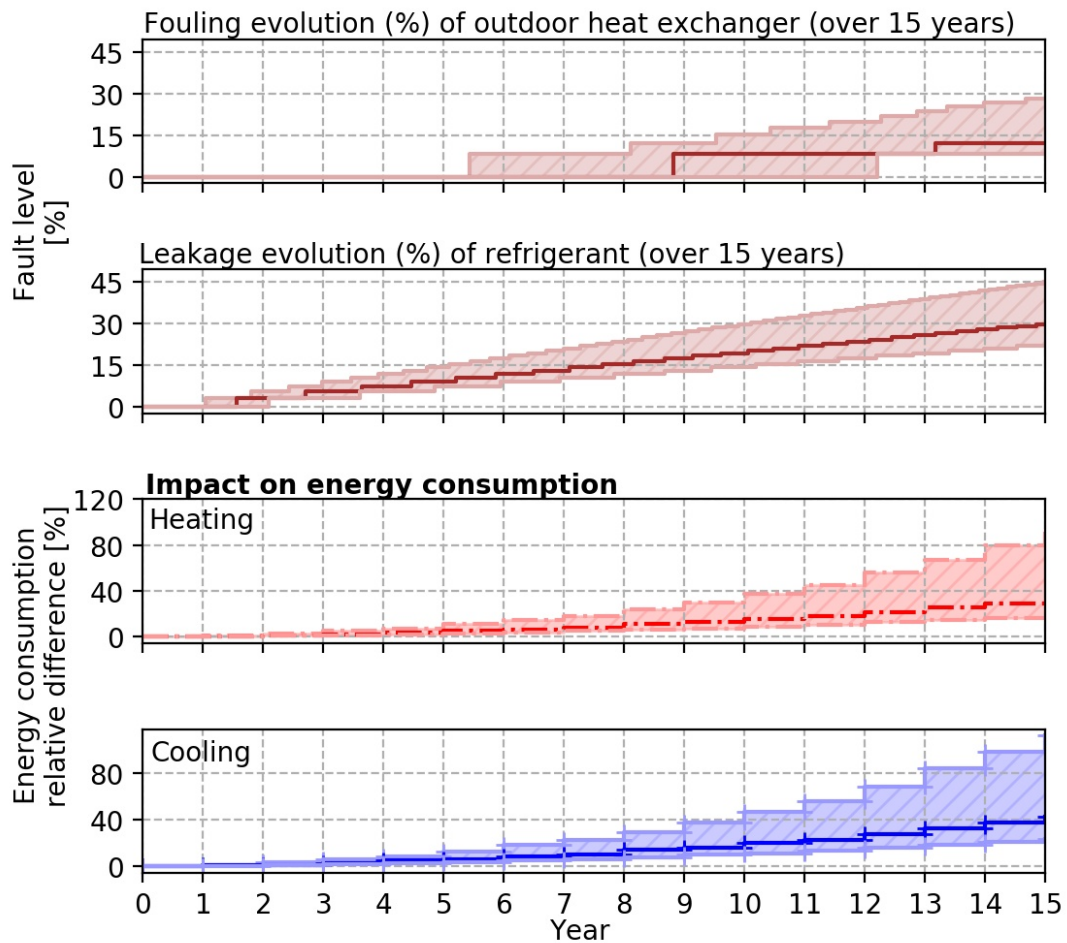


Figure 4.30: Impact of exterior fouling and refrigerant leakage faults on energy consumption during 15 years

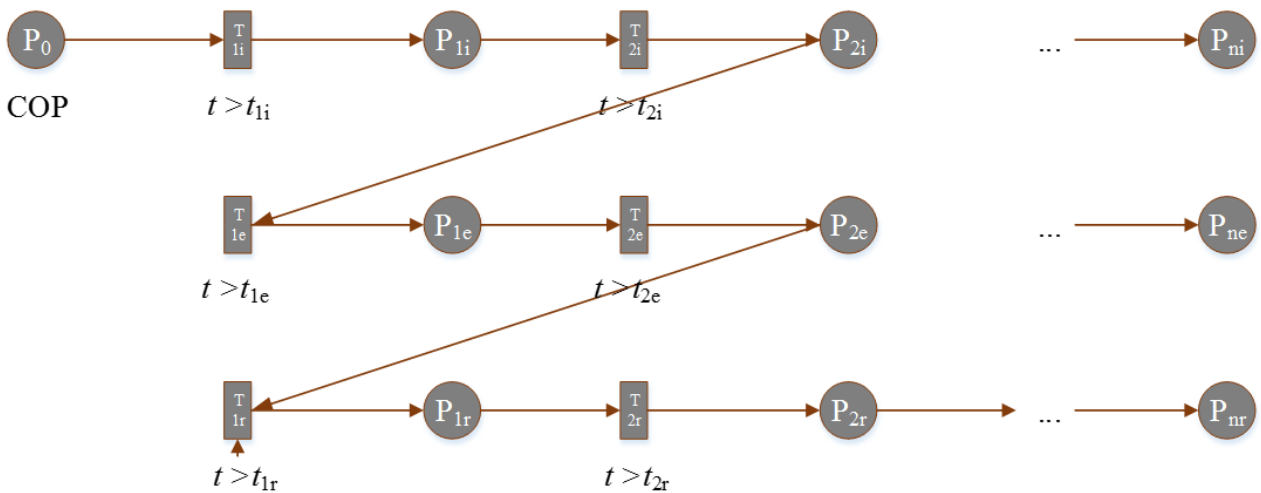


Figure 4.31: Petri net example for a three operating faults combination of an air-to-air heat pump

Four figures from Fig.4.26, Fig.4.29, Fig.4.30, and Fig.4.32 show the impact of four operating fault combinations on heating and cooling consumption during 15 years in Paris. As expected, the collective impact of simultaneous faults on energy consumption varies and depends on the faults considered. For the first combination of two fouling faults in heat

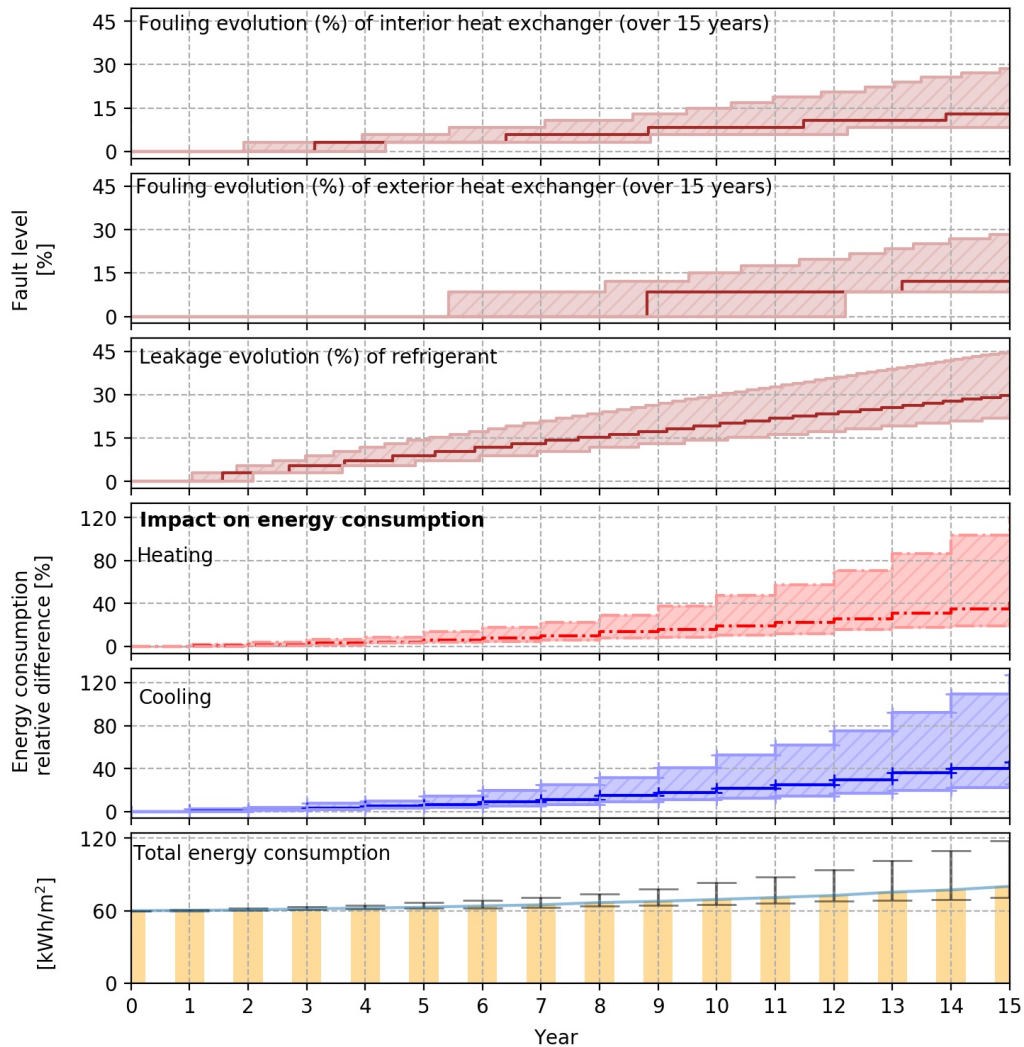


Figure 4.32: Impact of interior fouling, exterior fouling and refrigerant leakage faults on energy consumption during 15 years

exchangers, the collective effect can be described as exceeding additive in heating consumption and less additive in cooling consumption. At the 15th year, the heating increases by 27.8% which is higher than the sum of each fault impact 15.1% (interior fouling) + 10.8% (exterior fouling) =25.9%, while the cooling increases by 7.8%, which is lower than the sum of each fault impact 5.2% (interior fouling) + 10.7% (exterior fouling) =15.9%. However, when there is a refrigerant leakage, the consumption trend is inverse. The collective effect can be described as being less additive in heating consumption and exceed additive in cooling consumption. For example, in the second fault combination of interior fouling and refrigerant leakage, in the 15th year, the heating increases by 98.6%, which is lower than the sum of each fault impact 15.1% (interior fouling) + 101,8% (refrigerant leakage) =116.9%, while the cooling increases by 122.6%, which is too higher than the sum of each fault impact 5.2% (interior fouling) + 24.9% (exterior fouling) =30.1%.

Particularly, Fig.4.32 shows the relative consumption of the building, which covers the consumption of heating, cooling, lighting, hot water production, and auxiliaries (pumps and fans). The building is located in Paris, which respects the thermal regulation RT2012 for the

building's primary energy consumption, $60\text{kWh}/\text{m}^2/\text{year}$. As can be seen from Fig.4.32, the building consumption increases as soon as the faults occur. From the 3rd year, the building consumption remarkably increased, in which the primary energy consumption of the building exceeds $60\text{kWh}/\text{m}^2/\text{year}$. If there is no maintenance intervention, the operating faults impact more and more on the primary energy consumption. For example, in the 15th year, the Cep can increase approximately $120\text{kWh}/\text{m}^2/\text{year}$, double the standard value.

In this study, only three operating faults are considered. Their impacts on the building energy consumption are essential. These results show us a hypothesis that if there are more operating faults of HVAC systems, the more the building energy consumption. It should be taken into account the maintenance process to reduce the fault ratio during its life cycle.

Conclusions et perspectives

*“The most important thing is you go on the stage
and that you will be you and you have fun.”*

SIMON REINHARD

Conclusion

The overall objective of this work was to develop and demonstrate a methodology, which considers the operating faults during the life cycle of the residential air-to-air heat pump. The goal was to analyze the impact of these operating faults on the heat pump performance and the building energy consumption.

The approach for fault modeling realized begins with the model of the faults in the individual components, and ends up with the consequence of the fault to the whole system. The proposed method about the study of the impact of the operating faults, especially the fouling of heat exchangers, refrigerant leakage of the split residential air-to-air heat pump by using the refrigerant cycle model, white-box model. Once a fault appears and the cause of the fault is determined, the impact of three operating faults on the heat pump performance is presented. The more fouling the heat exchangers are and the more leakage of refrigerant in the circulation, the more significant the decrease in COP/EER value and the greater the increase in compressor power. The refrigerant cycle model shows a great capacity to model different heat pumps, in wide ranges of operating conditions.

Few experimental research studied operating faults and analyzed their impacts on heat pump performance over a wide range of operating conditions. There is still a lack of a integration of heat pump performance in design practice. The evolution of operating faults during the heat pump life cycle is therefore taken into account. In this study, based on the experiment results from the previous studies, we modeled the evolution of each operating fault. As the operating faults occur randomly, later, or sooner, we used the Petri net model to show every transition of operating faults under the graphical and mathematical form. The flow chart describes graphically parallel or concurrent activities. An equation system is established to, on the one hand, characterize the evolution of different activities. The graphic representation of Petri net describes the problem intuitively, which contains all possible evolutions and transitions of the fault throughout the heat pump life cycle: the interior fouling,

exterior fouling, and refrigerant leakage. These three operating faults are illustrated in two cases: separately and together. On the other hand, the Petri net model associates with the heat pump model to characterize the heat pump performance with different evolutions.

The association of the Petri net model and heat pump model provides consistent inputs to the building simulation, for example, heat pump performance evolution during the life cycle of the heat pump. To analyze the impact of fault on the building level, the Petri net model is associated with building energy simulation COMETH. The coupling of 3 computed models operated by Petri net (the heat pump model, the fault models, and the building model) can show the evolution of operating faults and quantify the operating fault's impact on the heat pump performance and the building energy consumption.

The impact of individual faults on performance, energy efficiency, and building energy consumption was evaluated for the residential air-to-air heat pump under a wide range of operating conditions. According to the results of this study, a refrigerant leakage of about 30% can result in an average 32% increase in heating consumption and a 5% rise in cooling capacity. For interior and exterior fouling, a 30% reduction in airflow increased the average heating consumption by 15% and 10%, respectively. As operating faults occur cumulatively, the impact of faults on performance and building energy consumption is also presented. When there are three operating faults with two states of faults, the Petri net model shows 54 scenarios of fault occurrence order. Based on the average occurrence time and its dispersion from the experiments, only a few scenarios can happen. We analyzed the impact of these three heat pump operating faults in a case study over 15 years. The building consumption increases as soon as the faults occur. As expected, the collective impact of simultaneous faults on energy consumption varies and depends on the faults considered. In most cases, the collective effect can be described as additive; however, the effect can exceed this additive value. Concerning the fault combination of three operating faults, the building consumption remarkably increased from the third year, in which the primary energy consumption of the building exceeds 60kWh/m²/year. If there is no maintenance intervention, the operating faults impact more and more on the primary energy consumption. For example, in the 15th year, the Cep can increase approximately 120 kWh/m²/year, double the standard value.

This study shows that the heat pump operation is also a great importance when it comes to energy efficiency. Throughout this study, we can see that each operating fault can have an impact not only on the heat pump performance but also on the building energy consumption. The proposed methodology is about system modeling, which takes into account the operating faults and their evolution during the execution phase. By simulating the heat pump performance with different operating faults, which approaches the heat pump performance in reality, the prospects for efficient energy use, the building energy consumption during overall operation are discovered.

Perspectives

The primary goal of this research is to detail a new methodology to evaluate the impact of a heat pump operating faults on its performance and building energy consumption. It is essential to mention the limitations of the current study, which should be addressed in future research. Suggestions for future work can be divided into three groups. One is related to the refrigerant cycle model of heat pump, another related to building simulation model, the third is related to the maintenance process.

The amount of detail used in the refrigerant cycle model is dependent on the simulation accuracy required. As the simulation is used during the heat pump design, we would like to analyze accurately the impact of different design parameters. Therefore, a highly detailed simulation would be required. It is suggested that more research and development can be carried out to improve the capability of the refrigerant cycle model. These capabilities may include different environmental conditions as humidity level, in which we can generalize the refrigerant model for different types of climate.

This study evaluates only three heat pump operating faults, which frequently happen during the building life cycle. Other operating faults, as compressor leakage, liquid line restriction, presence of non-condensable gases fault, should be taken into account in future research. With more operating faults, we can evaluate heat pump performance accurately during its operation. At the building level, other HVAC systems should be taken into account. Using the same principle of the Petri net model on a heat pump for other HVAC systems, we can have a whole picture about the impact of the HVAC systems operating faults on the building energy consumption.

Concerning the proposed methodology about using the Petri net model in system designs integrating operating faults, there is still much to be done to make it more applicable. In this study, three common heat pump operating faults were identified and modeled with the Petri net model. These fault models have been added to a development version of COMETH to characterize the building energy consumption. Once the COMETH development team has approved these models and implementation strategies, they will be part of future official COMETH release versions. There is a strong need to develop libraries that will guide and assist users in building their systems, choosing inputs, validating results.

Finally, the impact of operating faults should be analyzed in the economic situation, for example, service cost. According to the economic benefits, it is also essential to set a reasonable threshold by comparing the service cost with the economic impact of the operating faults. From these analyses, we can have the right decision for the maintenance process, such as verification, reparation, and replacement. Furthermore, we can consider the maintenance in the calculation process. The fault ratio of operating faults can be recalculated during its life cycle, which approaches the heat pump performance. According to the new European directive about the heat pump performance, it is required that the heat pump has to be checked every two years to ensure the energy efficiency of systems, which maintain

the building energy consumption as design.

References

- Abergel T. [Heat Pump report](#), 2020.
- AFPAC. [Les derniers chiffres du marché du génie climatique !](#) 2020.
- Andreas Z., Markus L., Roger N., Philippe R., and Marek M. [Evaluation method for comparison of heat pump systems with conventional heating systems](#), 2011.
- AQC. [Installation de chauffage](#). Technical report, 2019.
- Bettgenhauser K., Offermann M., Boermans T., Bosquet M., Grozinger J., von Manteuffel B., and Surmeli N. [Heat pump implementation scenarios until 2030](#), 2013.
- Breuker M. S. and Braun J. E. [Common faults and their impacts for rooftop air conditioners](#). *HVAC&R Research*, 4(3):303–318, 1998.
- BSI. [British Standard BS 3811: 1964–Glossary of Maintenance Management Terms in Terotechnology](#), 1993.
- Campbell J. M. [Gas conditioning and processing-Volume 2: The Equipment modules](#). Campbell petroleum series, 1992.
- Carl E. S. and Marianne S. [Guide to Refrigeration Cfc's](#). 1992.
- Cho J. M., Heo J., Payne W. V., and Domanski P. A. [Normalized performance parameters for a residential heat pump in the cooling mode with single faults imposed](#). *Applied Thermal Engineering*, 67(1):1 – 15, 2014. ISSN 1359-4311.
- Choi H., Cho H., and Choi J. M. [Refrigerant amount detection algorithm for a ground source heat pump unit](#). *Renewable Energy*, 42:111–117, 2012. ISSN 0960-1481. International Symposium on Low Carbon and Renewable Energy Technology 2010 (ISLCT 2010).
- CSTB. [Méthode de calcul Th-BCE 2012](#). 2012.
- CSTB. [Méthode de calcul Th-BCE - Annexes techniques](#), 2012.
- Danfoss M. [How thermostatic expansion valves work](#). 2017.
- Davis B. and Robison D. [Field Monitoring of High Efficiency Residential Heat Pumps](#). 2008.
- Deboyser B. [France : forte progression du chauffage par pompe à chaleur](#), 2020.

- Devotta S. [Alternative heat pump working fluids to CFCs](#). *Heat Recovery Systems and CHP*, 15(3):273 – 279, 1995. ISSN 0890-4332.
- Downey T. and Proctor J. [What can 13,000 air conditioners tell us](#). *the Proceedings of the 2002 ACEEE Summer Study on Energy Efficiency in Buildings*, 1:53–67, 2002.
- Du Z., Domanski P. A., and Payne W. V. [Effect of common faults on the performance of different types of vapor compression systems](#). *Applied Thermal Engineering*, 98:61 – 72, 2016. ISSN 1359-4311.
- EHPA. [European Heat Pump Market and Statistics Report 2014](#) . 2014.
- Elbel S. and Hrnjak P. [Flash gas bypass for improving the performance of transcritical R744 systems that use microchannel evaporators](#). *International Journal of Refrigeration*, 27(7):724–735, 2004.
- Elbel S. and Hrnjak P. [Ejector refrigeration: an overview of historical and present developments with an emphasis on air-conditioning applications](#). 2008.
- Eric D., Thomas M., Florence M., Frédéric V., Laurence F., Romuald H., Denis L., and Anthony D. [Etude sur le confinement des fluides frigorigènes](#), 2015.
- Fang Y., Croquer S., Poncet S., Aidoun Z., and Bartosiewicz Y. [Drop-in replacement in a R134 ejector refrigeration cycle by HFO refrigerants](#). *International Journal of Refrigeration*, 77:87–98, 2017. ISSN 0140-7007.
- Fizel Y. [Evolution des fluides frigorigènes : point réglementaire et tendances](#) , 2019.
- Gasche J. L., Andreotti T., and Maia C. R. M. [A model to predict R134a refrigerant leakage through the radial clearance of rolling piston compressors](#). *International Journal of Refrigeration*, 35(8):2223–2232, 2012. ISSN 0140-7007.
- Guzda A. and Szmolke N. [Compressors in heat pumps](#). *Machine Dynamics Research*, 39(2), 2016.
- Hourahan G. and Baxter V. D. [Impact of Installation Faults on Heat Pump Performance](#). *IEA Heat Pump Center Newsletter (Online)*, 33(1), 2015.
- IEA. [Key World Energy Statistics 2019](#). 2019.
- Inc A. T. [BJAC exchanger design help manual](#). 2003.
- Jacques B., Michel L. G., and Jean L. [Climatisation, conditionnement d'air - Production de chaud et de froid](#). Parisiennes, Paris, 1997. ISBN 2-86243-041-2.
- Katipamula S. and Brambley M. R. [Methods for fault detection, diagnostics, and prognostics for building systems—a review](#). *Hvac&R Research*, 11(1):3–25, 2005.

- Kim B., Lee S. H., Lee D., and Kim Y. [Performance comparison of heat pumps using low global warming potential refrigerants with optimized heat exchanger designs](#). *Applied Thermal Engineering*, 171:114990, 2020. ISSN 1359-4311.
- Kim J., Cai J., and Braun J. E. [Common faults and their prioritization in small commercial buildings](#), 2018.
- Kim M. and Kim M. S. [Performance investigation of a variable speed vapor compression system for fault detection and diagnosis](#). *International Journal of Refrigeration*, 28(4):481–488, 2005. ISSN 0140-7007.
- Kim M., Payne W. V., Domanski P. A., and Hermes C. [Performance of a Residential Heat Pump Operating in the Cooling Mode with Single Faults Imposed \(NISTIR 7350\)](#). Technical report, 2006.
- Kim M., Payne W. V., Domanski P. A., Yoon S. H., and Hermes C. J. [Performance of a residential heat pump operating in the cooling mode with single faults imposed](#). *Applied Thermal Engineering*, 29(4):770 – 778, 2009. ISSN 1359-4311.
- Madani H. and Roccatello E. [A comprehensive study on the important faults in heat pump system during the warranty period](#). *International journal of refrigeration*, 48:19–25, 2014.
- Madani H., Claesson J., and Lundqvist P. [Capacity control in ground source heat pump systems: Part I: modeling and simulation](#). *International Journal of Refrigeration*, 34(6):1338–1347, 2011.
- Maddah S., Goodarzi M., and Safaei M. R. [Comparative study of the performance of air and geothermal sources of heat pumps cycle operating with various refrigerants and vapor injection](#). *Alexandria Engineering Journal*, 2020. ISSN 1110-0168.
- Mader G., Thybo C., and Rasmussen H. [An electronic expansion valve with automatic refrigerant distribution control](#). *Deutsche Kälte-Klima-Tagung. Magdeburg, Germany*, 2010.
- Mehrabi M. and Yuill D. [Generalized effects of faults on normalized performance variables of air conditioners and heat pumps](#). *International Journal of Refrigeration*, 85:409–430, 2018. ISSN 0140-7007.
- Mowris R., Blankenship A., and Jones E. [Field Measurements of Air Conditioners with and without TXVs](#). In *ACEEE Summer Study Proceedings*, 2004.
- Norford L., Socolow R., Hsieh E., and Spadaro G. [Two-to-one discrepancy between measured and predicted performance of a ‘low-energy’ office building: insights from a reconciliation based on the DOE-2 model](#). *Energy and Buildings*, 21(2):121–131, 1994. ISSN 0378-7788.

- Payne W. V., Payne W. V., Yoon S. H., and Domanski P. A. [Heating Mode Performance Measurements For A Residential Heat Pump With Single-Faults Imposed](#). Technical report, 2017.
- Roth K. W., Westphalen D., Llana P., and Feng M. [The energy impact of faults in US commercial buildings](#). 2004.
- Schiffmann J. and Favrat D. [Experimental investigation of a direct driven radial compressor for domestic heat pumps](#). *International Journal of Refrigeration*, 32(8):1918 – 1928, 2009. ISSN 0140-7007.
- Siegel J., Walker I., and Sherman M. [Dirty air conditioners: Energy implications of coil fouling](#). Technical report, Lawrence Berkeley National Lab.(LBNL), Berkeley, CA (United States), 2002.
- Staffell I., Brett D., Brandon N., and Hawkes A. [A review of domestic heat pumps](#). *Energy Environ. Sci.*, 5:9291–9306, 2012.
- Swan W. P., Fernandes D. P., Khade A., and Chen D. H. [Abnormal Situation Management: Detection of Fouling and Longitudinal Bypass in Heat Exchangers](#). *International Journal of Chemical Engineering and Applications*, 9(1):9–15, 2018.
- Underwood C. [Heat pump modelling](#). In Rees S. J., editor, *Advances in Ground-Source Heat Pump Systems*, pages 387 – 421. Woodhead Publishing, 2016. ISBN 978-0-08-100311-4.
- Wang C.-C. [System performance of R-1234yf refrigerant in air-conditioning and heat pump system – An overview of current status](#). *Applied Thermal Engineering*, 73(2):1412–1420, 2014. ISSN 1359-4311. Special Issue for the 2nd International Workshop on Heat Transfer Advances for Energy Conservation and Pollution Control (IWHT2013).
- Xiao B., Chang H., He L., Zhao S., and Shu S. [Annual performance analysis of an air source heat pump water heater using a new eco-friendly refrigerant mixture as an alternative to R134a](#). *Renewable Energy*, 147:2013 – 2023, 2020. ISSN 0960-1481.
- Xu X., Hwang Y., and Radermacher R. [Performance comparison of R410A and R32 in vapor injection cycles](#). *International Journal of Refrigeration*, 36(3):892–903, 2013. ISSN 0140-7007.
- Yang C.-Y. and Nalbandian H. [Condensation heat transfer and pressure drop of refrigerants HFO-1234yf and HFC-134a in small circular tube](#). *International Journal of Heat and Mass Transfer*, 127:218–227, 2018. ISSN 0017-9310.
- Yoon S. H., Payne W. V., and Domanski P. A. [Residential heat pump heating performance with single faults imposed](#). *Applied Thermal Engineering*, 31(5):765 – 771, 2011. ISSN 1359-4311. MNF 2009 Special Issue.

Appendices

Appendix A

Heat pump types

Exhaust air

Exhaust-air heat pumps use aerothermal energy. Part of the energy used comes from a re-use (via heat exchangers) of indoor air, part of it comes from outdoor air that is drawn into the building. Initial analysis shows that 30% to 50% of the energy used comes from outdoor air. In order to provide (yet again) a cautious estimate, the contribution from exhaust air heat pumps is generally weighted with a factor of 0,3*.

Heat pumps using exhaust air as energy source use ambient energy, and such heat pumps therefore supply renewable energy. But simultaneously such heat pumps recover the energy in the exhaust air, which is not aerothermal energy according to the Directive (9). It is therefore only the aerothermal energy that is counted as renewable energy.

H-air/water

Reversible heat pumps connected to hydronic systems are always counted, as their primary use as heating system can be assumed.

H-ground/water

Reversible air-air W/heating

Firstly, reversible heat pumps in warm and to some extent average climates are often installed with the purpose of cooling the indoor environment, although they are also used to provide heating during the winter. As the cooling demand in the summer is higher than the heating demand in the winter, the rated capacity reflects the cooling demand rather than the need for heating. As the installed capacity is used as an indicator of heating demand, it implies that the statistics of installed capacity will not reflect the capacity installed for heating purposes. Moreover, reversible heat pumps are often installed in parallel to existing heating systems, implying that these heat pumps are not always used for heating purposes.

The use of air/air heat pumps predominantly for heating is assumed for countries in cold climates (Estonia, Denmark, Finland, Lithuania, Norway). The number of units reported results from total sales adjusted by a correction factor (around 10 Air/air units sold in the average climate zone have not been counted, due to a lack of reliable information on their use for heating or cooling. For countries in the warm climate zone (France, Italy, Portugal and Spain) only a share of the total sales number has been included in the report. A study of the Italian market comes to the conclusion that in 9.5

As described earlier, a large number of reversible air-air heat pumps are installed in Europe. In Scandinavian and Baltic climates, their use for heating is simply assumed on the basis of the prevailing cold climate. For southern Europe a different approach has been taken. It is based on a study done for the Italian market to determine the type of heating systems used. This study has been used as guidance for the calculation of the share of heating provided by heat pumps in the EHPA methodology. It has now been translated in modified heating hours for the Mediterranean markets in the commission study.

Reversible other

Reversible HP - air/water

Sanitary hot water

Sanitary hot water heat pumps are the fastest growing heat pump segment across Europe. This category is the only one showing double-digit growth. Sanitary hot water units combine a heat pump and a hot water storage tank. They are either sold as stand alone units with the heat pump and the tank in one casing or as systems combining a heat pump and a separate tank.

Others

Hybrid HP

There is no clear definition of what a hybrid heat pump is, due to the manyfold ways to integrate heat pumps with other technologies. In order to integrate this new class of systems into our database, the national heat pump associations and EHPA agreed on the following broad definition: A hybrid heat pump is the combination of a heat pump and a fossil fuel based boiler that has a controller between both heaters and is designed to be sold together under one commercial reference.

For a part of the housing stock, so-called 'hybrid' heat pumps have proven to be particularly suitable for heating. A hybrid heat pump comprises an 'electric heat pump' and a 'fossil fuel boiler'. The combination of the two systems has been around for a long time (boiler back-up heat pump) but 'hybrid heat pumps', which recently came on to the market, go further thanks to a high-tech control system that is implemented between the two systems. The performance of these new-generation hybrid machines is optimal in every aspect: in terms of CO₂ emissions, customer's energy bills and balancing supply and demand across the national grid. This last point, hardly known by the general public, is crucial as it helps to secure the supply of electricity in the country and to retain a high-quality network. The performance of these hybrid heat pumps remains high both in terms of energy (high COP) and in terms of the environment (low CO₂ emissions) thanks to the heat pump's high operating rate (> 70%)

Industrial heat pumps

Larger heat pumps for commercial, industrial and district heating applications are increasingly popular. They quite often use geothermal or hydrothermal energy. However also here, air is an energy source used by a number of installations. Air, water and ground can either carry renewable energy or waste heat from processes. In the later case, this type of heat pump improves energy efficiency, but does not use a renewable source.

District heating

Heating capacity >500 kW, smaller central heat pumps for heating several buildings have to be included under point 1

VRF

Variable Refrigerant Flow / Variable Refrigerant Volume